The Causal Effects of Global Supply Chain Disruptions on Macroeconomic Outcomes: Evidence and Theory*

Xiwen Bai† Jesús Fernández-Villaverde‡ Yiliang Li§

Francesco Zanetti¶

October 3, 2023

Abstract

We study the causal effects and policy implications of global supply chain disruptions on the U.S. economy. We construct a new index of supply chain disruptions from the Automatic Identification System data of containerships, developing a novel spatial clustering algorithm that determines real-time congestion from the positions and speeds of containerships in major ports around the globe. We show important differences between our index and the Global Supply Chain Pressure Index that are important for the interpretation of supply chain disruptions. We develop a new theoretical framework with search frictions between exporters and importers in the goods market, transportation costs, and spare capacity that provides us with unique identification restrictions arising from the co-movements of spare capacity, price, and output for the causal effects of supply chain disruptions. A structural VAR with these restrictions establishes that supply chain disruptions: (i) depress real GDP, raise prices, generate a surge in spare capacity, and (ii) increase the effectiveness of contractionary monetary policy in taming inflation while reducing the sensitivity of output to monetary policy.

JEL Classification: E32, E58, J64.

Keywords: supply chain disruptions, search-and-matching in the goods market, SVAR, state-dependence of monetary policy.

*We thank our discussant Frank Smets, and Dennis Bonam, Sebastian Heise, Bo Hu, Elena Maria Diaz, Ekaterina Peneva, Omar Rachedi, Ricardo Reis, Bo Sun, Li Yu, Yuan Zi and participants at the Inflation: Drivers and Dynamics Conference 2023 (ECB and the Cleveland Fed), EEA-ESEM Barcelona 2023, AMES Singapore 2023, 11th Shanghai Macroeconomics Workshop at SUFE, AMES China 2023, CEMA 2023, 26th T2M Conference, Leuven Summer Event 2023, 2nd Asia-Pacific SaM Online Workshop, and 4th UIBE CCTER Workshop on Transportation Research for valuable comments and suggestions. Francesco Zanetti gratefully acknowledges financial support from the British Academy.

†Tsinghua University, China. xiwenbai@mail.tsinghua.edu.cn.

‡University of Pennsylvania, U.S. jesusfv@econ.upenn.edu

§University of International Business and Economics, China. yiliang_li@uibe.edu.cn.

¶University of Oxford, U.K. francesco.zanetti@economics.ox.ac.uk.

1. Introduction

Sudden and large imbalances in the supply and demand for goods, often stemming from disruptions to the supply chain, can lead to protracted deterioration in macroeconomic performance. For instance, the severe disruptions to the flow of goods worldwide during the Covid-19 pandemic led to an unprecedented fall in global trade and a sharp rise in prices, culminating in the second-largest recession in U.S. history.[1] Other prominent examples of potent supply chain disruptions include the blockage of the Suez Canal in 2021 and the war in Ukraine in 2022, both of which resulted in a shortage of goods, increased transportation costs, and raised inflation globally.[2]

Despite the fundamental role of supply chain disruptions in shaping macroeconomic performance and economic policy, research on this topic is scant and progress is challenged by two key issues. First, existing indices of supply chain disruptions are often inferred from changes in shipping prices or information from surveys on potential disruptions gleaned from the Purchasing Managers' Index (PMI). These measures are problematic since prices internalize endogenous movements in the demand for goods while being disconnected from output during supply chain disruptions, and surveys are notoriously prone to measurement errors accruing to the subjective perceptions of purchasing managers on supply chain issues, thus providing a potentially biased measurement of supply chain disruptions. The ideal measurement of supply chain disruptions requires data that track the disruptions to the regular flows of goods that are central to the mismatch between supply and demand and the consequent increase in prices. Second, there is no theoretical framework that studies supply chain disruptions considering the spare capacity resulting from the imbalances between the supply and demand for goods. Against this backdrop, mounting evidence points to the adjustment in the spare capacity as a systematic attribute of supply chain disturbances, which is critical to the response of prices and the ensuing policy tradeoffs for the contemporaneous stabilization of prices and output.[3]

1. During the Covid-19 recession (February-April 2020), the decline in GDP from peak to trough was 19.2%. During the Great Depression (August 1929-March 1933), the fall in GDP was 26.7%.

2. See https://www.nytimes.com/2021/03/24/world/middleeast/suez-canal-blocked-ship.html (accessed on July 25, 2023) for coverage on the Suez Canal blockage.

3. Several articles in newspapers and policy institutions discuss the relevance of disruptions to the supply

Our paper addresses these issues by developing: (i) a new index of global supply chain disruptions derived from maritime satellite data of containerships, and (ii) a novel theoretical framework that accounts for the spare capacity arising from the imbalances between the supply and demand for goods consequent to the disruption to the supply chain. Using our new data and theory, we shed new lights on the causal effects of global supply chain disruptions and their implications for the effectiveness of monetary policy.

The measurement of supply chain disruptions. We study disruptions to the supply chain by examining congestion at container ports. Given the pivotal role of container ports in international trade, through which approximately 60% of the total value of world seaborne trade passes (UNCTAD 2019; OECD and EUIPO 2021), even a mild increase in port congestion can significantly impair regular supply chains and generate large imbalances between the supply and demand for tradable goods. More importantly, the itineraries of containerships are rarely altered due to significant switching costs, and the routes of these vessels remain unchanged for the duration of contracts that normally average more than one year, ensuring that congestion at a seaport is minimally influenced by strategic decisions of shipping companies to adjust capacity across routes following changes in demand (Stopford 2008; Song and Dong 2012; Wang, Meng, and Jia 2019; Brancaccio, Kalouptsidi, and Papageorgiou 2020; Brancaccio et al. 2023).[4,5] This feature of the shipping segment of containerships separates port congestion from the forces of demand, hence enabling us to detect supply chain disturbances from the density of inactive vessels stationed at ports.

chain for economic performance and macroeconomic policies. See for instance Attinasi et al. (2021), Forster van Aerssen et al. (2021), Grimes and Edgecliffe-Johnson (2021), The White House (2021), Dempsey (2022), Lane (2022), and World Bank (2022).

4. In the maritime shipping industry, long-term contracts between exporters and shipowners often have a validity period of one year, with a significant proportion of them lasting even longer due to heightened uncertainty on some specific routes (Bhonsle 2023).

5. Stopford (2008), Kalouptsidi (2014), Brancaccio, Kalouptsidi, and Papageorgiou (2020), Fuchs and Wong (2022), Wong (2022), and Brancaccio et al. (2023) discuss the different segments of the maritime shipping industry, namely, containerized liner services and tramp shipping. Specifically, in his textbook on maritime economics, Stopford (2008) states, "A liner service is a fleet of ships … which provide a fixed service, at regular intervals, between named ports, …. A fixed itinerary, inclusion in a regular service, and the obligation to accept cargo from all comers and to sail … on the date fixed by a published schedule are what distinguish the liner from the tramp". In addition, Brancaccio, Kalouptsidi, and Papageorgiou (2020) state, "The transportation sector … can be split into two categories: those that operate on fixed itineraries, much like buses, and those that operate on flexible routes, much like taxis. Containerships … belong to the first group". In Section 2.3, we also provide statistical evidence that corroborates the above definition of the containerized liner industry.

We quantify port congestion using granular shipping data from the Automatic Identification System (AIS), the mandatory real-time satellite tracking system for containerships across major ports around the globe from 2017 to 2022. By developing a novel machine learning clustering algorithm that utilizes the positions and speeds of containerships recorded in the AIS data, we provide the first mapping of global port congestion by constructing a high-frequency index of Average Congestion Rate (ACR) for major ports worldwide. Our ACR index is also the first measurement of global supply chain disruptions derived from maritime satellite data of containerships.[6]

Theoretical framework. To interpret the data and study the causal effects of supply chain disruptions, we develop a simple model that accounts for the imbalances in the supply and demand for goods and provides new insights into the effects of these disruptions on the tradeoffs of economic policy. Our model is based on search and matching frictions between exporters and importers in the international product market, building on the disequilibrium model of Barro and Grossman (1971), recast in a microfounded framework by Michaillat and Saez (2015, 2022), and Ghassibe and Zanetti (2022). The presence of search frictions renders prices not allocative and unable to clear the supply and demand for goods, similar to the central effect of supply chain disruptions. In our model, exporters supply the goods demanded by importers, and the transactions are mutually costly since they require exporters and importers to pay transportation and visiting costs, respectively. In equilibrium, these costs generate spare capacity and costly congestion. Central to the realization of supply chain disruptions, exporters draw transportation costs from a given distribution in each period, and they decide to ship goods if the drawn cost falls below the threshold for profitable shipments. We assume that a disturbance to the supply chain increases the transportation costs for all exporters, as evinced by the large empirical evidence linking supply chain disturbances and transportation costs (Benigno et al. 2022; Finck and Tillmann 2022; Alessandria et al. 2023; Dunn and Leibovici 2023). We model the general rise in transportation costs as a shift of the distribution of costs to the right of the domain, making it more likely for each exporter

6. The global nature of our ACR index "averages out" any changes in port congestion resulting from infrequent adjustments in shipping capacity across routes, thus further underpinning the exogeneity of our ACR index. In addition, since the AIS data offer unparalleled accuracy in tracking real-time movements of tradable goods across the globe, our ACR index is not subject to the same measurement errors as those in the PMI stemming from the subjective perceptions of purchasing managers on supply chain issues.

to draw transportation costs that exceed the profitability threshold and thus increasing the likelihood of a halt in the shipping of goods. Consequently, the number of unprofitable shipments increases, leading to a fall in the supply of goods available to importers. The model shows that the supply chain shock disrupts economic trade, drives up prices, and widens the spare capacity of exporters.

Our model demonstrates that the responses of macro aggregates to a supply chain disruption shock differ from standard shocks to the demand and supply of goods. Unlike demand shocks, disruptions to the supply chain result in negative co-movements between the quantity and price of goods. While such a property also holds for traditional labor supply shocks, disruptions to the supply chain uniquely increase spare capacity (or equivalently, unemployment), whereas labor supply shocks decrease it. Such a distinction is intuitive, as transportation costs do not change the domestic capacity to produce, but affect whether selling abroad is profitable. Therefore, the changes in the spare capacity resulting from the disequilibrium between the supply and demand for goods play a crucial role for the identification of supply chain disruptions.

The causal effects of supply chain disruptions. Drawing directly from the prediction of our model, we apply our theoretical restrictions on the responses of endogenous variables in the Structural Vector Autoregressions (SVARs), allowing us to uniquely identify the shocks to the supply chain and distinguish them from traditional labor supply and demand shocks. We estimate the SVAR model using the Bayesian approach, as in Arias, Rubio-Ramirez, and Waggoner (2018), Arias, Caldara, and Rubio-Ramírez (2019), and Arias et al. (2023), and establish several key results. First, a disruption shock to the supply chain leads to a large and immediate drop in real GDP, sharp and persistent increases in both inflation and import prices, and a substantial jump in unemployment. In addition, similar to a labor supply shock, a supply chain disruption shock tends to generate a persistent positive response of inflation, an observation consistent with recent evidence (e.g., Bekaert, Engstrom, and Ermolov (2020) and Gordon and Clark (2023)). Furthermore, the two aggregate supply shocks differ in terms of their effects on unemployment, which is representative of spare capacity. While the initial fall in unemployment in response to the labor supply shock is transitory, the initial increase in unemployment in response to the supply chain

disruption shock is persistent, with the median response reverting to zero slightly before the two-quarter mark.

Second, the decomposition of historical variance shows that the sharp fall in inflation in early 2020 was mainly driven by a significant contraction of aggregate demand that coincided with the first wave of the Covid-19 pandemic across the world. Subsequently, aggregate demand started to rebound, while global supply chain disruptions escalated and made a significant contribution to the rise in inflation. This pattern continued until the end of 2021, with labor supply shocks emerging as the primary driving force for the elevated inflation. In addition, we show that the sharp increase in the Global Supply Chain Pressure Index (GSCPI) – a prominent index to measure supply chain disruptions in both the literature and media – during the first seven months of the pandemic (January-July 2020) was not caused by disruptions to the supply chain. During that time, port congestion was at historical average levels. Instead, the surge in the GSCPI was likely driven by sudden changes in demand and the management's mis-perception of supply chain issues as recorded by the surveys.[7] We show that the misclassification of disruptions to the supply chain has important implications for the statistical significance of supply chain disruption shocks and the associated policy response, as we discuss below.

Policy implications. Our analysis shows that supply chain disruptions generate stagflation and a simultaneous increase in spare capacity. The higher spare capacity constrains the supply of goods and leads to a tighter product market, thus escalating the mismatch between the supply and demand for goods and increasing the sensitivity of prices to movements in demand. As larger shifts in prices are needed to ration the product market, these changes in the relative movements of prices and output increase the effectiveness of monetary policy in stabilizing inflation amid supply chain disruptions. This reinforces findings that show state-dependence in the effectiveness of monetary policy (Benigno and Ricci 2011; Ikeda et al. 2022; Benigno and Eggertsson 2023; Harding, Lindé, and Trabandt 2023).[8]

7. Specifically, the GSCPI builds on the PMI, which does not differentiate whether the increase in "delivery times" is caused by a disruption to the supply chain, or to the actual production itself.

8. Benigno and Eggertsson (2023) introduce labor search and matching frictions, as well as wage rigidity, to a New Keynesian framework and proposes a nonlinear Philips curve, of which the slope increases when the labor market is tight. Such nonlinearities imply an "easy down" for the economy, meaning small output losses from bringing inflation under control. In contrast, while our theoretical framework also predicts an "easy down" for the economy through monetary tightening, it relies on the role of spare capacity in the

We test the theoretical prediction by developing a Threshold Vector Autoregression (TVAR) model that estimates the differences in the effects of a contractionary monetary policy shock for different levels of the ACR index. Consistent with our theory, we find that an exogenous tightening of monetary policy leads to a significantly larger and more persistent decline in inflation for a given decrease in output and employment during periods of supply chain disruptions. Our results support a more aggressive, yet less contractionary, monetary policy in response to the elevated inflation consequent to the disturbances to the supply chain. This approach is consistent with the progressive tightening of monetary policy in the U.S. during the supply chain disruptions in the post-Covid-19 recession.

Related literature. Our analysis is related to several realms of research. We develop a theoretical framework that maps the mismatch between the supply and demand for goods to changes in prices, real activity, and spare capacity. Our model builds on the disequilibrium framework of Barro and Grossman (1971) by incorporating search and matching frictions in the goods market that result in spare capacity, similar to the studies by Michaillat and Saez (2015, 2022) and Ghassibe and Zanetti (2022). We also link to Brancaccio, Kalouptsidi, and Papageorgiou (2020) and Brancaccio et al. (2023) who develop a search and matching framework to study the role of the transportation sector, as well as Comin, Johnson, and Jones (2023) who develop a New Keynesian model with imported inputs to investigate how potentially binding capacity constraints and demand/supply shocks to them shape inflation. Unlike these studies, however, we connect disequilibrium and spare capacity in the goods market with rising transportation costs resulting from the disruptions to the supply chain, and we focus on the impact on prices and real activity and the changes for the tradeoffs of economic policy.

We connect to studies linking the transportation sector to the real economy. Brancaccio, Kalouptsidi, and Papageorgiou (2020) demonstrate the chief role of transportation costs in equalizing comparative advantages across countries and dampening the response of trade flows to shocks. Brancaccio et al. (2023) show that search frictions in the transportation market distort the transportation network and the dynamic allocation of ships over space, requiring pricing rules or taxes to establish efficiency. Dunn and Leibovici (2023) study

goods market to endogenously generate strong nonlinearities in the aggregate supply curve.

the drivers of global shipping dynamics, showing that supply chain disruptions lead to an increase in shipping prices and generate aggregate implications. Allen and Arkolakis (2014) link transportation networks to real activity, and Fuchs and Wong (2022) connect them to infrastructure investment. Smirnyagin and Tsyvinski (2022) study the effect of supply chain disasters on asset prices. Li et al. (2022) estimate the patterns of global trade in crude oil, and Bai and Li (2022) investigate the role of congestion in shipping markets for international oil trade and the macroeconomy. In contrast to these studies, we concentrate on the macroeconomic consequences and policy implications of supply chain disruptions arising from the transportation sector.

Finally, we relate to the empirical research that develops SVAR models to study the causal effects of supply chain shocks and differentiate them from alternative shocks to aggregate demand. Representative studies in this large area of research include Balleer et al. (2020), Bekaert, Engstrom, and Ermolov (2020), Brinca, Duarte, and Faria-e-Castro (2021), Shapiro (2022), and Gordon and Clark (2023). Unlike these studies, we base the identification of disturbances to the supply chain on our theory of disequilibrium, and we are the first study to apply in the SVARs an index of global supply chain disruptions that is derived from granular shipping data.

The remainder of our study is organized as follows. Section 2 constructs our ACR index of supply chain disruptions from satellite data. Section 3 develops our theoretical model and the identification restrictions. Section 4 presents the baseline estimation results and a comparison with the estimation based on the GSCPI. Section 5 explores the state-dependent effects of monetary policy shocks following supply chain disruptions. Section 6 concludes.

2. Measuring Global Supply Chain Disruptions

In this section, we develop a novel index designed to track global supply chain disruptions by analyzing imbalances between the supply and demand for goods through the lens of containerized trade. Accounting for 60 percent of the total value of seaborne trade (UNCTAD 2019; OECD and EUIPO 2021), containerized seaborne trade plays an indispensable role in fostering the development and ensuring the smooth operation of global supply chains

(Notteboom, Pallis, and Rodrigue 2022).

In the realm of containerized trade, seaports serve as international hubs for freight collection and distribution. Any disruption to these hubs can lead to port congestion, which in turn significantly impairs regular supply chains and trade flows, culminating in far-reaching consequences for all parties involved in international trade.[9] By leveraging the most recent satellite data on the positions and speeds of containerships, available from 2017 onwards, we track port congestion and construct a granular measure of global supply chain disruptions.

2.1. AIS Data

We use satellite data from the AIS, the mandatory tracking system required by the International Maritime Organization (IMO) for international voyaging vessels larger than 300 gross tonnage (Heiland et al. 2022). The AIS can handle over 2000 reports per minute and may update information as often as every two seconds, providing comprehensive coverage of the movements of containerships around the globe from January 2017 to July 2022.[10] Each data entry includes the ship's IMO number, timestamp, current draught, speed, heading, and geographical coordinates.[11] The detailed positioning and sailing information enables us to track the behaviors of vessels within various port zones, facilitating the construction of an accurate measure of port congestion.

9. Port congestion is a multifaceted issue that imposes significant costs on various stakeholders in the shipping industry. Prior to the pandemic, waiting times at ports were typically measured in hours; however, stringent COVID-19 restrictions led to extended delays, with waiting times reaching 2-3 days at several major ports worldwide, incurring substantial daily financial losses. Shippers and freight forwarders encountered unexpected delays, compounded by surcharges such as the Port Congestion Surcharge (PCS), with charges escalating to USD 1,250 per container in certain cases. Importers and exporters faced disruptions in their supply chains, resulting in potential profit losses, additional costs such as demurrage and detention, and challenges in fulfilling market demands and contractual obligations. Container owners were directly impacted by the PCS, while truckers and terminal operators experienced restricted transport efficiency and increased operational costs. Considering that the average value of goods in a 40-foot container is around USD 100,000, the PCS alone represents a sizable share of the total value, underscoring the substantial economic impact of port congestion on all parties involved.

10. Over 99 percent of international container shipments are carried by containerships that exceed 500 gross tonnage.

11. The draught measures the vertical distance from the bottom of a vessel's keel to the water's surface, indicating how deeply the ship is situated in the water. Although the draught typically reflects a vessel's cargo load (Bai and Li 2022; Li et al. 2022), this measurement can be less informative for containerships since loading and unloading operations often occur simultaneously.

2.2. A Density-Based Spatial Clustering Algorithm

In order to accurately quantify port congestion, we follow the maritime literature by estimating the likelihood that a vessel will first moor in an anchorage area within the port before docking at a berth (Talley and Ng 2016; Karimi-Mamaghan et al. 2020; Bai et al. 2023).[12] Such an estimation requires the precise identification of berth and anchorage areas, a task for which practitioners before us have largely relied on navigational charts for individual ports, making it both labor-intensive and challenging to generalize to global ports. Hence, we automate the process by developing an iterative, multi-attribute, density-based spatial clustering algorithm that is not only accurate in identifying different port areas but also applicable to ports worldwide.

This algorithm identifies different port areas by focusing on the density of ships' mooring points recorded in the AIS data, which includes all historical visits of containerships to each port, with each visit containing numerous AIS data points. Our algorithm operates in two layers of clustering. The first layer identifies high-density areas, which are considered potential berth and anchorage areas. The second layer refines these areas by considering additional domain knowledge, such as the heading of ships during mooring, since vessels are observed to dock at berths in an orderly and close fashion, while they moor in the anchorage areas more randomly (Figure 1).

Our algorithm is specifically designed to address two primary challenges inherent in the identification of berth and anchorage areas that existing clustering algorithms struggle to handle. The primary challenge is the variability in the density of ships' mooring points *across* ports with large differences in trade volume handled, frequency of vessel visits, and geographical morphology and boundaries. This variability necessitates an adaptive approach to parameter setting for different ports. Our algorithm is designed to automatically iterate and refine its clustering parameters for each individual port, thus facilitating the handling of varied and complex port environments. This iterative process not only streamlines the algorithm but also enhances its generalizability. Another challenge is to accurately distin-

12. An anchorage is a location within a port where ships can lower anchors, while a berth is a designated spot within a port where vessels moor to load and unload cargo. If port congestion were not a concern, a ship would dock at a berth immediately upon its arrival in the port to begin loading or unloading cargo.

(a) Headings at a Berth **(b)** Headings at an Anchorage

Figure 1: Information on Headings

Notes. In both figures, a tip represents the bow of a ship. In (a), the headings are either in the same direction or exactly opposite. As a result, two clusters can be formed with exact opposite headings. In (b), the headings are random, with some of them appearing in a ring shape.

guish between berth and anchorage areas *within* ports, as they both have a high density of ships' mooring points. Our algorithm overcomes this by leveraging both the spatial (i.e., geographical coordinates) and non-spatial attributes (i.e., headings) in its two layers of clustering. This innovative approach, based on our domain knowledge, significantly increases the granularity and accuracy of our analysis.[13,14]

To illustrate our algorithm, Figures 2a to 2d show the berth (red, yellow, blue, purple, pink, cyan, and orange markers) and anchorage (markers of other colors) areas in the following major container ports: Singapore (Panel a), Ningbo-Zhoushan in China (Panel b), Rotterdam in the Netherlands (Panel c), and Los Angeles and Long Beach in the U.S.

13. The identification of berth and anchorage areas in global ports lays the foundation for a series of granular measures of port performance, such as port handling efficiency and waiting time. Furthermore, while our algorithm is tailored to identify berth and anchorage areas, its core mechanism – transforming domain knowledge into non-spatial attributes and using them as additional metrics between data points in an iterative clustering process – has broader applications, as it provides a versatile framework for classifying clusters of varied densities with specific labels in other contexts as well (e.g., identification of disease hotspots, urban planning).

14. Appendix A and the companion paper (Bai et al. 2023) provide details on our clustering algorithm, including pseudo-codes and a case study involving the Port of Ningbo-Zhoushan in China, which illustrates the effectiveness of our methodology in identifying berth and anchorage areas in ports with different morphologies compared to alternative methods.

(Panel d). Our algorithm accurately captures the berth and anchorage areas in each port, despite the large spectrum of geographical and operational port conditions. By applying our algorithm to the real-time AIS satellite data, we construct a comprehensive, high-frequency measure of global port congestion, as we discuss in the next section.

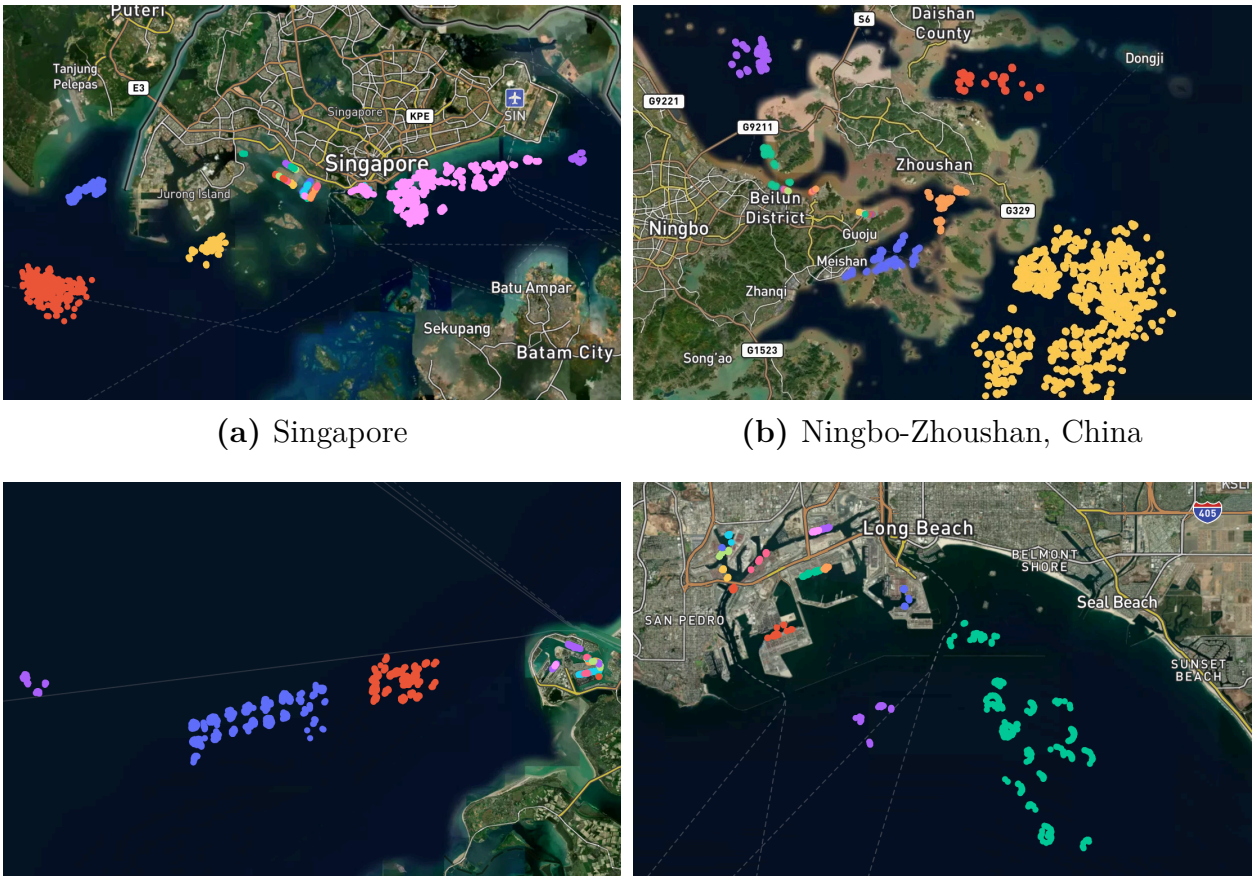

(a) Singapore

(b) Ningbo-Zhoushan, China

(c) Rotterdam, Netherlands

(d) Los Angeles and Long Beach, U.S.

Figure 2: Identification of Anchorage and Berth Areas of a Port Using Machine Learning

Notes. The figures plot the identification results of the berth and anchorage areas for each of the following representative container ports worldwide: the Port of Singapore, Port of Ningbo-Zhoushan in China, Port of Rotterdam in the Netherlands, and the Ports of Los Angeles and Long Beach in the U.S. We use different colors to depict various clusters identified by our machine learning clustering algorithm (IMA-DBSCAN; see Appendix A for details); specifically, we use red, yellow, blue, purple, pink, cyan, and orange to represent clusters identified as anchorages, and the other colors to represent clusters identified as berths. The underlying sample for each figure takes the first 50,000 AIS observations of containerships entering each port since 1 January 2020.

2.3. Port Congestion and the Index of Average Congestion Rate

Port congestion arises when ships cannot immediately load and/or unload cargo upon arrival at ports, resulting in the vessels having to wait in an anchorage area for an opportunity to dock at a berth. We define the Average Congestion Rate (ACR) for a port as the ratio of containerships that moor at an anchorage before docking at a berth to the total number of ship visits at the port.[15] We calculate the monthly ACR for the top 50 container ports worldwide during the sample period.

We derive a time series measure of global supply chain disruptions by computing the weighted average of the ACR series for the top 50 container ports worldwide, with the weights determined by the number of ship visits and thus reflecting the distinctive roles of different ports within the global supply chain.[16] Figure 3 displays our ACR index. Prior to 2019, the index remained stable around the sample median (17.8%), and it declined to 16% from early 2019 to mid-2020. Subsequently, the index consistently rose to reach its peak at 25% in June 2021, indicative of the significant disruptions to the supply chain caused by the Covid-19 pandemic.

Figure 4 presents the monthly ACR series for the top ten container ports worldwide that are located in China, Singapore, South Korea, and the Netherlands, as well as the Ports of Los Angeles and Long Beach in the U.S., for the period from January 2017 to July 2022 when the AIS data are available. These ports are pivotal in the global supply chain, as they jointly account for more than 30% of the total volume of containerized seaborne trade in the world. Following the onset of the Covid-19 pandemic in March 2020, the ACR indices for several ports remained largely stable (e.g., Port of Rotterdam, Netherlands), while only a few decreased (e.g., Port of Shanghai, China). However, as the pandemic progressed from October 2020 onwards, congestion increased in the majority of ports, as evinced by the increase in chromatic intensity in the figure.[17] This implies that containerships

15. A ship visit, which is also known as a port call, refers to the arrival of a ship at a specific port where it docks to load or unload cargo.

16. The weighting considers the differential impact on global supply chain disruptions resulting from changes in the ACR at different ports. For instance, a slight increase in the ACR at the Port of Hong Kong in China would likely have triggered a more pronounced global supply chain disruption than a significant increase at the Port of Manila in the Philippines.

17. By our calculation, in late-2020, over 80% of inbound ships at the Port of Los Angeles in the U.S.

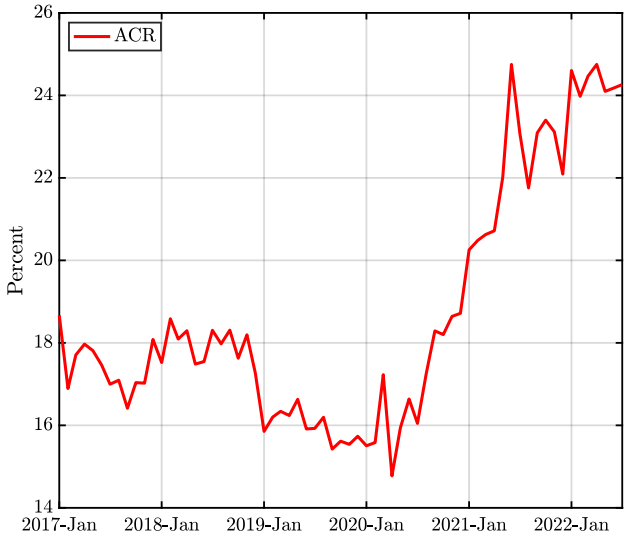

Figure 3: ACR Index of Global Supply Chain Disruptions

Notes. The ACR index of global supply chain disruptions is derived by taking a weighted average of the ACR series for the top 50 global container ports. The number of ship visits serves as the weight for each port. The index is presented in percentage terms and has been seasonally adjusted. For the complete ranking of container ports, please refer to https://www.worldshipping.org/top-50-ports (Accessed June 15, 2022).

encountered significant delays in the loading and/or unloading operations since October 2020, thus disrupting the international freight collection and distribution of tradable goods.

Figure 5a plots the ACR index against the Harper Peterson Charter Rates Index (HARPEX). The HARPEX is a widely-used composite indicator of container shipping rate changes in the time charter market for eight different classes of containerships (Attinasi et al. 2021; Benigno et al. 2022; Finck and Tillmann 2022), and is also used in the construction of the GSCPI as a measure of cross-border transportation costs. Not surprisingly, we observe that the two indices have moved similarly since the onset of the pandemic. As delays in container processing became more prevalent and port congestion escalated, ships were tied up at ports. This led to a significant shortage in the supply of shipping services, resulting in surging shipping prices. However, it is also noteworthy that the two series did not align closely with each other before the onset of the pandemic and in its aftermath. This observation is intuitive, as the shipping price is an equilibrium object, and its fluctuations are influenced by both

were unable to dock at a berth immediately upon arrival. This observation aligns with official statistics. According to figures released by the Pacific Merchant Shipping Association, the percentage of containerships at Los Angeles waiting five or more days for unloading surged from 10% in August to 26% in December 2020. Additionally, the Marine Exchange of Southern California reported that the number of vessels anchored in Los Angeles waters also rose from fewer than 20 in August to more than 35 in December 2020.

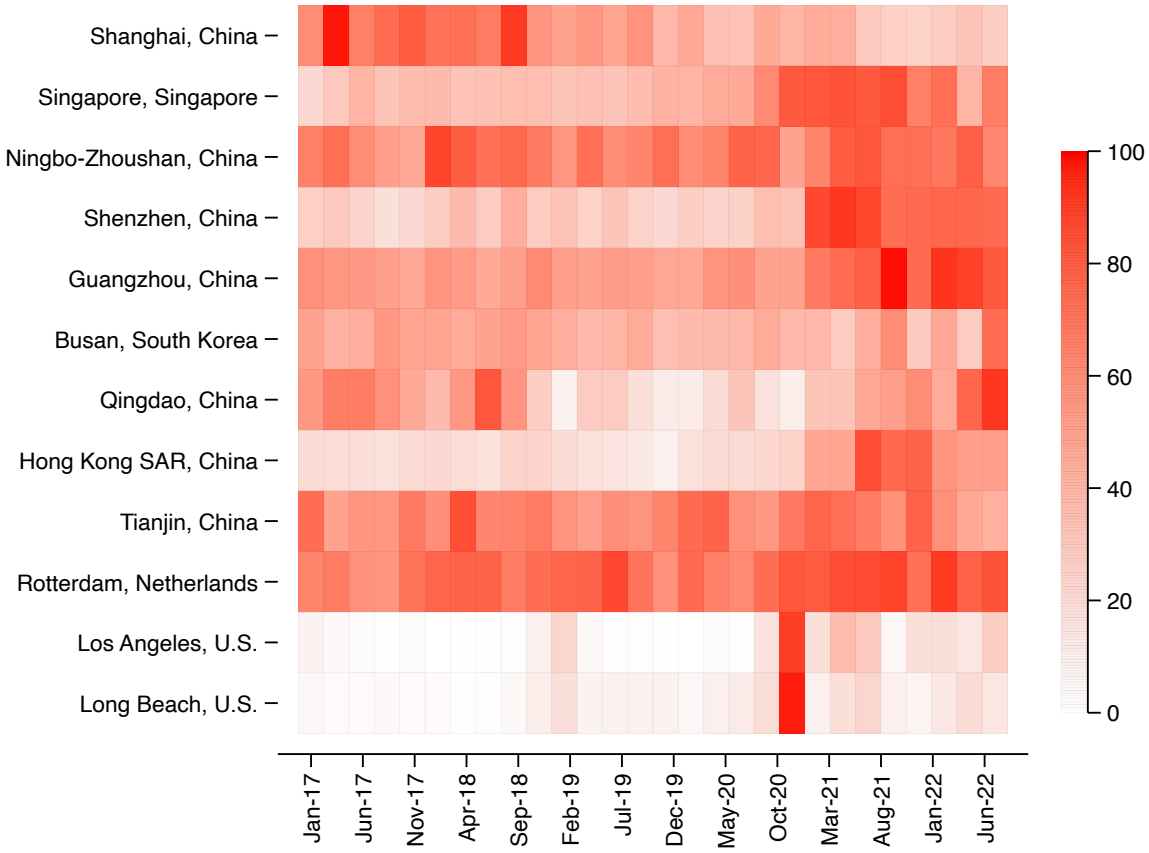

Figure 4: ACR for the Major Container Ports Worldwide

Notes. The heatmap presents the monthly ACR series for the top ten global container ports and the Ports of Los Angeles and Long Beach in the U.S., covering the period from January 2017 to July 2022. These ports jointly represent more than 30% of the total volume of containerized seaborne trade in the world. The ACR series for each port is normalized, expressed as a percentage of its peak value observed within the sample period. Cells in a darker shade indicate greater congestion for the corresponding port during the designated month. The ACR of a port is defined as the proportion of containerships that moor at an anchorage area before docking at a berth, relative to the total number of ship visits at the port.

demand and supply-side factors.

Lastly, we compare our ACR index with the GSCPI to highlight the differences in the measurement of supply chain disruptions. The GSCPI uses information on cross-border transportation costs and sub-components of the country-specific manufacturing PMI to infer supply chain disruptions. As discussed in the introduction, the GSPI is potentially problematic since it relies on: (i) transportation costs reflecting the mismatch between the supply and demand for goods, while prices become disjoint from output during supply chain disruptions, and (ii) information gathered from purchasing managers that may reflect subjective

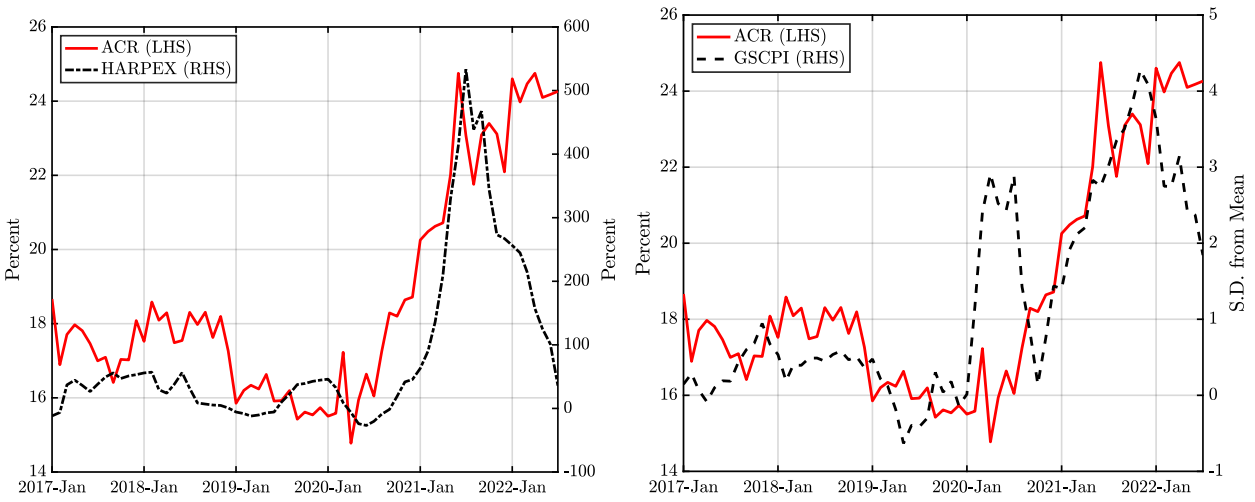

(a) ACR vs. HARPEX **(b)** ACR vs. GSCPI

Figure 5: Comparison Between the ACR and Other Measures of Supply Chain Disruptions

Notes. Figure 5a plots the ACR (red solid line) against the HARPEX (black dotted line), while Figure 5b plots the ACR against the GSCPI (black dashed line) during the sample period from January 2017 to July 2022. The ACR is computed using the AIS data of containerships and the IMA-DBSCAN algorithm developed in Appendix A. The original series of HARPEX is published by Harper Peterson and retrieved from the Refinitiv data platform. Following Attinasi et al. (2021) and Benigno et al. (2022), we transform the original series by computing the year-on-year percentage changes. The GSCPI is retrieved from the New York Fed's website (Source: https://www.newyorkfed.org/research/policy/gscpi#/overview (Accessed August 10, 2022)). Both the ACR and HARPEX are measured in percent, while the GSCPI is measured in standard deviations from the mean. All the series are seasonally adjusted.

views rather than realized disturbances to the supply chain.[18]

In contrast, our ACR index uses maritime satellite data to estimate the congestion at seaports around the globe. Our approach avoids the main shortcomings of the alternative measures. Since containerships operates on fixed itineraries, as extensively documented in Stopford (2008), Song and Dong (2012), Wang, Meng, and Jia (2019), Brancaccio, Kalouptsidi, and Papageorgiou (2020), and Brancaccio et al. (2023),[19] our index is instead independent from the mismatch between the supply and demand of goods, as evinced by Table 1

18. Appendix B elaborates on the shortcomings of using the shipping cost, sub-components of the manufacturing PMI, and other indices of supply chain disruptions in the causality assessment. In particular, we compare the U.S. supply disruptions index (SDI) by Smirnyagin and Tsyvinski (2022) to the ACR and GSCPI indices. We find that the SDI and GSCPI align well, and an alternative estimation with the SDI included as a measure of supply chain disruptions yields quantitatively similar results to those obtained using the GSCPI.

19. Routes are rarely altered since diversions in shipping routes usually incur a large transition cost. Changes in routes severely affect the stability of shipping operations and the loyalty of customers (Wang, Meng, and Jia 2019).

that shows that our ACR series is statistically uncorrelated with the number of ship visits at each port (column, 1), whereas the HARPEX index that captures the shipping price is significantly correlated with the number of ship visits (column 2).[20] Furthermore, any infrequent adjustments in shipping capacity across routes, and the resulting changes in congestion at different ports, are canceled out when we aggregate the indices of port congestion to construct the ACR index, hence enhancing the exogeneity of our ACR index to imbalances between supply and demand in measuring global supply chain disruptions. Finally, we avoid the issue of biased managerial perceptions by tracking the congestion of ports in real time. Overall, we believe our index provides a powerful measure of supply chain disruptions.

Table 1: ACR, HARPEX, and Ship Visits

	(1) ACR	(2) HARPEX
# Ship Visits	-0.0018	-0.0286^{***}
	(0.00183)	(0.00614)
Port FE	Yes	N/A
Time FE	Yes	N/A
Obs	3,256	67
R^2	0.0355	0.2499

Notes. Column (1) displays the estimated coefficient when we regress the port-specific ACR on the number of ship visits to each port, controlling for both port and time fixed effects (FE). Column (2) presents the estimated coefficient when we regress the HARPEX on the total number of ship visits across the top 50 container ports worldwide. Both the ACR and the number of ship visits are computed using the AIS data of containerships and the IMA-DBSCAN algorithm developed in Appendix A. Meanwhile, the HARPEX is constructed by taking the year-on-year percentage changes of the original series. *** indicates $p < 0.01$.

Figure 5b displays the ACR and GSCPI indices over the sample period from January 2017 to July 2022. Before 2020, the dynamics of the two indices were similar, but the GSCPI substantially increased at the onset of the Covid-19 pandemic in early 2020 and remained elevated in the first half of the year. From mid-2020 onwards, the two series

20. It should be noted that the correlation between the HARPEX and the number of ship visits is estimated at the global level, as there is no disaggregated data on shipping prices at the port level. We also check the robustness of our baseline results in Section 4.1 by applying a fitted ACR in our estimation after regressing the port-specific ACR on the Oxford Stringency (OS) index (Mathieu et al. 2020) and port fixed effects; as shown in Appendix F.1, such results are quantitatively similar to those obtained using the ACR directly.

increased similarly until January 2022. di Giovanni et al. (2022) attribute the jump in the GSCPI in early 2020 to the onset of the Chinese lockdown, and the sudden fall in the second half of 2020 to the partial reopening of China and Europe. Our index of port congestion indicates that the initial lockdown in China did not lead to congestion of a magnitude that would generate a global supply chain disruption, and equally, the reopening of China and Europe did not substantially ease the congestion in ports. Thus, the changes in the GSCPI are likely driven by sudden changes in demand and management's misperception of supply chain issues as recorded by the PMI surveys. We also observe that the two series diverged from each other again in early 2022, as the ACR remained elevated while the GSCPI had already started plummeting. We argue that the high ACR could be largely attributed to the stringent containment measures that were still in place in China during the first half of 2022, continuously exerting pressure on the global supply chain.

3. A Model of Congestion and Spare Capacity

In this section, we develop a model featuring imbalances in the supply and demand for goods that result in spare capacity. The model is based on search and matching frictions in the international product market similar to the framework in Michaillat and Saez (2015, 2022) and Ghassibe and Zanetti (2022), and incorporates transportation costs that generate the separation of unprofitable matches; both features render prices no longer allocative and unable to clear the goods market.[21] Our model illustrates the central role of spare capacity in uniquely identifying supply chain disruptions (Section 4) and links these disruptions to the efficacy of monetary policy in controlling inflation (Section 5).

The economy is composed of maximizing firms and households. Firms can be either exporters or importers. Exporters produce goods using a fixed amount of labor supplied by households and incur transportation costs to sell the goods. Importers buy these goods from exporters and sell them to the households.[22] Households purchase goods from importers

21. Appendix C provides a discussion on the evidence of matching frictions in the international product market and the separation of commercial trade linked to transportation costs.

22. Our approach is similar to the standard assumption that firms require internationally imported intermediate goods for the production of final goods. See, for instance, Costinot, Vogel, and Wang (2013), Kasahara and Lapham (2013), and Ramondo and Rodríguez-Clare (2013) and the references therein.

using money that is the numeraire in the economy.

In the rest of this section, we begin by studying the separate problems of exporting and importing firms that face transportation and visiting costs, respectively, to derive the aggregate supply. We then study the problem of households, who determine the aggregate demand. Subsequently, we show that in equilibrium, search frictions and transportation costs determine the spare capacity in the economy whose adjustment is critical to the study of disruptions to the supply chain.

3.1. Firms

Firms comprise exporters and importers. Exporters produce goods with a capacity determined by the inelastic labor inputs $l > 0$. Exporters sell goods to the importers in a frictional goods market that prevents the sale of the full capacity. Each unmatched (identified by the subscript U) importer makes visits i_U to unmatched exporters at a unitary cost $\rho > 0$ and upon a successful trade, resells the purchased goods to households at the set price p.

Matching process. In each period, a constant-returns-to-scale matching function encapsulates the search frictions in the product market, determining the number of meetings ($\mathscr{m}$) between unmatched exporters and importers according to:

$$\mathscr{m} = (x_U^{-\xi} + i_U^{-\xi})^{-\frac{1}{\xi}}, \tag{1}$$

where x_U and i_U are the number of unmatched exporters and importers, respectively, and the parameter ξ is the elasticity of substitution between the inputs of the matching function. We assume $\xi > 0$, such that $\mathscr{m} \leq \min\{x_U, i_U\}$.

We define the product market tightness θ as the ratio between the number of visits by the unmatched importers and the number of unmatched exporters, such that $\theta \equiv i_U/x_U$. Given the law of large numbers, product market tightness is taken as given by single exporters and importers, and it determines the probabilities that exporters and importers meet each others given the constant returns to scale in the matching function. Specifically, the probability for

an exporter to meet an importer is:

$$f(\theta) = \frac{m}{x_U} = (1 + \theta^{-\xi})^{-\frac{1}{\xi}}, \tag{2}$$

and the probability for an importer to meet an exporter with probability:

$$q(\theta) = \frac{m}{i_U} = (1 + \theta^{\xi})^{-\frac{1}{\xi}}. \tag{3}$$

The function $f(\theta)$ is smooth and strictly increasing in the domain $[0, +\infty)$, with $f(0) = 0$, $\lim_{\theta \to +\infty} f(\theta) = 1$, and $f'(\theta) > 0$, whereas the function $q(\theta)$ is smooth and strictly decreasing in the same domain $[0, +\infty)$, with $q(0) = 1$, $\lim_{\theta \to +\infty} q(\theta) = 0$, and $q'(\theta) < 0$. Two properties that will be useful later are that $f(\theta)/q(\theta) = \theta$ and $df(\theta)/d\theta = q(\theta)^{1+\xi}$.

Transportation cost. Exporters pay an idiosyncratic transportation cost to export goods.[23] In each period, exporters draw a transportation cost z from the log-normal distribution $G(z)$ with a scaling parameter γ and the standard deviation σ, i.e., $G(z) \equiv \Phi\big[(\log z - \gamma)/\sigma\big]$, where $\Phi(\cdot)$ is the standard normal cumulative density function.[24] As we discuss later, there exists a reservation level of transportation cost $\bar{z}$, above which matches are unprofitable and therefore severed. Consequently, the matches with a draw of transportation cost higher than the reservation level ($z > \bar{z}$) are severed, whereas they continue otherwise ($z \leq \bar{z}$).

Recursive value functions. At the beginning of each period, the matched exporters sell the produced goods to importers and pay the transportation costs, and the matched importers sell their imported goods to households and pay the import prices. The exporters and importers that are unmatched search to form a match with each other. At the beginning of the next period, each exporter draws a new transportation cost and they continue in the match if the new cost is sufficiently low for the match to remain profitable while the unprofitable matches are severed (we describe the match separation decision later in the

23. Our results continue hold if the transportation cost is borne by importers instead. This is because the match separation condition (12) is invariant to such a modeling choice.

24. We could also apply a more general setup that each exporter maintains its previous draw of transportation cost with probability $1 - \varphi$, and with probability φ, the exporter draws a new transportation cost from $G(z)$. This setup is often found in the traditional labor search and matching theory that studies the labor market outcomes following a rise in economic turbulence (den Haan, Ramey, and Haefke 2005; Fujita 2018). Despite more tedious algebra, our main results still hold.

section).

Four recursive value functions describe the values for the different status of exporters and importers. The value for a matched (identified by the subscript M) exporter, $X_M(z)$, is equal to:

$$X_M(z) = r(z) - z + \beta \mathbb{E}_{z'}\big[\max\big(X_M(z'), X_U\big)\big], \tag{4}$$

where $r(z)$ is the price of the imported goods that is endogenously determined, z is the cost of transportation, β for the discount factor, and z' for the draw of transportation cost at the beginning of the next period. Equation (4) shows that the present value of being a matched exporter is the profit margin $r(z) - z$, plus the continuation value which depends on whether the exporter endogenously separates from the match. Such a decision is determined by z', and hence the max operator characterizes the optimal continuation/separation decision.

The value for an unmatched exporter, X_U, is:

$$X_U = \beta f(\theta) \mathbb{E}_{z'}\big[\max\big(X_M(z'), X_U\big)\big] + \beta\big(1 - f(\theta)\big) X_U. \tag{5}$$

With probability $f(\theta)$, the unmatched exporter meets an importer and then decides whether to endogenously separate if the given draw of transportation cost makes the match unprofitable. With probability $1 - f(\theta)$, the exporter forgoes a successful match with an importer and remains unmatched in the next period.

The value of matched importer, $I_M(z)$, is:

$$I_M(z) = p - r(z) + \beta \mathbb{E}_{z'}\big[\max\big(I_M(z'), I_U\big)\big]. \tag{6}$$

The importer earns the price p by selling the imported goods to the households and it pays the import price $r(z)$ to the exporter. The max operator characterizes the optimal continuation/separation decision conditional on the draw of transportation cost at the beginning of the next period. If the drawn transportation cost makes the match unprofitable, the importer endogenously separates from the match and hence starts the next period with a value equal to:

$$I_U = -\rho + \beta q(\theta) \mathbb{E}_{z'}\big[\max\big(I_M(z'), I_U\big)\big] + \beta\big(1 - q(\theta)\big) I_U, \tag{7}$$

where ρ is a fixed cost to pay per visit. We assume free entry into the international product market that drives the value for an unmatched importer to zero in equilibrium, i.e., $I_U = 0$.

Nash bargaining. Nash bargaining splits the total surplus from the matching between the exporter and the importer. The total surplus from matching is equal to:

$$S(z) = X_M(z) - X_U + I_M(z) - I_U. \tag{8}$$

The exporter earns a constant share η of the total surplus, and the importer earns the remaining share $1 - \eta$, which in equilibrium yields:

$$\eta\big(I_M(z) - I_U\big) = (1 - \eta)\big(X_M(z) - X_U\big). \tag{9}$$

Given the equilibrium rule (9), the value functions (4), (5), (6), and the free entry condition $I_U = 0$, the import price that splits the surplus is equal to:

$$r(z) = \eta(p + \rho\theta) + (1 - \eta)z. \tag{10}$$

Equation (10) shows that the bargaining power η is central to the determination of the import price. When the exporters have significant bargaining power ($\eta \to 1$), they earn the total surplus accrued to the importers from selling the goods to the household ($p + \rho\theta$). On the other hand, when the bargaining power of the exporter is low ($\eta \to 0$), the import price is close to the cost of transportation (z). Intermediate values for the bargaining parameter proportionally split the total surplus between exporters and importers, with the share of surplus determined by the bargaining parameter. Important to our analysis, congestion in the matching process, captured by tightness in the product market, worsens the bargaining position of importers by lowering their matching probability, thus increasing the price they are willing to pay to buy goods from exporters.

Match separation. Since the total value for a matched exporter and a matched importer, i.e., $X_M(z) + I_M(z)$, strictly decreases with the cost of transportation z, there exists a cut-off transportation cost $\bar{z}$, above which the costs are too high and the matches become unprofitable and are severed. This cut-off makes the total surplus in Equation (8) equal to

zero, as follows:

$$S(\bar{z}) = 0. \tag{11}$$

By substituting the value functions (4), (5), (6), and the free entry condition $I_U = 0$ into Equation (11), we can express the match separation condition as a function of price p, reservation transportation cost $\bar{z}$, and product market tightness θ, defined for all $p \in (0, +\infty)$, $\bar{z} \in (0, +\infty)$, and $\theta \in [0, +\infty)$, satisfying:

$$\mathbb{F}(p, \bar{z}, \theta) = p - \bar{z} + \big(1 - \eta f(\theta)\big)\beta \mathbb{E}_{z'} S(z') = 0, \tag{12}$$

where the expected surplus is defined by $\mathbb{E}_{z'} S(z') = \int_0^{\bar{z}} S(z') dG(z')$.

Match creation. Using the value function for an unmatched importer (7) and the free entry condition $I_U = 0$, we define the match creation condition as a function of reservation transportation cost $\bar{z}$ and product market tightness θ, defined for all $\bar{z} \in (0, +\infty)$ and $\theta \in [0, +\infty)$, satisfying:

$$\mathbb{H}(\bar{z}, \theta) = \frac{\rho}{q(\theta)} - (1 - \eta)\beta \mathbb{E}_{z'} S(z') = 0. \tag{13}$$

Aggregate supply. The aggregate supply in the economy results from the steady-state equilibrium in the international product market, which is defined as:

Definition 1. *The steady-state equilibrium in the international product market consists of a price $p \in (0, +\infty)$, a reservation transportation cost $\bar{z} \in (0, +\infty)$, and a product market tightness $\theta \in [0, +\infty)$ such that the conditions for match separation (12) and match creation (13) simultaneously hold:*

$$\mathbb{F}(\bar{z}, \theta, p) = \mathbb{H}(\bar{z}, \theta) = 0.$$

Definition 1 indicates that the equilibrium product market tightness is a function of price and reservation transportation cost. This relationship is determined by the conditions of match separation and creation, as stated in Equations (12) and (13), respectively.

Proposition 1. *In equilibrium, the price p, reservation transportation cost $\bar{z}$, and product market tightness θ satisfy the relationship:*

$$\theta(p, \bar{z}) = \frac{1 - \eta}{\eta \rho}\big(p - \bar{z} + \beta \int_0^{\bar{z}} G(z') dz'\big), \tag{14}$$

where $G(.)$ is the log-normal cumulative density function. Hence, the product market tightness θ has the following properties:

1. *$\theta(p^{min}, \bar{z}) = 0$ and $\lim_{p\to+\infty} \theta(p, \bar{z}) = +\infty$, where p^{min} satisfies:*

$$p^{min} - \bar{z} + \beta \int_0^{\bar{z}} G(z')dz' = 0;$$

2. *$\theta(p, \bar{z})$ is strictly increasing on $[p^{min}, +\infty)$;*

3. *$\theta(p, \bar{z})$ is linear on $[p^{min}, +\infty)$;*

4. *$\lim_{\bar{z}\to 0^+} \theta(p, \bar{z}) = (1-\eta)p/(\eta\rho)$ and $\theta(p, \bar{z}^{max}) = 0$, where $\bar{z}^{max}$ satisfies:*

$$p - \bar{z}^{max} + \beta \int_0^{\bar{z}^{max}} G(z')dz' = 0;$$

5. *$\theta(p, \bar{z})$ is strictly decreasing on $(0, \bar{z}^{max}]$; and*

6. *$\theta(p, \bar{z})$ is convex on $(0, \bar{z}^{max}]$.*

Proof. See Appendix D.1. ■

Proposition 1 establishes that the product market tightness strictly increases with the price of goods and decreases with the reservation transportation cost. These properties are intuitive. When the total surplus rises due to a higher price, importers visit more exporters. Conversely, a higher reservation transportation cost reduces the total surplus shared between exporters and importers at the margin. This, in turn, dampens the incentives for importers to visit exporters, leading to a slack product market.[25]

Next, the aggregate supply comprises the quantity of goods traded by the importers and exporters that survive separation for a given productive capacity l. To determine the steady-state number of matched exporters, we consider the law of motion for the number of matched exporters at the beginning of the next period:

$$x'_M = G(\bar{z})x_M + f(\theta)G(\bar{z})x_U,$$

25. An increase in the reservation transportation cost increases the expected total surplus $\beta\mathbb{E}_{z'}S(z')$, since matches are less likely to be dismissed in the next period. However, such a positive effect is outweighed by the loss in the profit margin $p - \bar{z}$, resulting in a negative net effect on the total surplus.

and that for the number of unmatched exporters at the beginning of the next period:

$$x'_U = \big[1 - f(\theta) + f(\theta)\big(1 - G(\bar{z})\big)\big]x_U + \big(1 - G(\bar{z})\big)x_M.$$

By focusing on the steady-state equilibrium and normalizing the total number of matched and unmatched exporters to one, i.e., $x_M + x_U = 1$, we derive the equilibrium number of matched exporters x_M^{eqm} equal to:

$$x_M^{eqm}(\bar{z}, \theta) = \frac{f(\theta)G(\bar{z})}{1 - G(\bar{z}) + f(\theta)G(\bar{z})}.$$

The aggregate supply in the economy is equal to the quantity of goods supplied by matched exporters for a given productive capacity l:

$$c_s(\bar{z}, \theta) = x_M^{eqm}(\bar{z}, \theta) \cdot l = \frac{f(\theta)G(\bar{z})}{1 - G(\bar{z}) + f(\theta)G(\bar{z})} l. \tag{15}$$

By substituting the expressions for $f(\theta)$ and θ from Equations (2) and (14) into Equation (15), we express the aggregate supply in the economy as a function of price and reservation transportation cost, as stated in the next definition.

Definition 2. *The aggregate supply c_s, expressed as a function of price p and reservation transportation cost $\bar{z}$, is equal to:*

$$c_s(p, \bar{z}) = \frac{\Big\{1 + \Big[\frac{1-\eta}{\eta\rho}\big(p - \bar{z} + \beta \int_0^{\bar{z}} G(z')dz'\big)\Big]^{-\xi}\Big\}^{-\frac{1}{\xi}} G(\bar{z})}{1 - G(\bar{z}) + \Big\{1 + \Big[\frac{1-\eta}{\eta\rho}\big(p - \bar{z} + \beta \int_0^{\bar{z}} G(z')dz'\big)\Big]^{-\xi}\Big\}^{-\frac{1}{\xi}} G(\bar{z})} l, \tag{16}$$

for all $(p, \bar{z}) \in (0, +\infty) \times (0, +\infty)$ satisfying:

$$p - \bar{z} + \beta \int_0^{\bar{z}} G(z')dz' \geq 0. \tag{17}$$

Since the aggregate supply in (16) is determined by two endogenous variables, there exists infinite combinations of the price and reservation transportation cost that yield the same aggregate supply, as long as they satisfy the constraint (17).[26] We resolve the indeterminacy

26. The indeterminacy of the equilibrium is standard in search models. For instance, it arises in Michaillat and Saez (2015), where either price or tightness must be assumed fixed to select an equilibrium. Our model also does not allow for an equilibrium in which both the price and reservation transportation cost can be determined simultaneously. The reason is similar: each importer-household pair decides the price in a situation of bilateral monopoly. Since the solution to the bilateral monopoly problem is indeterminate (Howitt and McAfee 1987; Hall 2005), it cannot be used to impose a condition on the price.

by selecting the equilibrium where the reservation transportation cost is to remain fixed at an arbitrary level τ, and prices move to satisfy the aggregate supply condition. By considering the equilibrium with freely adjusting prices, we can study the responses of prices to the distinct disturbances to demand, supply, and the supply chain, and use the comovements across variables to formulate unique restrictions to estimate the causal effect of supply chain shocks in our SVAR model developed in Section 4.

Our next Definition 2′ recasts the original Definition 2 of aggregate supply as a function of the price p for an arbitrary transportation cost τ.

Definition 2′. *For an arbitrary reservation transportation cost $\tau \in (0, +\infty)$, the flexible-price aggregate supply c_s^{flex} is the function of price p defined by:*

$$c_s^{flex}(p) = \frac{\left\{1 + \left[\frac{1-\eta}{\eta\rho}\left(p - \tau + \beta \int_0^\tau G(z')dz'\right)\right]^{-\xi}\right\}^{-\frac{1}{\xi}} G(\tau)}{1 - G(\tau) + \left\{1 + \left[\frac{1-\eta}{\eta\rho}\left(p - \tau + \beta \int_0^\tau G(z')dz'\right)\right]^{-\xi}\right\}^{-\frac{1}{\xi}} G(\tau)} l, \tag{18}$$

for all $p \in [p^{min}, +\infty)$, where p^{min} satisfies:

$$p^{min} - \tau + \beta \int_0^\tau G(z')dz' = 0.$$

The next proposition outlines the properties of the aggregate supply when the price moves to satisfy the aggregate supply condition.[27]

Proposition 2. *The flexible-price aggregate supply c_s^{flex} has the following properties:*

1. *$c_s^{flex}(p^{min}) = 0$ and $\lim_{p\to+\infty} c_s^{flex}(p) = G(\tau)l$;*
2. *$c_s^{flex}(p)$ is strictly increasing in p on $[p^{min}, +\infty)$; and*
3. *$c_s^{flex}(p)$ is concave on $[p^{min}, +\infty)$.*

Proof. See Appendix D.2. ■

The aggregate supply $c_s^{flex}(p)$ represents the quantity of goods traded that satisfy (18) for a given transportation cost τ. Therefore, the dynamics of the aggregate supply is uniquely

27. Appendix E discusses the alternative pricing mechanism in which the price of goods is fixed while the reservation transportation cost can vary. In addition to the derivation of the analytical properties, we apply numerical methods to approximate such a fixed-price aggregate supply and illustrate the behavior over different values of the reservation transportation cost.

determined by the interaction between the price and tightness in the product market. A higher price first leads to a higher total surplus by increasing the value of the matched importer. This, in turn, increases the incentives for importers to visit exporters, resulting in a higher product market tightness and a greater probability for an exporter to match with an importer. More matches are created, leading to an increase in aggregate supply. Thus, while transportation costs and matching frictions decrease the aggregate supply, and the economy entails spare capacity, the model retains the standard positive relationship between the price and the aggregate supply.

Figure 6 graphically shows the equilibrium of the aggregate supply in the quantity-price (Q,p) space. For a given capacity of the economy l (yellow line), the transportation costs reduce the production capacity to $G(\tau)l$ (green line), and the search frictions further reduce the supply to the produced level $c_s^{flex}(p)$ (blue line) that standardly increases with the price, as discussed in the previous paragraph. Spare capacity, represented by the difference between the capacity of the economy and the actual production (i.e., $l - c_s^{flex}(p)$), results from the transportation and the search and matching costs. It is worth noting that in our model the spare capacity is equivalent to unemployment since it represents the difference the supply of labor linked to the capacity of the economy and the demand of labor linked with the actual production.

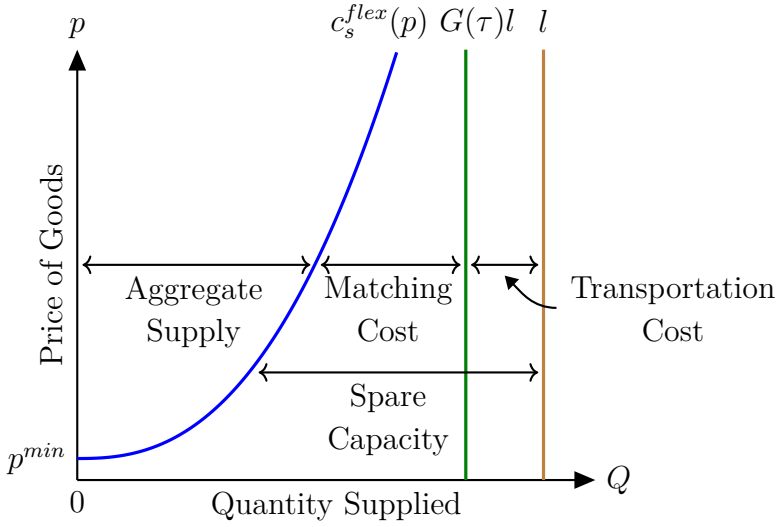

Figure 6: Supply Side of the Economy when the Price of Goods is Flexible

3.2. Households

The representative household derives utility from consuming goods and holding real money balances.[28] The household's utility is given by:

$$u\big(c, \frac{m}{p}\big) = \frac{\chi}{1+\chi} c^{\frac{\epsilon-1}{\epsilon}} + \frac{1}{1+\chi}\big(\frac{m}{p}\big)^{\frac{\epsilon-1}{\epsilon}},$$

where c denotes consumption, m is the nominal money balance, p is the price, the parameter $\chi > 0$ represents the taste for consumption relative to holding money, and the parameter $\epsilon > 1$ is the elasticity of substitution between consumption and real money balances.

Taking the price as given, the representative household chooses consumption and nominal money balances to maximize utility, subject to the budget constraint. The household, with an endowment $\mu > 0$ of nominal money, purchases c goods at price p from importers and holds m units of nominal money balances. This leads to the following budget constraint:

$$pc + m \leq \mu.$$

Solving the utility-maximization problem yields the optimal condition for the household:

$$\frac{\chi}{1+\chi} c^{-\frac{1}{\epsilon}} = \frac{1}{1+\chi}\big(\frac{m}{p}\big)^{-\frac{1}{\epsilon}}, \tag{19}$$

implying that she is indifferent between consumption and holding money at the margin.

Aggregate Demand. The aggregate demand in the economy is equal to the level of consumption that maximizes utility at a given price when all resources are consumed:

Definition 3. *The aggregate demand c_d for a given price $p \in (0, +\infty)$ equals:*

$$c_d(p) = \frac{\chi^\epsilon}{1+\chi^\epsilon}\frac{\mu}{p}. \tag{20}$$

Proposition 3. *$c_d(p)$ is strictly decreasing and convex on $(0, +\infty)$.*

Proof. Direct proof from Equation (20). ■

28. We borrow the money in the utility function directly from Michaillat and Saez (2015) to ensure that aggregate demand plays a meaningful role in driving the macro aggregates. More importantly, the presence of money is necessary for studying the state-dependent effects of a contractionary monetary policy shock, as outlined in Section 5.

Figure 7 in the next section shows the aggregate demand, which is downward sloping in the (c, p) plane. Since a higher price leads to lower real money balances, the households' indifference between consumption and holding money implies that they would behave optimally and desire lower consumption when the price is higher. Hence, the aggregate demand in the economy decreases with the price.

3.3. Flexible-Price Equilibrium

With the flexible-price aggregate supply and aggregate demand sketched out, we define a flexible-price equilibrium as an equilibrium in which the reservation transportation cost is an external parameter:

Definition 4. *A flexible-price equilibrium parameterized by $\tau > 0$ consists of a price p and a reservation transportation cost $\bar{z}$ such that the flexible-price aggregate supply equals the aggregate demand:*

$$c_s^{flex}(p) = c_d(p), \tag{21}$$

while the reservation transportation cost is given by the parameter τ, i.e., $\bar{z} = \tau$.

Proposition 4. *For any $\tau > 0$, there exists a unique flexible-price equilibrium parameterized by τ that features positive price and consumption.*

Proof. See Appendix D.3. ■

Figure 7 depicts the flexible-price aggregate supply, the aggregate demand, and the corresponding flexible-price equilibrium. The equilibrium price is at the intersection of the flexible-price aggregate supply and aggregate demand in the (c, p) plane. Both the theoretical upper bound of the flexible-price aggregate supply if the matching frictions were absent and productive capacity are also plotted in the figure for comparison.

3.4. Comparative Statics

We use comparative statics to derive the responses of the macro aggregates to adverse shocks to demand, labor supply, and supply chain, respectively. The responses will provide unique

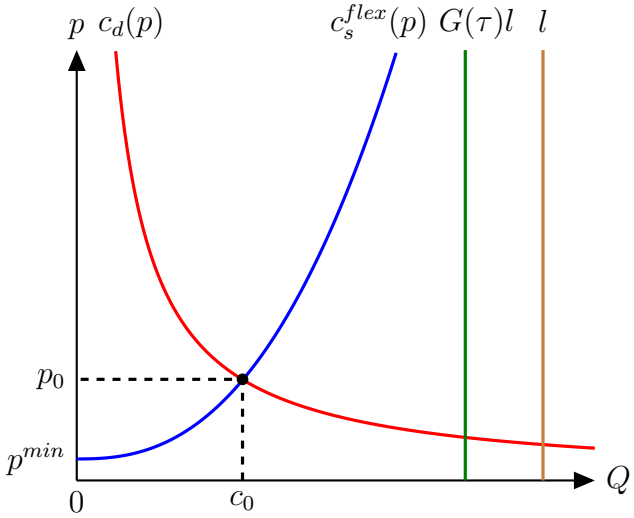

Figure 7: Flexible-Price Aggregate Supply, Aggregate Demand, and Flexible-Price Equilibrium

identifying restrictions for studying the causal effects of supply chain disturbances in the empirical SVAR model in the next section. In our model, an adverse shock to aggregate demand is either a decrease in the money supply, μ, or in the preference for consuming goods, χ. An adverse shock to labor supply is a negative disturbance to the labor supply (or equivalently, productive capacity), l. An adverse shock to supply chain is a comprehensive increase in the distribution of transportation costs, encapsulated by a rise in γ, the scale parameter of the log-normal distribution of transportation costs. *Ceteris paribus*, an increase in γ implies a higher average transportation cost, i.e., $exp(\gamma + \sigma^2/2)$. Proposition 5 summarizes the responses of the macro aggregates to these distinct shocks.[29]

Proposition 5. *In equilibrium:*

- ***An adverse shock to aggregate demand*** *increases matching cost and spare capacity (or equivalently, unemployment), while it decreases consumption (or equivalently, output), price, product market tightness, and import price.*

- ***An adverse shock to labor supply*** *increases price, product market tightness, and import price, while it decreases consumption (or equivalently, output), matching cost, and spare capacity (or equivalently, unemployment).*

29. Unlike Michaillat and Saez (2015) in which there is a matching cost that differentiates consumption from output, consumption and output are equivalent in our model.

- ***An adverse shock to supply chain*** *increases price and spare capacity (or equivalently, unemployment), while it decreases consumption (or equivalently, output). The responses of product market tightness, import price, and matching cost are undetermined.*

Proof. See Appendix D.4. ■

Table 2 summarizes the signs of the responses of the macro aggregates to the three different shocks. Figure 8 graphically illustrates the comparative statics (left panels), alongside the corresponding equilibrium condition between product market tightness and price (right panels) from Equation (14) that describes the optimal interplay between product market tightness and price.

Table 2: Comparative Statics for Adverse Shocks to Aggregate Demand, Labor Supply, and Supply Chain

Adverse Shock To:	**Effects On:**					
	Consumption (or Output) c	Price p	Product Market Tightness θ	Import Price r	Matching Cost $G(\tau)l-c$	Spare Capacity (or Unemployment) $l-c$
Aggregate Demand	$-$	$-$	$-$	$-$	$+$	$+$
Labor Supply	$-$	$+$	$+$	$+$	$-$	$-$
Supply Chain	$-$	$+$	N/A	N/A	N/A	$+$

Notes. The table summarizes the comparative statics in Proposition 5. An adverse shock to aggregate demand is a decrease in money supply, μ, or in the taste for consumption of goods, χ. An adverse shock to labor supply is a decrease in labor supply (or equivalently, productive capacity), l. An adverse shock to supply chain is an increase in the scale parameter of the log-normal distribution of transportation costs, γ.

Panel (a) in Figure 8 shows the response of the system to a decline in aggregate demand. The aggregate demand curve shifts inwards, driven by the preference for lower consumption by households, either because they hold less money or prefer to consume less. In equilibrium, the price decreases to clear the market. As the price decreases, importers visit fewer exporters to participate in trade, hence lowering product market tightness. The declines in price and product market tightness then contribute to a lower import price, as not only does a trade itself become less profitable, but also the probability of getting into a trade for an importer becomes higher, given the weakened congestion. Consequently, exporters sell a

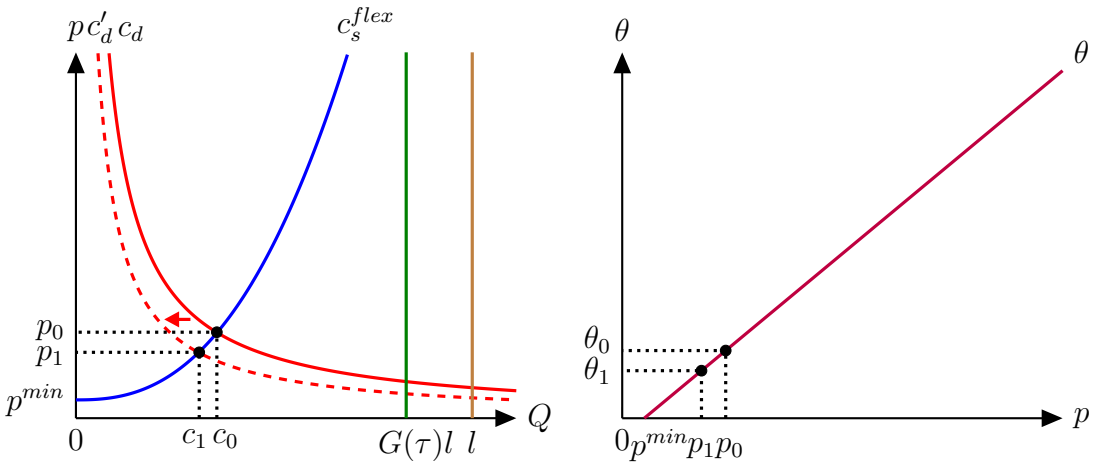

(a) An Adverse Shock to Aggregate Demand, i.e., $\mu \downarrow$ or $\chi \downarrow$

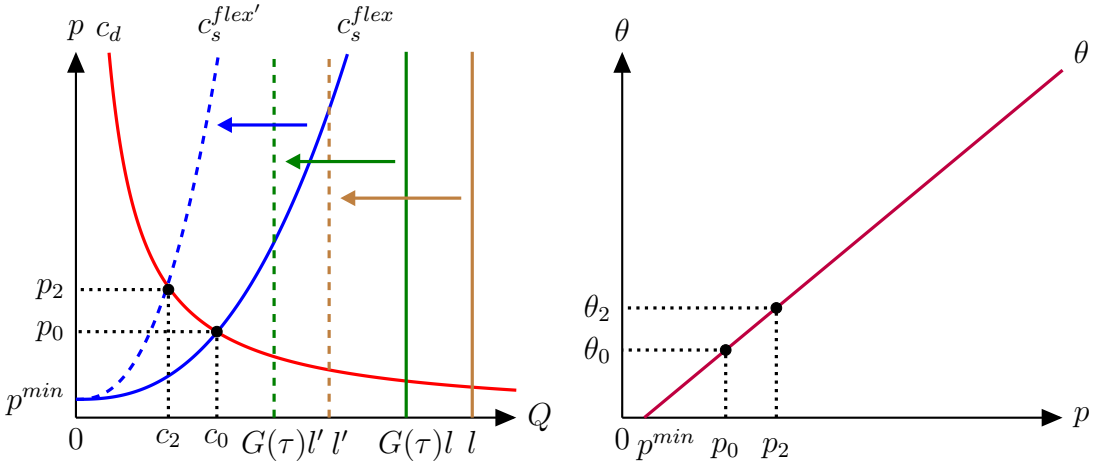

(b) An Adverse Shock to Labor Supply, i.e., $l \downarrow$

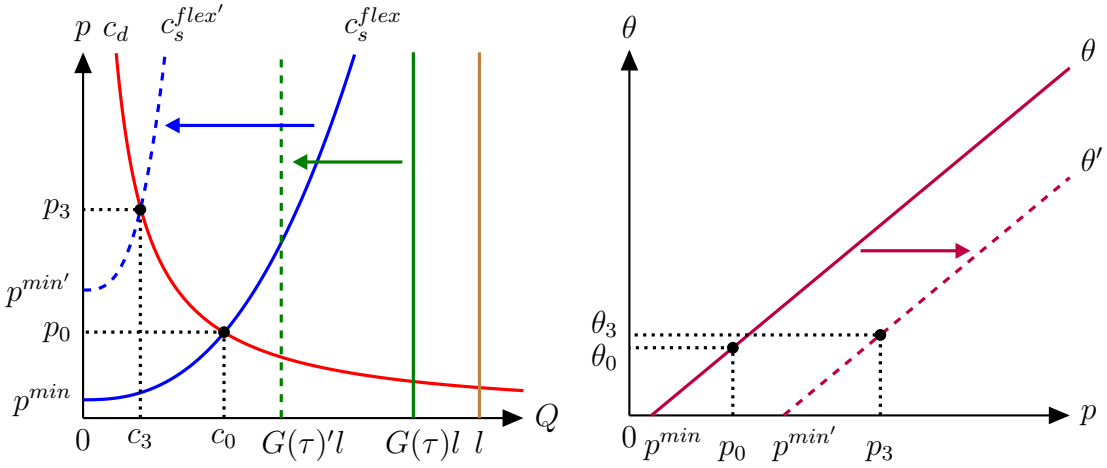

(c) An Adverse Shock to Supply Chain, i.e., $\gamma \uparrow$

Figure 8: Graphical Representation of Comparative Statics

lower fraction of their productive capacity to importers, resulting in a decrease in consumption (or equivalently, output). This leads to an increase in matching cost and spare capacity (or equivalently, unemployment).

Panel (b) in Figure 8 shows the response of the system to a negative labor supply shock that decreases productive capacity.[30] The negative shock to the aggregate supply causes it to rotate inwards while leaving p^{min} unchanged. The price increases to clear the market, and consumption (or equivalently, output) decreases as the equilibrium moves upwards along the aggregate demand curve. The increase in the price raises product market tightness. This simultaneous rise in price and product market tightness leads to a higher import price. Along with the contraction in productive capacity, this results in lower matching costs and reduced spare capacity (or equivalently, unemployment).

Lastly, Panel (c) in Figure 8 shows the response of the system to an increase in transportation costs corresponding to a negative supply chain shock, encapsulated by the increase in the scale parameter of the log-normal distribution of transportation costs. The increase generates a higher mean transportation cost, increasing the probability of drawing a transportation cost above the reservation threshold. Since the reservation threshold is fixed, the expected total surplus from a trade decreases without a change in the price. To continue benefiting from trade, importers raise the price of imported goods to households and pass on these costs to consumers. Consequently, the price rises while consumption (or equivalently, output) falls. Graphically, this process is represented by an inward shift of the aggregate supply curve, and unlike in the negative labor supply shock, p^{min} increases in response to the shock. Since the productive capacity (or equivalently, labor supply) is fixed, spare capacity (or equivalently, unemployment) increases in response to the negative supply chain shock.

In terms of the effect on product market tightness, as seen in Equation (22),

$$\theta(\gamma) = \frac{1-\eta}{\eta\rho}\Big[\underbrace{p(\gamma)-\tau}_{\text{Profit Margin }\uparrow} + \underbrace{\beta\int_0^{\tau}\Phi\Big(\frac{\log z'-\gamma}{\sigma}\Big)dz'}_{\text{Expected Total Surplus }\downarrow}\Big], \tag{22}$$

the result remains ambiguous. On the one hand, an increase in γ reduces the expected

30. This shock is commonly termed as a "supply shock" and has been studied intensively in the literature. See, for instance, del Rio-Chanona et al. (2020), Bonadio et al. (2021), Brinca, Duarte, and Faria-e-Castro (2021), and Leyva and Urrutia (2022).

total surplus, since it becomes more likely to obtain a bad draw that severs trade. On the other hand, an increase in γ raises the price, and thus, the profit margin. Therefore, if the price rises to a level that offsets the negative effect of a lower expected total surplus, product market tightness will increase, as depicted in Panel (c) of Figure 8. Alternatively, if the price increase is insufficient to reverse the aforementioned relationship, product market tightness will decrease accordingly.

Lastly, as discussed in Appendix D.4, the corresponding changes in import price and matching cost depend on how the price and product market tightness evolve following an adverse shock to supply chain. Therefore, their comparative statics also remain ambiguous.

4. The Causal Effects of Supply Chain Disruptions

In this section, we study the causal effects of supply chain disruptions by developing a SVAR model that uses our ACR index and restricts the responses of the macro aggregates according to our theoretical results.[31] We also study the differences between our index and the alternative GSCPI, focusing on the statistical significance and historical contribution of disruption shocks to the supply chain during the Covid-19 pandemic.

4.1. A SVAR Model with Sign and Zero Restrictions

Our empirical model is based on Rubio-Ramirez, Waggoner, and Zha (2010) and Arias, Rubio-Ramirez, and Waggoner (2018):

$$\boldsymbol{y}_t'\boldsymbol{A}_0 = \sum_{l=1}^{L} \boldsymbol{y}_{t-l}'\boldsymbol{A}_l + \boldsymbol{\omega}_t'\boldsymbol{C} + \boldsymbol{\epsilon}_t', \quad 1 \leq t \leq T, \tag{23}$$

where $\boldsymbol{y}_t$ is an $n \times 1$ vector of endogenous variables, $\boldsymbol{\omega}_t = [1, t]'$ is a 2×1 vector of a constant and a linear trend, $\boldsymbol{\epsilon}_t$ is an $n \times 1$ vector of structural shocks, $\boldsymbol{A}_l$ is an $n \times n$ matrix of structural parameters for $0 \leq l \leq L$ with $\boldsymbol{A}_0$ invertible, $\boldsymbol{C}$ is a $2 \times n$ matrix of parameters,

31. When we disentangle the causal effects of a supply chain disruption shock from others, it is important to include the relevant variable(s) necessary for identification in the econometric models. This step is crucial to prevent the omitted variable bias, which could introduce a serious flaw in certain scenarios. For instance, an oil price shock could influence real GDP, inflation, and unemployment similarly to a supply chain disruption shock (Känzig 2021; Gagliardone and Gertler 2023).

L is the lag length, and T is the sample size. The vector $\boldsymbol{\epsilon}_t$, conditional on past information and the initial conditions $\boldsymbol{y}_0, \ldots, \boldsymbol{y}_{1-L}$ is Gaussian with mean zero and covariance matrix $\mathbf{1}_{n\times n}$, i.e., the $n \times n$ identity matrix. The SVAR described in Equation (23) can be written compactly as:

$$\boldsymbol{y}_t' \boldsymbol{A}_0 = \boldsymbol{x}_t' \boldsymbol{A}_+ + \boldsymbol{\epsilon}_t', \quad 1 \leq t \leq T, \tag{24}$$

where $\boldsymbol{A}_+' = [\boldsymbol{A}_1' \ \ldots \ \boldsymbol{A}_L' \ \boldsymbol{C}']$ and $\boldsymbol{x}_t' = [\boldsymbol{y}_{t-1}' \ \ldots \ \boldsymbol{y}_{t-L}' \ \boldsymbol{\omega}_t']$ for $1 \leq t \leq T$. The dimension of $\boldsymbol{A}_+$ is $m \times n$, where $m = nL + 2$. The reduced-form representation implied by Equation (24) is given by:

$$\boldsymbol{y}_t' = \boldsymbol{x}_t' \boldsymbol{B} + \boldsymbol{u}_t', \quad 1 \leq t \leq T,$$

where $\boldsymbol{B} = \boldsymbol{A}_+ \boldsymbol{A}_0^{-1}, \boldsymbol{u}_t' = \boldsymbol{\epsilon}_t' \boldsymbol{A}_0^{-1}$, and $\mathbb{E}(\boldsymbol{u}_t \boldsymbol{u}_t') = \boldsymbol{\Sigma} = (\boldsymbol{A}_0 \boldsymbol{A}_0')^{-1}$. The matrices $\boldsymbol{B}$ and $\boldsymbol{\Sigma}$ are the reduced-form parameters, while $\boldsymbol{A}_0$ and $\boldsymbol{A}_+$ are the structural parameters.

We estimate the model using the monthly U.S. series for real GDP, GDP deflator, unemployment, import price, as well as our ACR index over the period from January 2017 to July 2022, with all series being seasonally adjusted. All the variables are from the Federal Reserve Economic Data (FRED), maintained by the Federal Reserve Bank of St. Louis.[32,33] The real GDP, GDP deflator, and import price are in log percent, while the unemployment and ACR are in percent. We set the number of lags to two in the baseline specification, but the results are robust to considering one or three lags.[34]

Our identification scheme applies the sign restrictions from our theoretical model, which are summarized in Table 2, as well as the zero restrictions on the responses of the ACR

32. The mnemonics of the variables are: `GDPC1` (real GDP), `INDPRO` (industrial production), `GDPDEF` (GDP implicit price deflator), `CPIAUCSL` (consumer price index), `PPIFG` (producer price index), `UNRATE` (unemployment), and `IREXFDFLS` (import price). The monthly time series for real GDP and GDP deflator are constructed using interpolation of the corresponding quarterly time series, as in Bernanke and Mihov (1998) and Arias, Caldara, and Rubio-Ramírez (2019). Specifically, we apply the Chow-Lin method for temporal disaggregation (Chow and Lin 1971) to interpolate the real GDP based on the industrial production index, while interpolating the GDP deflator based on the consumer price index and the producer price index. The unemployment and import price are raw series from the U.S. Bureau of Labor Statistics.

33. Considering that international trade in goods, rather than services, was primarily affected by global supply chain disruptions, we conduct a robustness check of our baseline results. We do this by replacing the monthly U.S. series of the GDP deflator with the Personal Consumption Expenditures (PCE) goods price index. The mnemonic for this index in the FRED database is `DGDSRG3M086SBEA`. As shown in Appendix F.2, while the baseline results remain consistent, the identification of the causal effects of an adverse shock to the supply chain becomes even more pronounced.

34. Appendix F.3 demonstrates the robustness of our baseline results when considering different lag structures and extended horizons to impose the sign restrictions on IRFs.

index to adverse aggregate demand and labor supply shocks. We estimate the SVAR using a Bayesian approach as in Arias, Rubio-Ramirez, and Waggoner (2018), Arias, Caldara, and Rubio-Ramírez (2019), and Arias et al. (2023) with restrictions on the first period of response (i.e., $k = 1$), thus imposing a minimal structure as in Mumtaz and Zanetti (2012, 2015).[35] More concretely, we impose the following restrictions:

Restriction 1. ***An adverse shock to aggregate demand*** *leads to a negative response of real GDP, GDP deflator, and import price, as well as to a positive response of unemployment at $k = 1$. ACR does not respond at $k = 1$.*

Restriction 2. ***An adverse shock to labor supply*** *leads to a negative response of real GDP and unemployment, as well as to a positive response of GDP deflator and import price at $k = 1$. ACR does not respond at $k = 1$.*

Restriction 3. ***An adverse shock to supply chain*** *leads to a negative response of real GDP, as well as to a positive response of GDP deflator, unemployment, and ACR at $k = 1$.*

Figures 9, 10, and 11 present our baseline results for the responses of the endogenous variables to an adverse shock to aggregate demand, labor supply, and the supply chain respectively. The solid line shows the point-wise posterior median IRFs of the endogenous variables to each structural shock, and the gray-shaded bands represent the corresponding 68% and 90% posterior probability bands.[36] We start by discussing the IRFs to an adverse shock to aggregate demand in Figure 9. On impact, real GDP declines significantly by approximately 1.0%, while unemployment rises sharply by more than 0.5%. Such responses persist with a high posterior probability for the first six months after the shock. In contrast, the response of the GDP deflator is more muted, with its initial fall sitting at -0.1% before gradually reverting back to zero after a one-year window. Import price exhibits a similar

35. We impose a normal-generalized-normal (NGN) prior distribution over the structural parameters $\boldsymbol{A}_0$ and $\boldsymbol{A}_+$. The NGN prior is a conjugate prior characterized by four parameters $(\nu, \boldsymbol{\Phi}, \boldsymbol{\Psi}, \boldsymbol{\Omega})$. The parameters ν and $\boldsymbol{\Phi}$ govern the marginal prior distribution of $vec(\boldsymbol{A}_0)$, while the remaining parameters $\boldsymbol{\Psi}$ and $\boldsymbol{\Omega}$ govern the prior distribution of $vec(\boldsymbol{A}_+)$, conditional on $\boldsymbol{A}_0$. Our choice of the prior density parameterization is $\nu = 0, \boldsymbol{\Phi} = \boldsymbol{0}_{n\times n}, \boldsymbol{\Psi} = \boldsymbol{0}_{m\times n}$, and $\boldsymbol{\Omega}^{-1} = \boldsymbol{0}_{m\times m}$. This parameterization generates prior densities that are equivalent to those in Uhlig (2005). Nevertheless, our results are robust to using the prior robust approach in Giacomini and Kitagawa (2021), as illustrated in Appendix F.4.

36. The results are based on 100,000 independent draws from the posterior distribution of the structural parameters, and the structural shocks are of size one standard deviation.

pattern, although a zero response emerges much sooner at the six-month mark. Lastly, the response of the ACR index is less precisely estimated, with a large posterior probability mass centered around zero.

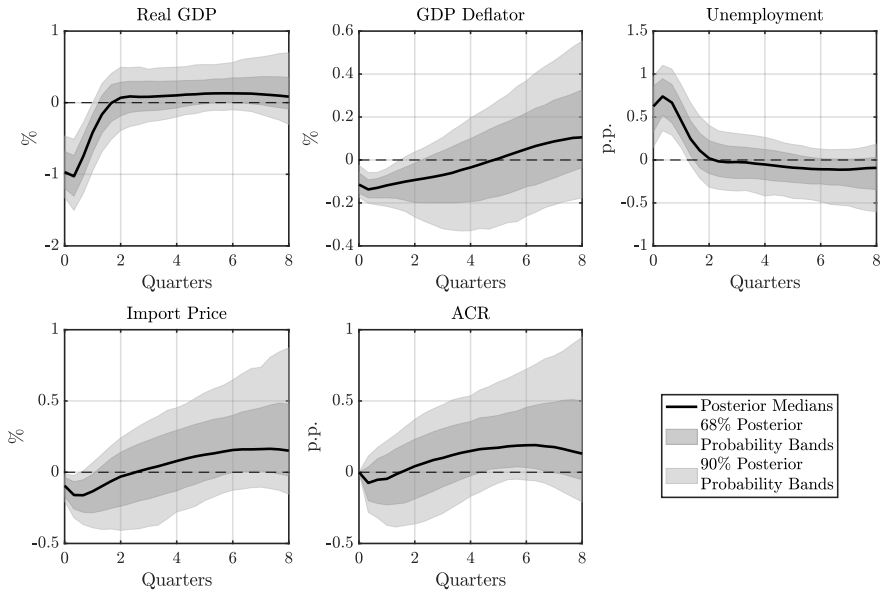

Figure 9: IRFs to an Adverse Shock to Aggregate Demand: Baseline

Notes. The IRFs to a one standard deviation adverse shock to aggregate demand are identified using the ACR index and Restrictions 1, 2, and 3. The solid line shows the point-wise posterior medians, and the shaded bands represent the 68% and 90% equal-tailed point-wise posterior probability bands. The figure is based on 100,000 independent draws.

Figure 10 shows the IRFs to an adverse shock to labor supply. On impact, following Restriction 2, both the responses of real GDP and unemployment are negative. Subsequently, real GDP continues to fall, with a zero response almost at the boundary of the 90% confidence set near the trough, which occurs about three months after the shock. Largely due to such a fall in real GDP, the initial decline in unemployment is quickly reversed, and it turns significantly positive within one quarter from the shock, peaking at approximately 0.25% before reverting back to zero. The GDP deflator increases and remains elevated for approximately one year, reflecting the lag effects of supply-side shocks. Import price again exhibits a similar pattern, but the peak is reached at a much earlier horizon. Lastly, the median response of ACR is zero on impact and consistently above zero for almost one year afterwards.

Finally, Figure 11 shows the IRFs following a negative shock to the supply chain. The

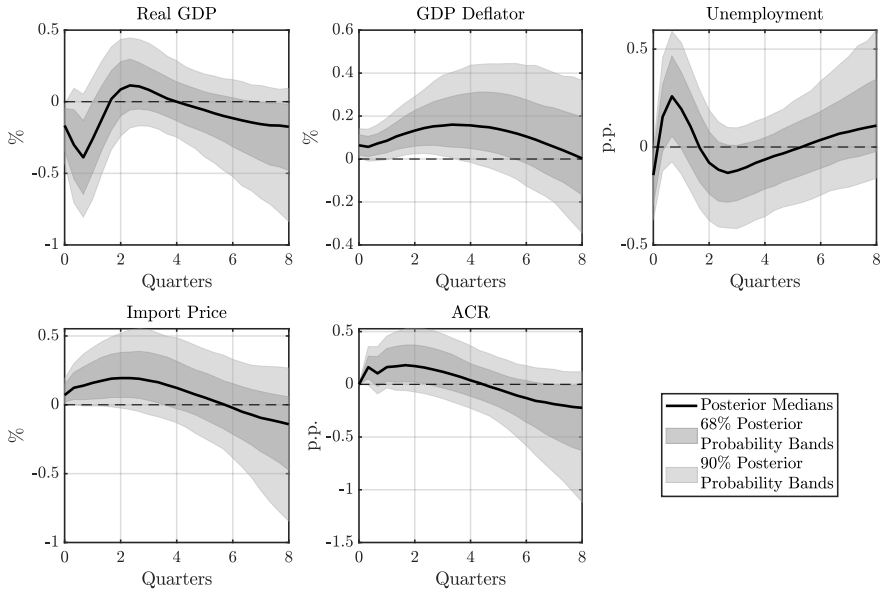

Figure 10: IRFs to an Adverse Shock to Labor Supply: Baseline

Notes. The IRFs to a one standard deviation adverse shock to labor supply are identified using the ACR index and Restrictions 1, 2, and 3. The solid line shows the point-wise posterior medians, and the shaded bands represent the 68% and 90% equal-tailed point-wise posterior probability bands. The figure is based on 100,000 independent draws.

median response of real GDP is negative on impact, and it remains below zero for more than one quarter after the shock. The unemployment response mirrors that of real GDP in magnitude. The increases in both the GDP deflator and import price align with the magnitude observed in the labor supply shock, highlighting the significant role of supply chain disruptions in driving up prices. Despite the uncertainty around our estimates, as evinced by the wide posterior probability bands, the positive responses of both the GDP deflator and import price are still statistically significant at the 68% level of significance. Lastly, the response of the ACR index remains elevated for nearly one year after the shock.

4.2. Comparison Between the ACR and GSCPI

In this section, we assess the implications of the differences between the ACR and GSCPI indices for the readings that the SVAR model makes regarding the causal effect of supply chain disruptions on inflation by studying: (i) IRFs to an adverse shock to supply chain, (ii) Forecast Error Variance Decomposition (FEVD), and (iii) Historical Decomposition (HD),

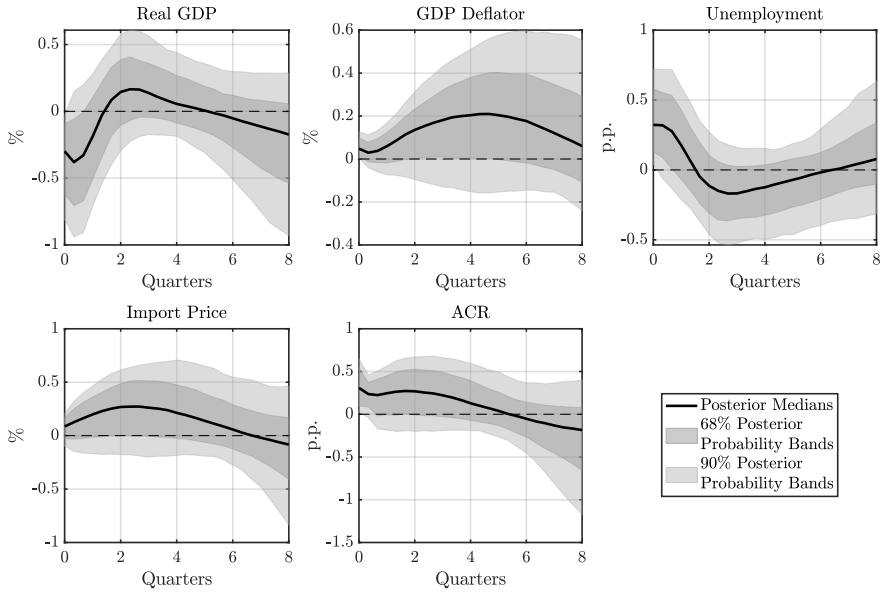

Figure 11: IRFs to an Adverse Shock to Supply Chain: Baseline

Notes. The IRFs to a one standard deviation adverse shock to supply chain are identified using the ACR index and Restrictions 1, 2, and 3. The solid line shows the point-wise posterior medians, and the shaded bands represent the 68% and 90% equal-tailed point-wise posterior probability bands. The figure is based on 100,000 independent draws.

using our empirical model and the sign and zero restrictions developed in Section 4.1.[37] As illustrated in Section 2.3, we find that the behaviors of the two indices diverge significantly from early 2020 onwards, and the substantial increase in the GSCPI at the onset of the Covid-19 pandemic is likely driven by sudden changes in demand and the management's misperception of supply chain issues as recorded by the PMI surveys.

Figure 12 shows the IRFs following an adverse shock to the supply chain for the GSCPI index. The responses of real GDP and unemployment closely resemble the baseline responses when we use the ACR index (Figure 11). The responses of the GDP deflator and import price are around zero and statistically insignificant, and the response of the GSCPI is positive on impact while returning to zero after the one-quarter mark.

Figures 13a and 13b illustrate the proportion of the forecast error variance explained by each of the three structural shocks, using the ACR and GSCPI indices, respectively. A comparison of the two figures reveals that aggregate demand shocks account for the largest

37. As a robustness check, Appendix F.5 estimates a version of the model without the zero restrictions imposed on the GSCPI, and the comparison results remain unchanged.

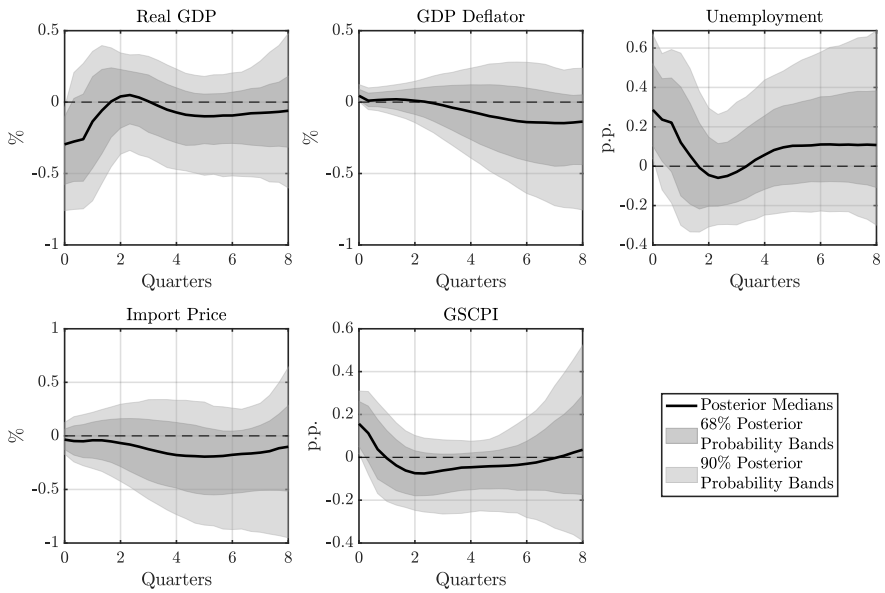

Figure 12: IRFs to an Adverse Shock to Supply Chain: The GSCPI and Restrictions 1, 2, and 3

Notes. The IRFs to a one standard deviation adverse shock to supply chain are identified using the GSCPI index and Restrictions 1, 2, and 3. The solid line shows the point-wise posterior medians, and the shaded bands represent the 68% and 90% equal-tailed point-wise posterior probability bands. This figure is based on 100,000 independent draws.

fraction of unexpected fluctuations in real GDP and unemployment for both indices. However, the supply chain shock explains a significant fraction of the unexpected fluctuations in the GDP deflator at longer horizons for the ACR index, while it only accounts for a minimal fraction for the GSCPI index. This latter finding is consistent with the zero response of the GDP deflator to the supply chain shock for the GSCPI index (Figure 12).

Finally, Figures 14a and 14b show the cumulative historical contribution of each of the three structural shocks to U.S. inflation for the ACR and GSCPI indices, respectively.[38] Our ACR index attributes the initial fall in inflation at the onset of the Covid-19 pandemic to a decline in demand, and the subsequent rise in inflation from April 2020 to adverse shocks to the supply chain, which remains influential for inflation throughout the sample period. Interestingly, our model shows that supply chain disturbances consistently exert a negative contribution to inflation prior to the global pandemic period that started in March 2020.[39]

38. To facilitate comparison of the series across different scales, we apply Z-score standardization, which re-scales data to have a mean of zero and a standard deviation of one.

39. The persistent negative contribution of shocks to the supply chain to U.S. inflation supports the political motives for the enhancements of supply chain operations to ease inflationary pressures. For instance, several

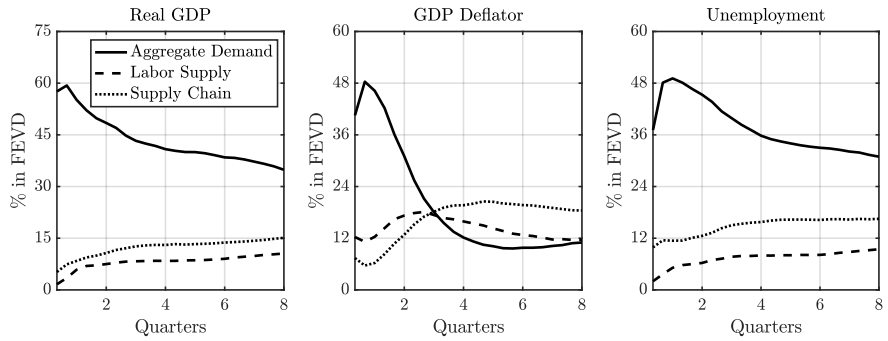

(a) Baseline

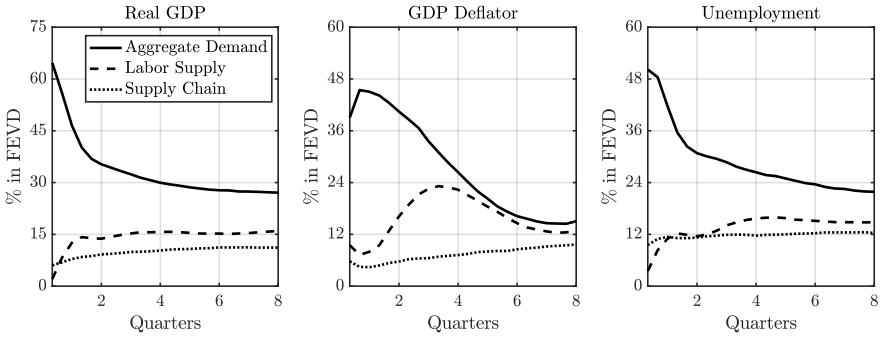

(b) The GSCPI and Restrictions 1, 2, and 3

Figure 13: FEVD from the SVAR

Notes. Each line presents the median fraction of the forecast error variance for each endogenous variable, explained by each of the three identified structural shocks at various time horizons. The FEVD is estimated using the ACR/GSCPI index and Restrictions 1, 2, and 3, and based on 100,000 independent draws.

In contrast, the results based on the GSCPI index attribute the early fall in inflation to positive shocks to the supply chain, while the rise in inflation subsequent to the onset of the pandemic is principally explained by demand shocks.

Taken together, we find significant differences between the ACR and GSCPI indices and show that they provide contrasting interpretations of the contributions of different shocks to U.S. inflation over the sample period.

U.S. ports underwent considerable infrastructure upgrades in the period 2017-2019, aiming to enhance their capacity, efficiency, and resilience against potential disruptions.

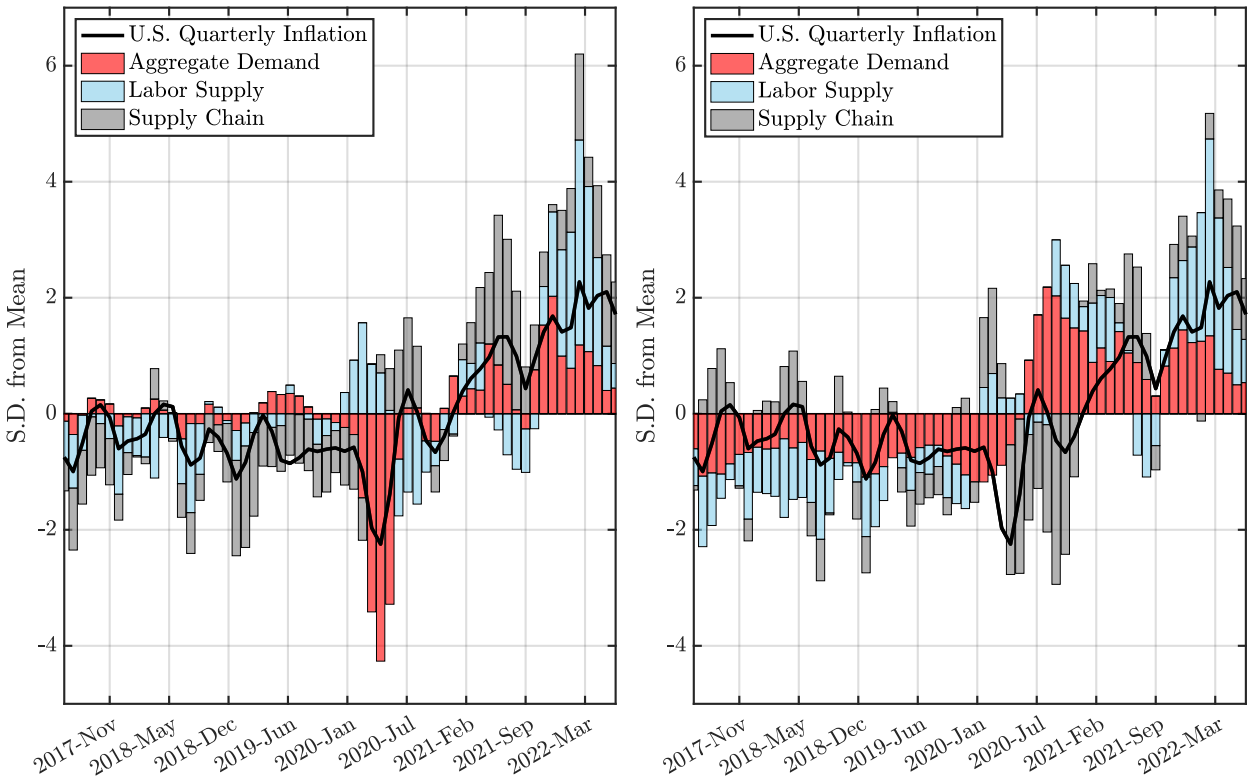

(a) Baseline **(b)** The GSCPI and Restrictions 1, 2, and 3

Figure 14: HD of U.S. Inflation

Notes. In both panels, the solid line represents the standardized quarterly inflation rate in the U.S., i.e., quarter-on-quarter growth of the GDP deflator. The shaded bar represents the standardized cumulative historical contribution of each of the three structural shocks identified using the ACR/GSCPI index and Restrictions 1, 2, and 3 to U.S. inflation. The estimation results are obtained with each variable measured in percent change from the previous period, and are calculated based on 100,000 independent draws.

5. The Effectiveness of Monetary Policy

In this section, we study the interplay between supply chain disruptions and the effectiveness of monetary policy to control inflation and output. We show through our theoretical model that a disruption to the supply chain increases the sensitivity of inflation and reduces the sensitivity of output to a contractionary monetary policy shock, generating state-dependence that changes the stabilization tradeoff of monetary policy. Subsequently, we test and corroborate our theoretical predictions using a Threshold Vector Autoregression (TVAR) model.

5.1. Theoretical Prediction

We derive the theoretical prediction for the state-dependence of monetary policy using our theoretical model described in Section 3. The monetary supply parameter μ encapsulates the action of monetary policy, and the transportation cost parameter γ captures the disruption to the supply chain. We study the comparative statics of the impact of a tightening in monetary policy, focusing on whether the effects of the policy intervention on inflation and output are different amid the supply chain disruption. The results are summarized in Proposition 6.

Proposition 6. *For any given threshold of transportation cost $\tau > 0$ and parameter values $\mu \in \mathbb{R}^+$ and $\gamma \in \mathbb{R}$ such that the following constraint holds:*

$$\frac{\partial \theta(\mu,\gamma)}{\partial \gamma} > \frac{\theta(1+\theta^{\xi})}{\big(1-G(\tau)\big)G(\tau)} \frac{1}{\sigma\sqrt{2\pi}} \exp\Big[-\frac{(\log\tau-\gamma)^2}{2\sigma^2}\Big], \tag{25}$$

where $G(\tau) \equiv \Phi[(\log\tau - \gamma)/\sigma]$, $\Phi(.)$ is the standard normal cumulative density function, the responses of the endogenous variables to a change in monetary policy are described by the partial derivatives:

$$\frac{\partial c(\mu,\gamma)}{\partial \mu} > 0, \ \frac{\partial p(\mu,\gamma)}{\partial \mu} > 0, \ \frac{\partial \theta(\mu,\gamma)}{\partial \mu} > 0, \ \frac{\partial r(\mu,\gamma)}{\partial \mu} > 0,$$
$$\frac{\partial}{\partial \mu}\big[G(\tau)l - c(\mu,\gamma)\big] < 0, \ \frac{\partial}{\partial \mu}\big[l - c(\mu,\gamma)\big] < 0.$$

The cross derivatives that describe the variation in the responses of the endogenous variables ascribed to the supply chain disruption satisfy:

$$\frac{\partial^2 c(\mu,\gamma)}{\partial \mu \partial \gamma} < 0, \ \frac{\partial^2 p(\mu,\gamma)}{\partial \mu \partial \gamma} > 0, \ \frac{\partial^2 \theta(\mu,\gamma)}{\partial \mu \partial \gamma} > 0, \ \frac{\partial^2 r(\mu,\gamma)}{\partial \mu \partial \gamma} > 0,$$
$$\frac{\partial^2}{\partial \mu \partial \gamma}\big[G(\tau)l - c(\mu,\gamma)\big] > 0, \ \frac{\partial^2}{\partial \mu \partial \gamma}\big[l - c(\mu,\gamma)\big] > 0,$$

where $c, p, \theta, r, G(\tau)l - c$, and $l - c$ represent consumption (or equivalently, output), price, product market tightness, import price, matching cost, and spare capacity (or equivalently, unemployment), respectively.

Proof. See Appendix D.5. ■

In words, the partial and cross derivatives in Proposition 6 imply that at an equilibrium

where the product market tightness is sufficiently reactive to the supply chain disruption (as evinced by equation (25)), the contractionary monetary policy shock induces a smaller decrease in consumption (or equivalently, output) and a larger decrease in price, as evinced by the second derivatives.[40]

Figure 15 provides a graphical representation of our theoretical prediction. In response to a contractionary monetary policy shock, households reduce consumption at a given price level due to decreased money holdings. This causes the aggregate demand curve to shift inwards, leading to a reduced price and lower consumption of goods. Consequently, product market tightness diminishes as importers visit fewer exporters for trade. This reduction in price and product market tightness subsequently results in a lower import price. Exporters, in turn, sell a smaller fraction of their productive capacity to importers, leading to a decrease in output. Correspondingly, matching costs and spare capacity (or equivalently, unemployment) increase.

[TO Y: I HAVE TRIED TO IMPROVE THE EXPLANATION HERE, BUT IT IS STILL UNCLEAR. COULD YOU PLEASE HAVE A SECOND GO AT IT?] The increase in transportation costs that generates the supply chain disruption decreases the likelihood that the randomly drawn transportation cost of the exporters falls below the reservation transportation cost, and consequently a lower number of matches materializes. Simultaneously, the contractionary monetary policy shock suppresses the demand of the importers. To instigate such a pronounced decrease in product market tightness, prices must experience a more dramatic drop. Taken together, these dynamics suggest that supply chain disruptions enhance the sensitivity of prices to fluctuations in goods supply. This heightened sensitivity becomes notably significant when product market tightness proves to be more reactive to the supply chain disruption, as outlined in the constraint (25) of Proposition 6.

[TO Y: THIS SENSENTE IS UNCLEAR. PLEASE REVISE IT.] Subsequently, these more pronounced decreases in price and product market tightness will result in a more significant drop in the import price. Furthermore, since changes in consumption (or equivalently, output) inversely mirror those in price, a steeper decline in price will be paralleled by a

40. Proposition 6 also shows that the responses of product market tightness and import price are greater while the responses of matching cost and spare capacity (or equivalently, unemployment) are weaker during the supply chain disruption.

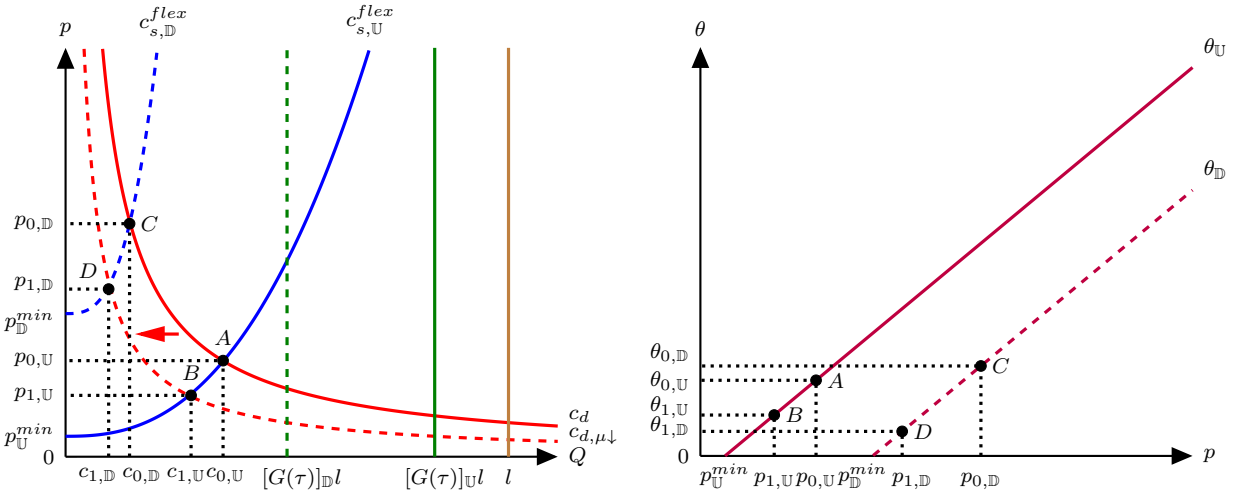

Figure 15: State-Dependent Effects of a Contractionary Monetary Policy Shock: Theoretical Prediction

Notes. The two figures illustrate how in theory the economy adjusts to a contractionary monetary policy shock and how such an adjustment depends on whether the supply chain is disrupted or not. The two respective states – i.e., supply chain disrupted ($\mathbb{D}$) versus undisrupted ($\mathbb{U}$) – are plotted against each other. $c^{flex}_{s,\mathbb{D}}$ and $c^{flex}_{s,\mathbb{U}}$ represent the flexible-price aggregate supply curves in the two states, while $\theta_{\mathbb{D}}$ and $\theta_{\mathbb{U}}$ represent the schedules of product market tightness in the two states. c_d and $c_{d,\mu\downarrow}$ represent the aggregate demand curves before and after the contractionary monetary policy shock. The labels on the axes corresponding to each state are differentiated by their subscripts, and the capital letters ($A \to B, C \to D$) are also included to facilitate comparison between the two states.

less substantial drop in consumption (or equivalently, output). Accordingly, the increases in matching cost and spare capacity (or equivalently, unemployment) will be smaller when responding to a contractionary monetary policy shock.

5.2. Empirical Validation

We test the theoretical result of the state-dependence of monetary policy by developing a structural TVAR model – building on Chen and Lee (1995) – that allows for endogenous variation in the estimated parameters based on the estimated threshold of our ACR index. The reduced-form model is the following:

$$\boldsymbol{y}_t = I_t\Big[\sum_{l=1}^{L} \boldsymbol{B}'_{\mathbb{D},l}\boldsymbol{y}_{t-l} + \boldsymbol{C}'_{\mathbb{D}}\boldsymbol{\omega}_t + \boldsymbol{\Sigma}^{1/2}_{\mathbb{D}}\boldsymbol{\epsilon}_t\Big] + (1 - I_t)\Big[\sum_{l=1}^{L} \boldsymbol{B}'_{\mathbb{U},l}\boldsymbol{y}_{t-l} + \boldsymbol{C}'_{\mathbb{U}}\boldsymbol{\omega}_t + \boldsymbol{\Sigma}^{1/2}_{\mathbb{U}}\boldsymbol{\epsilon}_t\Big], \quad (26)$$

where $1 \leq t \leq T$, $\boldsymbol{y}_t$ is an $n \times 1$ vector of endogenous variables, $\boldsymbol{\omega}_t = [1, t]'$ is a 2×1 vector of a constant and a linear trend, $\boldsymbol{\epsilon}_t$ is an $n \times 1$ vector of structural shocks, $\boldsymbol{B}_{\mathbb{D},l}$ and $\boldsymbol{B}_{\mathbb{U},l}$ are two $n \times n$ matrices of coefficients for the lagged endogenous variables $\boldsymbol{y}_{t-l}$, $\boldsymbol{C}_{\mathbb{D}}$ and $\boldsymbol{C}_{\mathbb{U}}$ are two $2 \times n$ matrices of coefficients for the constant and linear trend, $\boldsymbol{\Sigma}_{\mathbb{D}}$ and $\boldsymbol{\Sigma}_{\mathbb{U}}$ are the covariance matrices, L is the lag length, and T is the sample size.[41] The vector $\boldsymbol{\epsilon}_t$, conditional on past information and the initial conditions $\boldsymbol{y}_0, \ldots, \boldsymbol{y}_{1-L}$, is Gaussian with mean zero and covariance matrix $\mathbf{1}_{n \times n}$, i.e., an $n \times n$ identity matrix. Switches between the two regimes – i.e., supply chain disrupted ($\mathbb{D}$) vs. undisrupted ($\mathbb{U}$) – are governed by the indicator variable $I_t \in \{0, 1\}$, which is equal to one if the ACR in period $t-1$, ACR_{t-1}, is above the threshold $\overline{ACR}$, and equal to zero otherwise:

$$I_t = \begin{cases} 1, & \text{if } ACR_{t-1} > \overline{ACR}; \\ 0, & \text{if } ACR_{t-1} \leq \overline{ACR}. \end{cases} \tag{27}$$

Under the Normal-Inverse-Wishart conjugate prior for the TVAR parameters and conditional on the value of the threshold $\overline{ACR}$, the posterior distribution of the TVAR parameter vector is a conditional Normal-Inverse-Wishart distribution, and we use the Gibbs sampler to draw from the distribution. Since the posterior distribution of the threshold $\overline{ACR}$ conditional on the TVAR parameters is unknown, we use a Metropolis-Hastings algorithm to obtain its posterior distribution, similar to Chen and Lee (1995), Lopes and Salazar (2006), and Pizzinelli, Theodoridis, and Zanetti (2020). Appendix G.1 provides the details on the Normal-Inverse-Wishart prior.

To retain comparability with our previous results, we include the same variables used in our SVAR model in Section 4.1, with the addition of the Federal Funds Rate to reflect the changes in the stance of U.S. monetary policy. For consistency, we also retain the same sample period 2017M1-2022M7.[42]

To identify the contractionary monetary policy shock, we impose the following standard restriction on IRFs:

41. Note that we allow the covariance matrix to be regime-specific.

42. All the series are seasonally adjusted, except the Federal Funds Rate. Real GDP, GDP deflator, and import price enter the TVAR in log percent, whereas the Federal Funds Rate, unemployment, and ACR enter the TVAR in percent.

Restriction 4. ***A contractionary monetary policy shock*** *leads to a negative response of real GDP, GDP deflator, and import price, as well as to a positive response of unemployment and Federal Funds Rate at* $k = 1$*. ACR does not respond at* $k = 1$*.*[43]

We compute the identified set of IRFs using the Bayesian approach similar to Pizzinelli, Theodoridis, and Zanetti (2020) and Bratsiotis and Theodoridis (2022).[44] We use one lag in the baseline estimation, and select the one-month lag of the ACR index as the variable determining the state I_t.[45]

Figure 16 plots the IRFs to a contractionary monetary policy shock for both the supply chain disrupted (black) and undisrupted (red) regimes, reporting both the point-wise posterior medians (solid lines) and the 68% equal-tailed point-wise posterior probability bands (shaded area and dotted lines) for the horizon $k = 12$ (i.e., four quarters). The figure shows significant differences in the responses of the variables to the contractionary monetary policy shock between the two regimes. In accordance with our theoretical results, the GDP deflator and import price are more responsive, while the output and unemployment are less responsive in the regime of supply chain disruptions, and the differences in the responses are statistically significant.

Appendix H shows that our results hold across several variations to the benchmark model, namely: (i) different lag structures, (ii) a looser prior (i.e., $\lambda = 0.5$ instead of 0.25; see Appendix G.1 for the details on the tightness of the prior), and (iii) longer horizons for the sign restrictions (i.e., $k = 1$ to $k = 1, 2, 3$). Appendix I shows that our results continue to hold when we use local projections with interaction terms, as in Ghassibe and Zanetti (2022), to estimate the state-dependent effects of a contractionary monetary policy shock.

43. Restriction 4 enriches Restriction 1, which is intended for the identification of an adverse shock to aggregate demand, with the positive response of the Federal Funds Rate on impact.

44. To implement the sign and zero restrictions on IRFs, we use the penalty function approach (PFA) developed in Uhlig (2005) and Mountford and Uhlig (2009). The PFA consists of using a loss function to find an orthogonal matrix that satisfies the zero restrictions and that satisfies or comes close to satisfying the sign restrictions. Appendix G.2 provides the details on the PFA.

45. Appendix G.3 plots the posterior distribution of the threshold $\overline{ACR}$, together with the time series of the identified regimes using the median of the posterior $\overline{ACR}$.

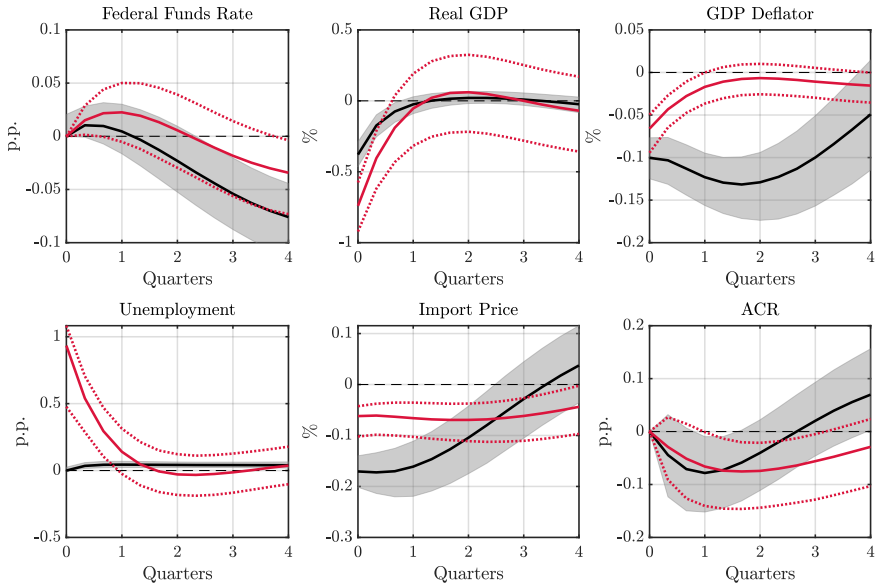

Figure 16: State-Dependent Effects of a Contractionary Monetary Policy Shock: Empirical Validation

Notes. The figure shows the IRFs to a one standard deviation contractionary monetary policy shock identified using Restriction 4 for both the supply chain disrupted and undisrupted regimes. The black solid (red solid) line shows the point-wise posterior medians, and the black shaded area (red dotted lines) depicts the 68% equal-tailed point-wise posterior probability bands for the supply chain disrupted (undisrupted) regime. The figure is based on 10,000 independent draws from the posterior.

6. Conclusion

Our study constructs the first index of global supply chain disruptions using data from the Automatic Identification System – a mandatory tracking system installed on containerships serving major ports worldwide – that was made publicly available since 2017. We quantify supply chain disruptions by estimating congestion in major global ports by developing a novel spatial clustering algorithm that tracks vessel positions and speeds in berth and anchorage areas within ports.

We develop a theoretical framework to study supply chain disruptions in the context of imbalances between the supply and demand for goods that generate changes in prices and spare capacity. Our framework demonstrates that disturbances to the supply chain reduce output and inflate prices, as in standard models, but also lead to an increase in the economy's spare capacity. The co-movements of spare capacity, prices, and output allow us to uniquely identify the supply chain shocks and explore their causal effects on macroeconomic

outcomes through an SVAR model with sign and zero restrictions. Our empirical model finds that supply chain shocks exert an immediate, large, and detrimental effect on real GDP and unemployment, while simultaneously causing a sharp rise in inflation.

We study the changes in the effectiveness of monetary policy consequent to supply chain disruptions. We show both theoretically and empirically that monetary policy exerts a stronger influence on inflation, albeit with diminished effect on output, during periods of supply chain disruptions. Therefore, disruptions to the supply chain enhance the effectiveness of contractionary monetary policy in taming inflation while reducing the sensitivity of output to the policy.

Our study opens several valuable avenues for future research. First, our new index reveals significant heterogeneity in the congestion of ports around the world. It would be interesting to study whether the spillovers between ports are primarily driven by geographical proximity or production synergies, and study the optimal redistribution of resources across ports in different locations to offset the negative impact of supply chain disruptions. Second, while our theoretical framework is based on single importer-exporter relationships to study the role of spare capacity, it would be worthwhile to extend the analysis to input-output networks and explore the role of spare capacity in the transmission of supply chain disruptions across firms in the network. The structure of the production network could potentially magnify or dampen the disturbances to the supply chain, which may trigger endogenous changes in the structure of the network, as recently documented in Ghassibe (2023). Third, with the incorporation of predictive analytics, our spatial clustering algorithm could be fine-tuned to anticipate supply chain disruptions by identifying and analyzing subtle changes in the positions and speeds of containerships, as recorded in real time by the AIS data. By effectively modeling these seemingly imperceptible changes, the algorithm could serve as a valuable tool for preemptive policy actions, enabling timely interventions to counter potential disruptions before they materialize. We plan to pursue some of these extensions in our future work.

References

Alessandria, George, Shafaat Yar Khan, Armen Khederlarian, Carter Mix, and Kim J. Ruhl. 2023. "The aggregate effects of global and local supply chain disruptions: 2020–2022." *Journal of International Economics,* 103788. ISSN: 0022-1996. https://doi.org/10.1016/j.jinteco.2023.103788.

Allen, Treb. 2014. "Information Frictions in Trade." *Econometrica* 82 (6): 2041–2083. ISSN: 0012-9682. https://doi.org/10.3982/ECTA10984.

Allen, Treb, and Costas Arkolakis. 2014. "Trade and the Topography of the Spatial Economy." *The Quarterly Journal of Economics* 129, no. 3 (May): 1085–1140. ISSN: 0033-5533. https://doi.org/10.1093/qje/qju016.

Arias, Jonas E., Dario Caldara, and Juan F. Rubio-Ramírez. 2019. "The systematic component of monetary policy in SVARs: An agnostic identification procedure." *Journal of Monetary Economics* 101 (January): 1–13. ISSN: 0304-3932. https://doi.org/10.1016/J.JMONECO.2018.07.011.

Arias, Jonas E., Jesús Fernández-Villaverde, Juan F. Rubio-Ramírez, and Minchul Shin. 2023. "The Causal Effects of Lockdown Policies on Health and Macroeconomic Outcomes." *American Economic Journal: Macroeconomics* 15, no. 3 (July): 287–319. https://www.aeaweb.org/articles?id=10.1257/mac.20210367.

Arias, Jonas E., Juan F. Rubio-Ramirez, and Daniel F. Waggoner. 2018. "Inference Based on Structural Vector Autoregressions Identified With Sign and Zero Restrictions: Theory and Applications." *Econometrica* 86 (2): 685–720. ISSN: 1468-0262. https://doi.org/10.3982/ECTA14468.

Attinasi, Maria Grazia, Mirco Balatti, Michele Mancini, and Luca Metelli. 2021. "Supply chain disruptions and the effects on the global economy." *Economic Bulletin*, Issue 8, ECB. https://www.ecb.europa.eu/pub/economic-bulletin/focus/2022/html/ecb.ebbox202108_01~e8ceebe51f.en.html.

Bai, Xiwen, and Yiliang Li. 2022. "The Congestion Effect of Oil Transportation and Its Trade Implications." *Working Paper.*

Bai, Xiwen, Zhongjun Ma, Yao Hou, Yiliang Li, and Dong Yang. 2023. "A Data-Driven Iterative Multi-Attribute Clustering Algorithm and Its Application in Port Congestion Estimation." *IEEE Transactions on Intelligent Transportation Systems,* 1–12. https://doi.org/10.1109/TITS.2023.3286477.

Baker, Scott R, Nicholas Bloom, and Steven J Davis. 2016. "Measuring Economic Policy Uncertainty." *The Quarterly Journal of Economics* 131 (4): 1593–1636. ISSN: 0033-5533. https://doi.org/10.1093/qje/qjw024.

Balleer, Almut, Sebastian Link, Manuel Menkhoff, and Peter Zorn. 2020. "Demand or Supply? Price Adjustment during the COVID-19 Pandemic." *IZA Discussion Paper No. 13568,* https://www.iza.org/publications/dp/13568/demand-or-supply-price-adjustment-during-the-covid-19-pandemic.

Bańbura, Marta, Domenico Giannone, and Lucrezia Reichlin. 2010. "Large Bayesian vector auto regressions." *Journal of Applied Econometrics* 25 (1): 71–92. https://doi.org/10.1002/jae.1137.

Barro, Robert J., and Herschel I. Grossman. 1971. "A General Disequilibrium Model of Income and Employment." *The American Economic Review* 61 (1): 82–93. http://www.jstor.org/stable/1910543.

Bekaert, Geert, Eric Engstrom, and Andrey Ermolov. 2020. "Aggregate Demand and Aggregate Supply Effects of COVID-19: A Real-time Analysis." *Finance and Economic Discussion Series 2020-049. Washington: Board of Governors of the Federal Reserve System,* https://doi.org/10.17016/FEDS.2020.049.

Benguria, Felipe. 2021. "The matching and sorting of exporting and importing firms: Theory and evidence." *Journal of International Economics* 131 (July): 103430. ISSN: 0022-1996. https://doi.org/10.1016/J.JINTECO.2021.103430.

Benigno, Gianluca, Julian di Giovanni, Jan J.J. Groen, and Adam I. Noble. 2022. "The GSCPI: A New Barometer of Global Supply Chain Pressures." *Federal Reserve Bank of New York Staff Reports No. 1017* (May). https://www.newyorkfed.org/research/staff_reports/sr1017.html..

Benigno, Pierpaolo, and Gauti B. Eggertsson. 2023. "It's Baaack: The Surge in Inflation in the 2020s and the Return of the Non-Linear Phillips Curve." *NBER Working Paper No. 31197,* https://doi.org/10.3386/w31197.

Benigno, Pierpaolo, and Luca Antonio Ricci. 2011. "The Inflation-Output Trade-Off with Downward Wage Rigidities." *American Economic Review* 101, no. 4 (June): 1436–66. https://doi.org/10.1257/aer.101.4.1436.

Bernanke, Ben S, and Ilian Mihov. 1998. "Measuring Monetary Policy." *The Quarterly Journal of Economics* 113 (3): 869–902. ISSN: 0033-5533. https://doi.org/10.1162/003355398555775.

Bhonsle, Jitendra. 2023. "Differences And Correlation Between Spot Rates And Contract Rates in Shipping." *Marine Insight*, May 11, 2023. Accessed July 26, 2023. https://www.marineinsight.com/maritime-law/differences-and-correlation-between-spot-rates-and-contract-rates-in-shipping/.

Bils, Mark, Yongsung Chang, and Sun-Bin Kim. 2011. "Worker Heterogeneity and Endogenous Separations in a Matching Model of Unemployment Fluctuations." *American Economic Journal: Macroeconomics* 3 (1): 128–154. http://www.jstor.org/stable/41237134.

Birant, Derya, and Alp Kut. 2007. "ST-DBSCAN: An algorithm for clustering spatial–temporal data." *Data & Knowledge Engineering* 60 (1): 208–221. ISSN: 0169-023X. https://doi.org/10.1016/J.DATAK.2006.01.013.

Bonadio, Barthélémy, Zhen Huo, Andrei A. Levchenko, and Nitya Pandalai-Nayar. 2021. "Global supply chains in the pandemic." *Journal of International Economics* 133 (November): 103534. ISSN: 0022-1996. https://doi.org/10.1016/J.JINTECO.2021.103534.

Brancaccio, Giulia, Myrto Kalouptsidi, and Theodore Papageorgiou. 2020. "Geography, transportation, and endogenous trade costs." *Econometrica* 88 (2): 657–691. https://doi.org/10.3982/ECTA15455.

Brancaccio, Giulia, Myrto Kalouptsidi, Theodore Papageorgiou, and Nicola Rosaia. 2023. "Search Frictions and Efficiency in Decentralized Transport Markets." *The Quarterly Journal of Economics* (May): qjad023. ISSN: 0033-5533. https://doi.org/10.1093/qje/qjad023.

Bratsiotis, George J., and Konstantinos Theodoridis. 2022. "Precautionary liquidity shocks, excess reserves and business cycles." *Journal of International Financial Markets, Institutions and Money* 77 (March): 101518. ISSN: 1042-4431. https://doi.org/10.1016/J.INTFIN.2022.101518.

Brinca, Pedro, Joao B. Duarte, and Miguel Faria-e-Castro. 2021. "Measuring labor supply and demand shocks during COVID-19." *European Economic Review* 139 (October): 103901. ISSN: 0014-2921. https://doi.org/10.1016/J.EUROECOREV.2021.103901.

Brown, Jennifer, Dominik Englert, and Jan Hoffmann. 2021. "International transport costs: Why and how to measure them?" *World Bank Blogs*, January 20, 2021. Accessed December 11, 2022. https://blogs.worldbank.org/transport/international-transport-costs-why-and-how-measure-them.

Burriel, Pablo, Iván Kataryniuk, Carlos Moreno Pérez, and Francesca Viani. 2023. "A New Supply Bottlenecks Index Based on Newspaper Data." *Banco de España Working Paper No. 2304,* https://doi.org/10.53479/25166.

Chaney, Thomas. 2014. "The Network Structure of International Trade." *American Economic Review* 104, no. 11 (November): 3600–3634. https://doi.org/10.1257/aer.104.11.3600.

Chen, Cathy W.S., and Jack C. Lee. 1995. "Bayesian Inference of Threshold Autoregressive Models." *Journal of Time Series Analysis* 16 (5): 483–492. ISSN: 1467-9892. https://doi.org/10.1111/J.1467-9892.1995.TB00248.X.

Chow, Gregory C, and An-loh Lin. 1971. "Best Linear Unbiased Interpolation, Distribution, and Extrapolation of Time Series by Related Series." *The Review of Economics and Statistics* 53 (4): 372–375. ISSN: 00346535, 15309142. https://doi.org/10.2307/1928739.

Comin, Diego A., Robert C. Johnson, and Callum J. Jones. 2023. "Supply Chain Constraints and Inflation." *NBER Working Paper No. 31179,* https://doi.org/10.3386/w31179.

Costinot, Arnaud, Jonathan Vogel, and Su Wang. 2013. "An Elementary Theory of Global Supply Chains." *The Review of Economic Studies* 80 (1): 109–144. ISSN: 0034-6527. https://doi.org/10.1093/restud/rds023.

del Rio-Chanona, R. Maria, Penny Mealy, Anton Pichler, François Lafond, and J. Doyne Farmer. 2020. "Supply and demand shocks in the COVID-19 pandemic: an industry and occupation perspective." *Oxford Review of Economic Policy* 36:S94–S137. ISSN: 14602121. https://doi.org/10.1093/OXREP/GRAA033.

Dempsey, Harry. 2022. "Is there an end in sight to supply chain disruption?" *Financial Times*, January 9, 2022. Accessed October 30, 2022. https://www.ft.com/content/21242e3b-298b-4a6f-a35f-32fdde905952.

den Haan, Wouter J., Garey Ramey, and Christian Haefke. 2005. "Turbulence and Unemployment in a Job Matching Model." *Journal of the European Economic Association* 3 (6): 1360–1385. http://www.jstor.org/stable/40004938.

di Giovanni, Julian, Şebnem Kalemli-Özcan, Alvaro Silva, and Muhammed A. Yildirim. 2022. "Global Supply Chain Pressures, International Trade, and Inflation." *NBER Working Paper No. 30240,* https://doi.org/10.3386/w30240.

Dunn, Jason, and Fernando Leibovici. 2023. "Navigating the Waves of Global Shipping: Drivers and Aggregate Implications." *Federal Reserve Bank of St. Louis Working Paper 2023-002,* https://doi.org/10.20955/wp.2023.002.

Eaton, Jonathan, and Samuel Kortum. 2002. "Technology, Geography, and Trade." *Econometrica* 70 (5): 1741–1779. ISSN: 0012-9682. https://doi.org/10.1111/1468-0262.00352.

Ester, Martin, Hans-Peter Kriegel, Jiirg Sander, and Xiaowei Xu. 1996. "A Density-Based Algorithm for Discovering Clusters in Large Spatial Databases with Noise." *KDD-96 Proceedings,* www.aaai.org.

Finck, David, and Peter Tillmann. 2022. "The macroeconomic effects of global supply chain disruptions." *BOFIT Discussion Paper No. 14/2022,* http://hdl.handle.net/10419/267906.

Forster van Aerssen, Katrin, Ramon Gomez-Salvador, Michel Soudan, and Tajda Spital. 2021. "The US and UK labour markets in the post-pandemic recovery." *Economic Bulletin*, Issue 8, ECB. https://www.ecb.europa.eu/pub/economic-bulletin/focus/2022/html/ecb.ebbox202108_02~0b5bde72b4.en.html.

Fuchs, Simon, and Woan Foong Wong. 2022. "Multimodal Transport Networks." *Federal Reserve Bank of Atlanta Working Paper No. 2022-13,* https://doi.org/10.29338/wp2022-13.

Fujita, Shigeru. 2018. "Declining labor turnover and turbulence." *Journal of Monetary Economics* 99 (November): 1–19. ISSN: 0304-3932. https://doi.org/10.1016/J.JMONECO.2017.12.005.

Fujita, Shigeru, and Garey Ramey. 2012. "Exogenous versus Endogenous Separation." *American Economic Journal: Macroeconomics* 4 (4): 68–93. https://doi.org/10.1257/mac.4.4.68.

Gagliardone, Luca, and Mark Gertler. 2023. "Oil Prices, Monetary Policy and Inflation Surges." *NBER Working Paper No. 31263,* https://doi.org/10.3386/w31263.

Ghassibe, Mishel. 2023. "Endogenous Production Networks and Non-Linear Monetary Transmission." *CREi Working Paper Series.*

Ghassibe, Mishel, and Francesco Zanetti. 2022. "State dependence of fiscal multipliers: the source of fluctuations matters." *Journal of Monetary Economics* (September). ISSN: 0304-3932. https://doi.org/10.1016/J.JMONECO.2022.09.003.

Giacomini, Raffaella, and Toru Kitagawa. 2021. "Robust Bayesian Inference for Set-Identified Models." *Econometrica* 89 (4): 1519–1556. ISSN: 0012-9682. https://doi.org/10.3982/ECTA16773.

Gordon, Matthew V., and Todd E. Clark. 2023. "The Impacts of Supply Chain Disruptions on Inflation." *Federal Reserve Bank of Cleveland, Economic Commentary 2023-08*, May 10, 2023. Accessed July 12, 2023. https://doi.org/10.26509/frbc-ec-202308.

Grimes, Christopher, and Andrew Edgecliffe-Johnson. 2021. "The supply chain crisis and US ports: 'Disruption on top of disruption'." *Financial Times*, October 14, 2021. Accessed May 30, 2022. https://www.ft.com/content/aa24d82e-16c7-4e3e-868e-42bd32f593be.

Hall, Robert E. 2005. "Employment Fluctuations with Equilibrium Wage Stickiness." *American Economic Review* 95, no. 1 (March): 50–65. https://doi.org/10.1257/0002828053828482.

Harding, Martín, Jesper Lindé, and Mathias Trabandt. 2023. "Understanding Post-COVID Inflation Dynamics." *Journal of Monetary Economics,* ISSN: 0304-3932. https://doi.org/10.1016/j.jmoneco.2023.05.012.

Heiland, Inga, Andreas Moxnes, Karen Helene Ulltveit-Moe, and Yuan Zi. 2022. "Trade From Space: Shipping Networks and The Global Implications of Local Shocks." *Working Paper.*

Howitt, Peter, and R. Preston McAfee. 1987. "Costly Search and Recruiting." *International Economic Review* 28 (1): 89–107. http://www.jstor.org/stable/2526861.

Ikeda, Daisuke, Shangshang Li, Sophocles Mavroeidis, and Francesco Zanetti. 2022. "Testing the Effectiveness of Unconventional Monetary Policy in Japan and the United States." *CAMA Working Paper 68/2022* (October). https://cama.crawford.anu.edu.au/publication/cama-working-paper-series/20722/testing-effectiveness-unconventional-monetary-policy.

Kalouptsidi, Myrto. 2014. "Time to Build and Fluctuations in Bulk Shipping." *American Economic Review* 104, no. 2 (February): 564–608. https://doi.org/10.1257/aer.104.2.564.

Kamali, Parisa, and Alex Wang. 2021. "Longer Delivery Times Reflect Supply Chain Disruptions." *IMF Blog*, October 25, 2021. Accessed October 31, 2022. https://www.imf.org/en/Blogs/Articles/2021/10/25/longer-delivery-times-reflect-supply-chain-disruptions.

Känzig, Diego R. 2021. "The Macroeconomic Effects of Oil Supply News: Evidence from OPEC Announcements." *American Economic Review* 111 (4): 1092–1125. ISSN: 0002-8282. https://doi.org/10.1257/AER.20190964.

Karimi-Mamaghan, Maryam, Mehrdad Mohammadi, Amir Pirayesh, Amir Mohammad Karimi-Mamaghan, and Hassan Irani. 2020. "Hub-and-spoke network design under congestion: A learning based metaheuristic." *Transportation Research Part E: Logistics and Transportation Review* 142 (October): 102069. ISSN: 1366-5545. https://doi.org/10.1016/J.TRE.2020.102069.

Kasahara, Hiroyuki, and Beverly Lapham. 2013. "Productivity and the decision to import and export: Theory and evidence." *Journal of International Economics* 89 (2): 297–316. ISSN: 0022-1996. https://doi.org/10.1016/J.JINTECO.2012.08.005.

Kilian, Lutz, and Daniel P Murphy. 2012. "Why Agnostic Sign Restrictions Are Not Enough: Understanding the Dynamics of Oil Market VAR Models." *Journal of the European Economic Association* 10 (5): 1166–1188. ISSN: 1542-4766. https://doi.org/10.1111/j.1542-4774.2012.01080.x.

Klachkin, Oren. 2021. "Supply-chain headwinds pummel the economy." *Research Briefing US*, September 22, 2021. Accessed October 31, 2022. https://resources.oxfordeconomics.com/hubfs/press-release/Supply-chain-headwinds-pummel-the-economy.pdf.

Krolikowski, Pawel M, and Andrew H McCallum. 2021. "Goods-market frictions and international trade." *Journal of International Economics* 129:103411. ISSN: 0022-1996. https://doi.org/10.1016/j.jinteco.2020.103411.

Lane, Philip R. 2022. "Bottlenecks and monetary policy." *The ECB Blog*, February 10, 2022. Accessed October 31, 2022. https://www.ecb.europa.eu/press/blog/date/2022/html/ecb.blog220210~1590dd90d6.en.html.

Lenoir, Clémence, Julien Martin, and Isabelle Mejean. 2022. "Search Frictions in International Goods Markets." *Journal of the European Economic Association* (August). ISSN: 1542-4766. https://doi.org/10.1093/jeea/jvac044.

Leyva, Gustavo, and Carlos Urrutia. 2022. "Informal labor markets in times of pandemic." *Review of Economic Dynamics* (January). ISSN: 1094-2025. https://doi.org/10.1016/J.RED.2022.01.002.

Li, Yiliang, Xiwen Bai, Qi Wang, and Zhongjun Ma. 2022. "A big data approach to cargo type prediction and its implications for oil trade estimation." *Transportation Research Part E: Logistics and Transportation Review* 165 (September): 102831. ISSN: 13665545. https://doi.org/10.1016/J.TRE.2022.102831.

Litterman, Robert B. 1986. "Forecasting with Bayesian Vector Autoregressions: Five Years of Experience." *Journal of Business & Economic Statistics* 4 (1): 25–38. ISSN: 07350015. https://doi.org/10.2307/1391384.

Lopes, Hedibert F, and Esther Salazar. 2006. "Bayesian Model Uncertainty In Smooth Transition Autoregressions." *Journal of Time Series Analysis* 27 (1): 99–117. https://doi.org/10.1111/j.1467-9892.2005.00455.x.

Mathieu, Edouard, Hannah Ritchie, Lucas Rodés-Guirao, Cameron Appel, Charlie Giattino, Joe Hasell, Bobbie Macdonald, et al. 2020. "Coronavirus Pandemic (COVID-19)." *Our World in Data,* https://ourworldindata.org/coronavirus.

Melitz, Jacques, and Farid Toubal. 2014. "Native language, spoken language, translation and trade." *Journal of International Economics* 93 (2): 351–363. ISSN: 0022-1996. https://doi.org/10.1016/j.jinteco.2014.04.004.

Melitz, Marc J. 2003. "The Impact of Trade on Intra-Industry Reallocations and Aggregate Industry Productivity." *Econometrica* 71 (6): 1695–1725. https://doi.org/10.1111/1468-0262.00467.

Menzio, Guido, and Shouyong Shi. 2011. "Efficient Search on the Job and the Business Cycle." *Journal of Political Economy* 119 (3): 468–510. https://doi.org/10.1086/660864.

Michaillat, Pascal, and Emmanuel Saez. 2015. "Aggregate Demand, Idle Time, and Unemployment." *The Quarterly Journal of Economics* 130 (2): 507–569. ISSN: 0033-5533. https://doi.org/10.1093/QJE/QJV006.

———. 2022. "An economical business-cycle model." *Oxford Economic Papers* 74 (2): 382–411. ISSN: 0030-7653. https://doi.org/10.1093/OEP/GPAB021.

Mountford, Andrew, and Harald Uhlig. 2009. "What are the effects of fiscal policy shocks?" *Journal of Applied Econometrics* 24 (6): 960–992. ISSN: 1099-1255. https://doi.org/10.1002/JAE.1079.

Mumtaz, Haroon, and Francesco Zanetti. 2012. "Neutral Technology Shocks and the Dynamics Of Labor Input: Results from an Agnostic Identification." *International Economic Review* 53 (1): 235–254. https://doi.org/10.1111/j.1468-2354.2011.00678.x.

———. 2015. "Labor Market Dynamics: A Time-Varying Analysis." *Oxford Bulletin of Economics and Statistics* 77 (3): 319–338. https://doi.org/10.1111/obes.12096.

Naudé, Wim, and Marianne Matthee. 2011. "The impact of transport costs on new venture internationalisation." *Journal of International Entrepreneurship* 9 (1): 62–89. ISSN: 1573-7349. https://doi.org/10.1007/s10843-010-0066-6.

Notteboom, Theo, Athanasios Pallis, and Jean-Paul Rodrigue. 2022. *Port Economics, Management and Policy.* 1st ed. Routledge, January. ISBN: 9780429318184. https://doi.org/10.4324/9780429318184.

OECD and EUIPO. 2021. *Misuse of Containerized Maritime Shipping in the Global Trade of Counterfeits.* OECD, February. ISBN: 9789264320086. https://doi.org/10.1787/e39d8939-en.

Pizzinelli, Carlo, Konstantinos Theodoridis, and Francesco Zanetti. 2020. "State Dependence in Labor Market Fluctuations." *International Economic Review* 61 (3): 1027–1072. ISSN: 1468-2354. https://doi.org/10.1111/IERE.12448.

Plagborg-Møller, Mikkel, and Christian K. Wolf. 2021. "Local Projections and VARs Estimate the Same Impulse Responses." *Econometrica* 89 (2): 955–980. ISSN: 0012-9682. https://doi.org/10.3982/ECTA17813.

Ramondo, Natalia, and Andrés Rodríguez-Clare. 2013. "Trade, Multinational Production, and the Gains from Openness." *Journal of Political Economy* 121 (2): 273–322. ISSN: 0022-3808. https://doi.org/10.1086/670136.

Rodrigue, Jean-Paul. 2020. *The Geography of Transport Systems.* 5th ed. Routledge, May. ISBN: 9780429346323. https://doi.org/10.4324/9780429346323.

Rubio-Ramirez, Juan F., Daniel F. Waggoner, and Tao Zha. 2010. "Structural Vector Autoregressions: Theory of Identification and Algorithms for Inference." *The Review of Economic Studies* 77 (2): 665–696. https://www.jstor.org/stable/40587642.

Samuelson, Paul A. 1954. "The Transfer Problem and Transport Costs, II: Analysis of Effects of Trade Impediments." *The Economic Journal* 64, no. 254 (June): 264–289. ISSN: 0013-0133. https://doi.org/10.2307/2226834.

Shapiro, Adam Hale. 2022. "How Much Do Supply and Demand Drive Inflation?" *FRBSF Economic Letter 2022-15*, June 21, 2022. Accessed November 2, 2022. https://www.frbsf.org/economic-research/publications/economic-letter/2022/june/how-much-do-supply-and-demand-drive-inflation/.

Smirnyagin, Vladimir, and Aleh Tsyvinski. 2022. "Macroeconomic and Asset Pricing Effects of Supply Chain Disasters." *NBER Working Paper No. 30503,* https://doi.org/10.3386/w30503.

Song, Dong-Ping, and Jing-Xin Dong. 2012. "Cargo routing and empty container repositioning in multiple shipping service routes." *Transportation Research Part B: Methodological* 46 (10): 1556–1575. ISSN: 0191-2615. https://doi.org/https://doi.org/10.1016/j.trb.2012.08.003.

Stamer, Vincent. 2021. "Thinking Outside the Container: A Sparse Partial Least Squares Approach to Forecasting Trade Flows." *Kiel Working Papers No. 2179,* https://www.ifw-kiel.de/experts/ifw/vincent-stamer/thinking-outside-the-container-a-sparse-partial-least-squares-approach-to-forecasting-trade-flows-15754/.

Stopford, Martin. 2008. *Maritime Economics.* 3rd ed. London: Routledge. https://doi.org/https://doi.org/10.4324/9780203891742.

Talley, Wayne K., and Man Wo Ng. 2016. "Port multi-service congestion." *Transportation Research Part E: Logistics and Transportation Review* 94 (October): 66–70. ISSN: 13665545. https://doi.org/10.1016/J.TRE.2016.07.005.

The White House. 2021. "Fact Sheet: Biden Administration Efforts to Address Bottlenecks at Ports of Los Angeles and Long Beach: Moving Goods from Ship to Shelf." *The White House Briefing Room*, October 13, 2021. Accessed: 27 August, 2023. https://www.whitehouse.gov/briefing-room/statements-releases/2021/10/13/fact-sheet-biden-administration-efforts-to-address-bottlenecks-at-ports-of-los-angeles-and-long-beach-moving-goods-from-ship-to-shelf/.

Uhlig, Harald. 2005. "What are the effects of monetary policy on output? Results from an agnostic identification procedure." *Journal of Monetary Economics* 52 (2): 381–419. ISSN: 0304-3932. https://doi.org/10.1016/J.JMONECO.2004.05.007.

UNCTAD. 2019. "Review of Maritime Transport 2019." *United Nations*, November 1, 2019. Accessed December 20, 2022. https://unctad.org/webflyer/review-maritime-transport-2019.

———. 2021. "Global Transport Costs Dataset for International Trade." *UNCTADstat*, January 20, 2021. Accessed December 10, 2022. https://unctadstat.unctad.org/wds/TableViewer/tableView.aspx?ReportId=207046.

Wang, Yadong, Qiang Meng, and Peng Jia. 2019. "Optimal port call adjustment for liner container shipping routes." *Transportation Research Part B: Methodological* 128:107–128. ISSN: 0191-2615. https://doi.org/10.1016/j.trb.2019.07.015.

Williamson, Chris. 2021. "Understanding…PMI suppliers' delivery times: A widely used indicator of supply delays, capacity constraints and price pressures." *PMI Research & Analysis, IHS Markit,* https://ihsmarkit.com/research-analysis/understanding--pmi-suppliers-delivery-times-a-widely-used-indicator-of-supply-delays-capacity-constraints-and-price-pressures-Jul21.html.

Wong, Woan Foong. 2022. "The Round Trip Effect: Endogenous Transport Costs and International Trade." *American Economic Journal: Applied Economics* 14 (4): 127–166. https://doi.org/10.1257/app.20190721.

World Bank. 2022. *Global Economic Prospects, June 2022.* Washington, DC: World Bank. https://doi.org/10.1596/978-1-4648-1843-1.

Online Appendices

A. A Density-Based Spatial Clustering Algorithm

In this appendix, we provide the technical details of our density-based spatial clustering algorithm, namely the iterative, multi-attribute, density-based spatial clustering of applications with noise (IMA-DBSCAN).[1] This algorithm is used to estimate port congestion for major container ports worldwide.[2] In subsequent sections, we first delve into the methodology underpinning our algorithm. We then present an illustrative case where we apply the algorithm to the Port of Ningbo-Zhoushan in China, demonstrating its capability to identify anchorage and berth areas of a port where other methods fall short.

A.1. Methodology

As depicted in Figure A.1, the proposed IMA-DBSCAN algorithm has several distinct features. Foremost among these is its two-tiered, iterative structure. At the first level, we extract the trajectory of each containership at every port in question from the AIS data. For each ship, a traditional DBSCAN (Ester et al. 1996) is employed to filter out noise and cluster all its mooring points. While this level can pinpoint mooring areas, it does not adequately differentiate between anchorage and berth areas of a port. The second level addresses this limitation. Here, a spatial-temporal-DBSCAN (ST-DBSCAN; see Birant and Kut (2007)) is applied to the clustering. During this phase, we employ an iterative method to determine a generalized and optimal parameter setting for the clustering algorithm. Another hallmark of IMA-DBSCAN is its integration of multiple attributes at the second level. Beyond spatial data (like coordinates), we also weave in non-spatial information (such as headings and timestamps) to enhance clustering accuracy. In the sections that follow, we elaborate on the specifics of each level of IMA-DBSCAN.

1. Most of the details provided in this appendix can also be found in the companion paper (Bai et al. 2023).
2. See https://www.worldshipping.org/top-50-ports (Accessed June 15, 2022) for the full list of ports. The Port of Tokyo Ko, Japan, is not included as its observations are merged with those of the Port of Keihin, Japan.

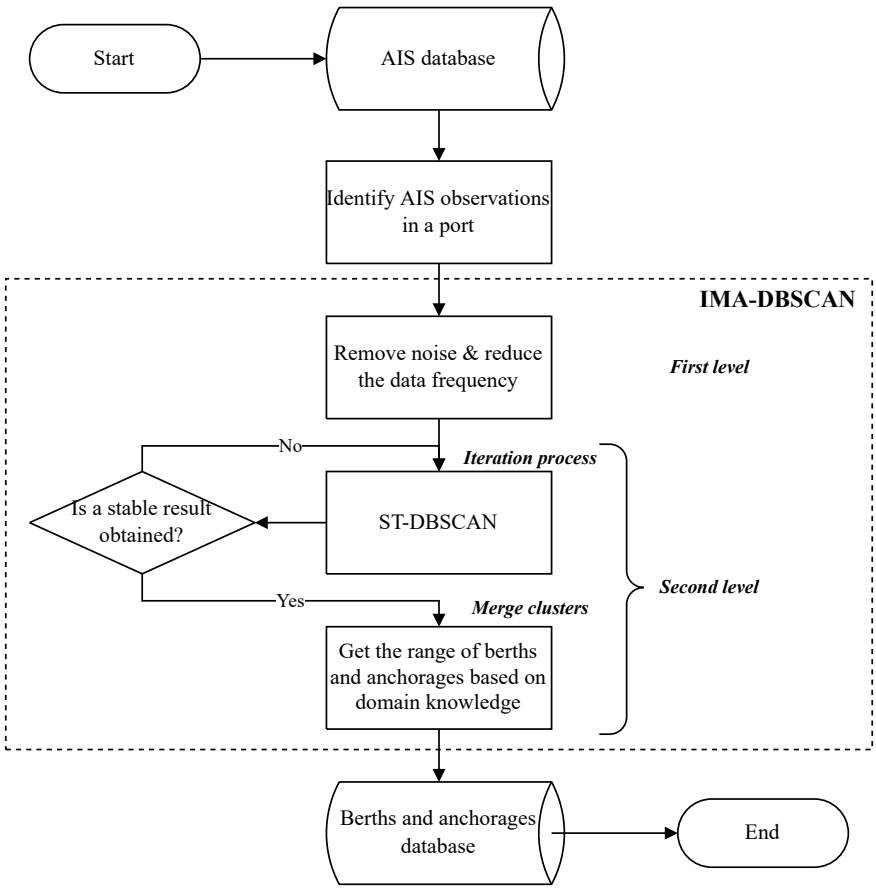

Figure A.1: Methodology Framework of IMA-DBSCAN

A.1.1. The First Level – Data Pre-Processing

While AIS data provides detailed information on the positions of each ship, direct clustering of these positions to determine the anchorage and berth areas of a port presents several challenges. Firstly, even if we restrict the data to a specific port area within a certain timeframe, the sheer volume of records means that inputting them directly into DBSCAN would lead to extended processing times. Secondly, a high incidence of incorrect AIS signal assignments could result in inaccurate clustering outcomes, such as identifying a cluster that is not an actual berth or one that covers an unusually large geographical area. Thirdly, if a ship stays in a port area for an extended period (e.g., for maintenance), the dense AIS data could lead DBSCAN to mistakenly identify it as a cluster. Given these challenges, it is essential to preprocess the AIS data before using it to pinpoint the anchorage and berth areas of a port.

In the first level of IMA-DBSCAN, we begin by filtering the AIS data for each ship in the port area, focusing on records indicating speeds of less than one knot. Such positions suggest that a ship is either berthed, anchored, or in an unusual situation (e.g., under maintenance). We then tally these positions; if their number falls outside an acceptable range (e.g., less than 100 or more than 100,000), we deem the ship's data abnormal and exclude it from further analysis. Since a ship might dock at a port multiple times, we establish a period, Δt (e.g., 12 hours), as the cut-off between two consecutive arrivals. If the gap between two arrivals exceeds Δt, we treat them as separate port calls. To streamline the data while maintaining consistency, we retain only the first data point for each hour. For every port call of a ship, its positions are clustered using the traditional DBSCAN with parameters *Eps* and $MinPts$. We choose an *Eps* value small enough to identify the ship's mooring areas and an appropriate $MinPts$ value to ensure transient stops are classified as noise. At this stage, the AIS data preprocessing is complete. The refined samples are then used to identify the anchorage and berth areas of a port in the second level of IMA-DBSCAN. For reference, the pseudo-code for the first level of IMA-DBSCAN is detailed in Algorithm 1.

A.1.2. The Second Level – Multiple Attributes and Iteration

Information on Headings. As highlighted in the main text, AIS data integrates both spatial (i.e., geographical coordinates) and non-spatial (i.e., headings) information. In Figure 1 from the main text, we illustrate the positions of a ship in a port alongside their headings. We observe that the headings of a ship at a berth are either aligned in the same direction or are exact opposites. In contrast, headings in an anchorage area appear random, with no discernible pattern. This observation aligns with real-world scenarios, where ships in anchorage areas often struggle to maintain consistent headings over time due to significant wind and wave variations.

Consequently, in the second level of IMA-DBSCAN, we leverage this heading information to enhance estimation accuracy.[3] Specifically, IMA-DBSCAN incorporates three parameters,

3. Such non-spatial information is also useful when we distinguish between different berths (see Algorithm 2). In our initial experiment, the coordinates could only help us identify the approximate locations of anchorage and berth areas of a port, not to mention the exact number of berths.

as opposed to the traditional two in DBSCAN. These are $Eps1$, $Eps2$, and $MinPts$. Here, $Eps1$ denotes the maximum geographical coordinate (spatial) distance, $Eps2$ represents the maximum non-spatial distance between two headings, and $MinPts$ is the minimum number of points within the distances defined by $Eps1$ and $Eps2$. The geographical coordinate (spatial) distance D is calculated using the Haversine formula:

$$D\Big[(x_1, x_2), (y_1, y_2)\Big] = 2 \cdot R \cdot \arcsin\left[\sqrt{\sin^2\left(\frac{x_1 - y_1}{2}\right) + \cos x_1 \cos y_1 \sin^2\left(\frac{x_2 - y_2}{2}\right)}\right], \quad \text{(A.1)}$$

where the coordinates are measured in radians, and $R = 6,371$ is the mean radius of Earth in kilometers. On the other hand, the non-spatial distance Δh is calculated as:

$$\Delta h(h_1, h_2) = \begin{cases} |h_1 - h_2|\,, & \text{if } |h_1 - h_2| \leq 180°; \\ 360° - |h_1 - h_2|\,, & \text{otherwise.} \end{cases} \quad \text{(A.2)}$$

With the two measures of distance defined above, the neighbors of a point are those with geographical coordinate (spatial) distance less than $Eps1$ and non-spatial distance less than $Eps2$, and a core is defined as a point with more than or equivalent to $MinPts$ neighbors. The clusters in IMA-DBSCAN contain only these cores.

Iteration Process. As previously discussed, there are three parameters to set in IMA-DBSCAN. Given that the geographical shapes of anchorage and berth areas vary significantly across ports, the values of these three parameters should ideally differ to achieve optimal estimation results. Therefore, we propose an iterative method to determine these parameter values. Specifically, while we fix $Eps2$ at 1°, our method allows the values of $Eps1$ and $MinPts$ to vary between different ports. During the iteration process, we define four intermediate variables: $Dist$, m, m', and $NumC$. Here, $Dist$ represents the average distance between a point in a cluster and the center of its respective cluster. m denotes the number of points, while m' represents the number of noisy points (initialized to zero). Lastly, $NumC$ indicates the number of clusters.[4] Using these intermediate variables, $MinPts$ and $Eps1$

4. Since there are no clusters at initialization, we treat all points as if they were part of the same cluster. Additionally, if all points are classified as noise, we set $NumC = 1$.

are calculated as:

$$Eps1 = \alpha \cdot Dist,\ MinPts = \beta \cdot \frac{m - m'}{NumC}.$$

Regarding α and β, even though there is no explicit constraint on their values, they should fall within a reasonable range to ensure both the algorithm's convergence and the validity of the identification results. After evaluating the performance of IMA-DBSCAN under various parameter settings, we find that an admissible range of ($0.4 \leq \alpha \leq 0.6$, $0.06 \leq \beta \leq 0.1$) is appropriate. We also introduce an intermediate variable, $Dist_0$, which records the value of $Dist$ from the previous iteration and is initialized to zero.

Following this, we iteratively execute ST-DBSCAN. In each iteration, ST-DBSCAN operates with $Eps1$ and $MinPts$ set to their current values, and $Eps2$ set to 1°. The outputs classify each point either into a cluster or as noise. Based on these outputs, the values of the intermediate variables, as well as those for $Eps1$ and $MinPts$, are updated. These updated values are then re-applied in ST-DBSCAN for the subsequent iteration. The entire process concludes when the difference $Dist - Dist_0$ is less than or equal to $\Delta Dist$ (e.g., 100 m). Consequently, each point is either assigned to a cluster or labeled as noise. We then interpret the cluster areas as berths and the areas of noisy points as anchorages.

Information on Timestamp. After running ST-DBSCAN, we find that there exists a large proportion of clusters that should be merged together as they essentially represent the same berth in reality. To achieve a more accurate identification of berth areas, we merge certain clusters by taking advantage of the time information (i.e., timestamps) in the AIS data (see Figure A.2 for an illustration). More precisely, we first calculate the start and end times of each port call in each cluster. Subsequently, since only one ship can dock at a berth for a given moment, for each cluster under consideration, we find the cluster that is the closest to it, and then check whether there is any overlap in the docking times. If there exists (at least) one overlap, the two clusters are considered to represent two different berths. If there is no overlap, the two clusters are merged together to represent one berth.

Furthermore, in order to differentiate between different anchorage areas, we perform another DBSCAN on those points that are classified as noise. In the process, the two parameters associated with the DBSCAN, i.e, Eps' and $MinPts'$, are set according to our

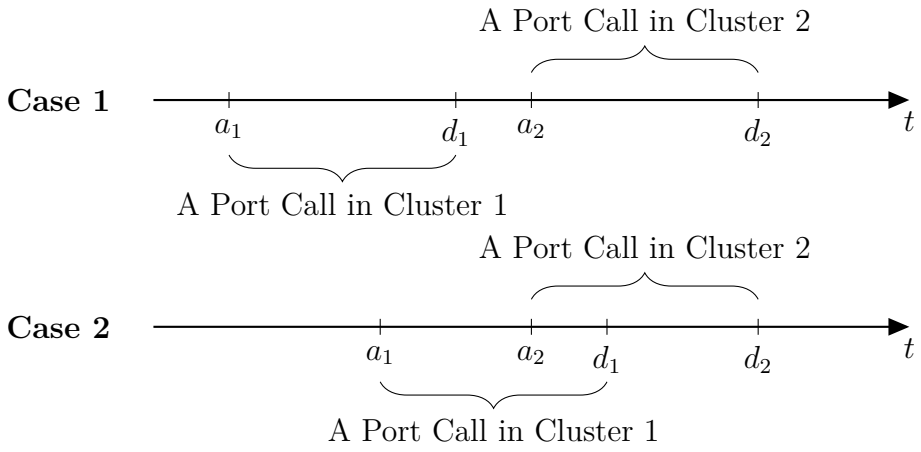

Figure A.2: Merging Clusters

Notes. The figure illustrates two scenarios and discusses the criteria for merging clusters after executing ST-DBSCAN on the second level. Here, a_1 and d_1 represent the arrival and departure times of a ship during a port call assigned to cluster 1. Similarly, a_2 and d_2 correspond to the times for a port call assigned to cluster 2, which is geographically the closest to cluster 1. In the first scenario, there is no overlap in the docking times, so clusters 1 and 2 are merged. In contrast, the second scenario shows an overlap in the docking times. As a result, clusters 1 and 2 are kept distinct since two ships cannot occupy a single berth simultaneously.

domain knowledge. Finally, we remove clusters with less than N port calls, with N set according to our domain knowledge. For reference, the pseudo-codes for the second level of IMA-DBSCAN can be found in Algorithms 2, 3, and 4.

Lastly, in the estimation of port congestion for the major container ports worldwide, the parameter values set for IMA-DBSCAN are provided in Table A.1.

Table A.1: Parameter Values for IMA-DBSCAN

	Parameter	**Value**
First Level	Δt	12 hours
	Eps	50 m
	$MinPts$	10
Second Level	α	0.5
	β	0.08
	$\Delta Dist$	100 m
	Eps'	1,000 m
	$MinPts'$	50
	N	5

Algorithm 1 Level 1 IMA-DBSCAN

Inputs:

$A_l = \{a_{1,l}, \ldots, a_{n,l}\}$: the set of coordinates recorded in the AIS data for a ship l
$S_l = \{s_{1,l}, \ldots, s_{n,l}\}$: the set of speeds recorded in the AIS data for a ship l
$T_l = \{t_{1,l}, \ldots, t_{n,l}\}$: the set of timestamps recorded in the AIS data for a ship l

Outputs:

$D_l = \{d_{1,l}, \ldots, d_{m,l}\}$: the coordinates of the first observation for each hour in B_l
$H_l = \{h_{1,l}, \ldots, h_{m,l}\}$: the headings of the first observation for each hour in B_l

/ Data Pre-Processing */*
$B_l = \{b_{1,l} \ldots b_{k,l}\} \leftarrow$ the set of coordinates in A_l that indicate a speed less than 1 knot
/ Exception Identification */*
if $|B_l| < 100$ **or** $|B_l| > 100,000$ **then**
    Remove the data and stop ▷ *The ship has an abnormal port call*
else
    Continue
end if
/ DBSCAN Clustering */*
$X \leftarrow b_{1,l}$
for $i \leftarrow 2 : k$ **do**
    if $t_i - t_{i-1} \leq \Delta t$ **then**
        Append $b_{i,l}$ to X
    else
        $DBSCAN(X, Eps, MinPts)$
        $X \leftarrow \emptyset$
        Append $b_{i,l}$ to X
    end if
end for
Remove the observations labeled as noise from B_l
Keep only the first observation for each hour in B_l ▷ *Note that only m observations remain in B_l at this stage*
$D_l = \{d_{1,l}, \ldots, d_{m,l}\} \leftarrow$ the coordinates of the first observation for each hour in B_l
$H_l = \{h_{1,l}, \ldots, h_{m,l}\} \leftarrow$ the headings of the first observation for each hour in B_l

Algorithm 2 Level 2 IMA-DBSCAN

Inputs:

$\boldsymbol{D} = \{D_1, \ldots, D_L\}$: the set of coordinates for all ships after Level 1 IMA-DBSCAN
$\boldsymbol{H} = \{H_1, \ldots, H_L\}$: the set of headings for all ships after Level 1 IMA-DBSCAN
$\boldsymbol{O} = \{\boldsymbol{D}, \boldsymbol{H}\} = \{o_1, \ldots, o_M\}$: the combined set of coordinates and headings

Outputs:

C_{berth}: the set of clusters marked as berths
$C_{anchorage}$: the set of clusters marked as anchorages

/ Parameter Initialization */*
$Dist \leftarrow$ the average distance between a point in $\boldsymbol{D}$ and the center of the mass of $\boldsymbol{D}$
$m \leftarrow |\boldsymbol{D}|$
$Eps1 \leftarrow \alpha \cdot Dist$
$MinPts \leftarrow \beta \cdot m$
/ Iteration Process */*
$Dist_0 \leftarrow 0$
while $Dist - Dist_0 > \Delta Dist$ km **do**
    $ST - DBSCAN(\boldsymbol{O}, Eps1, Eps2 = 1°, MinPts)$ ▷ *See function ST-DBSCAN*
    $Dist_0 \leftarrow Dist$
    $Dist \leftarrow$ the average distance between a non-noisy point in $\boldsymbol{D}$ and the center of the mass of its assigned cluster
    $m' \leftarrow |$noisy points in $\boldsymbol{O}|$
    $NumC \leftarrow |$clusters in $\boldsymbol{O}|$
    $Eps1 \leftarrow \alpha \cdot Dist$
    $MinPts \leftarrow \beta \cdot (m - m') / NumC$
end while
/ Merging Clusters */*
Use the center of the mass of each cluster to calculate the distance in between
for all clusters c in $\boldsymbol{O}$ **do**
    $c' \leftarrow$ the nearest cluster less than 500 m away from c
    if the docking times of c' and c do not overlap **then**
        Replace the cluster label of c' with that of c
    end if
end for
/ Berth and Anchorage Detection */*
$C_{berth} \leftarrow$ clusters in $\boldsymbol{O}$
$C_{anchorage} \leftarrow DBSCAN($Noisy points in $\boldsymbol{O}, Eps', MinPts')$
/ Exception Removal */*
for all clusters c **in** C_{berth} **and** $C_{anchorage}$ **do**
    $NumP \leftarrow$ the number of port calls in cluster c
    if $NumP < N$ **then**
        Remove c
    end if
end for

Algorithm 3 ST-DBSCAN

Inputs:

$\boldsymbol{O} = \{o_1, \ldots, o_M\}$: the combined set of coordinates and headings
$Eps1$: maximum geographical coordinate (spatial) distance
$Eps2$: maximum non-spatial distance
$MinPts$: minimum number of points within the distance of $Eps1$ and $Eps2$

Outputs:

$C = \{c_1, \ldots, c_M\}$: the set of clusters in $\boldsymbol{O}$

```
/* The codes are adapted from those in Birant and Kut (2007).                    */
function ST − DBSCAN(D, Eps1, Eps2, MinPts)
    ClusterLabel = 0
    for i ← 1 : m do
        if o_i is not in a cluster then
            Y ← RetrieveNeighbors(o_i, Eps1, Eps2)    ▷ See function RetrieveNeighbors
            if |Y| < MinPts then
                Mark o_i as noise
            else                                                ▷ Construct a new cluster
                ClusterLabel ← ClusterLabel + 1
                for j ← 1 : |Y| do
                    Mark all objects in Y with current ClusterLabel
                end for
                Push(all objects in Y)
                while not IsEmpty() do
                    CurrentObj = Pop()
                    Z ← RetrieveNeighbors(CurrentObj, Eps1, Eps2)
                    if |Z| ≥ MinPts then
                        for all objects o in Z do
                            if o is not marked as noise or it is not in a cluster then
                                Mark o with current ClusterLabel
                                Push(o)
                            end if
                        end for
                    end if
                end while
            end if
        end if
    end for
    C = {c_1, ..., c_M} ← the set of clusters in O
end function
```

Algorithm 4 RetrieveNeighbors

Inputs:

o: an observation in $\boldsymbol{O}$
$Eps1$: maximum geographical coordinate (spatial) distance
$Eps2$: maximum non-spatial distance

Outputs:

$Neighbors$: the set of neighbors for o

function $RetrieveNeighbors(o, Eps1, Eps2)$
  $Neighbors \leftarrow \emptyset$
  for all observations o' **in** O **do**
    $Dist1 \leftarrow D(o, o')$ ▷ *See Equation* (A.1)
    $Dist2 \leftarrow \Delta h(o, o')$ ▷ *See Equation* (A.2)
    if $Dist1 \leq Eps1$ **and** $Dist2 \leq Eps2$ **then**
      Append o' to $Neighbors$
    end if
  end for
  return $Neighbors$
end function

A.2. Illustrative Case: Port of Ningbo-Zhoushan, China

To demonstrate the capability of IMA-DBSCAN in accurately identifying anchorage and berth areas of a port, which other methods might fail to achieve, we apply the algorithm to the Port of Ningbo-Zhoushan in China. We choose this specific example primarily due to its intricate port layout. Figure A.3a showcases the first 50,000 AIS observations from January 2020 within the Port of Ningbo-Zhoushan.[5] The observations are represented by blue dots on the map, with each dot indicating the position of a low-speed containership. Before applying IMA-DBSCAN to the AIS data, we mark the approximate locations of anchorages and berths using both satellite images and nautical charts as benchmarks. The red boxes indicate the anchorage areas, while the yellow rectangles denote the berth locations.

Figure A.3b presents the clustering results of IMA-DBSCAN for the Port of Ningbo-Zhoushan, mirroring the map in Figure A.3a for a direct comparison between our algorithm's

5. This example focuses on a one-month snapshot. It is reasonable to assume that the identification results would be indicative of anchorage and berth areas in subsequent months, given that we do not expect significant short-term changes in the port areas. In real-world applications of IMA-DBSCAN, periodic identification can be conducted to monitor potential changes in port anchorages and berths.

outcomes and the actual observations. The clusters in Figure A.3b (colored in red, yellow, blue, purple, cyan, and orange) correspond closely with the anchorage areas in Figure A.3a (represented by red polygons).[6] Additionally, in Figure A.3e, we spotlight the locations of four terminals within Ningbo-Zhoushan: Beilun, Daxie, Pukou, and Yuandong. Using satellite maps as a reference, we confirm the accuracy of these identifications; each berth in the terminals is pinpointed precisely, and the delineated areas align closely with reality.[7]

To assess the performance of IMA-DBSCAN, we contrast it with the outcomes from ST-DBSCAN.[8] Given that ST-DBSCAN is capable of processing spatial-temporal databases and is recognized as one of the most prominent spatial clustering algorithms in the literature, this comparison is relevant. Figure A.3c illustrates the results derived from ST-DBSCAN, underscoring its lesser precision in comparison to IMA-DBSCAN. Notably, while ST-DBSCAN can generally detect points within the anchorages (highlighted in blue in A.3c), it mistakenly identifies several high-density regions as berths, even though they are not genuine berths. For example, within the blue rectangle in Figure A.3f, points that ought to be categorized as noise are marked as berths, given that ships stayed in these locations for extended periods (potentially for maintenance tasks). Additionally, in the black rectangle, ST-DBSCAN mislabels several points as berths when they should be designated as mooring areas. Consequently, while employing ST-DBSCAN on the sample data offers insights into the arrangement of anchorages, it does not succeed in precisely pinpointing berth locations.

Furthermore, in Figure A.4, we present the detailed results of berth identification for each of the four terminals, i.e., Beilun, Daxie, Pukou, and Yuandong, within the Port of Ningbo-Zhoushan. The outcomes from ST-DBSCAN are ambiguous and feature overlapping sections (proximate in position but with significant differences in heading). Although the general range of these terminals can be discerned, individual berths are scarcely distinguishable. In contrast, our IMA-DBSCAN method can produce clusters that align precisely with each berth within a terminal. Admittedly, increasing the $MinPts$ or reducing the $Eps1$ value could enhance the ST-DBSCAN results. However, this would require constant parameter

6. For clarity, we also display the convex hulls formed by these clusters in Figure A.3d.

7. Moreover, some of the blue dots in Figure A.3a do not correspond to any anchorage or berth in Figure A.3b, indicating that ships anchored in these areas for only a short duration.

8. For this comparison, the input parameters of ST-DBSCAN are set to $Eps1 = 2500$m, $Eps2 = 1°$, and $MinPts = 100$, as recommended by Ester et al. (1996).

adjustments, which is challenging to execute consistently for each port. Our IMA-DBSCAN algorithm, conversely, operates iteratively to automatically determine a set of parameters that can accurately identify both berths and anchorages.

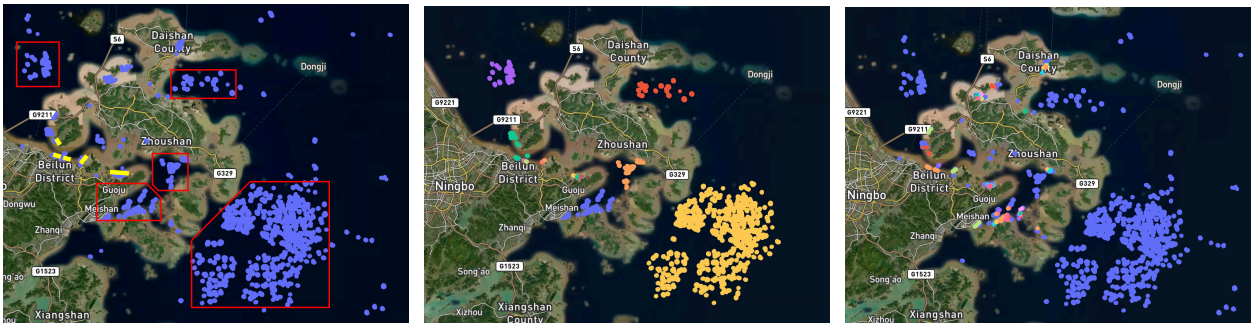

(a) Sample AIS Data **(b)** Result of IMA-DBSCAN **(c)** Result of ST-DBSCAN

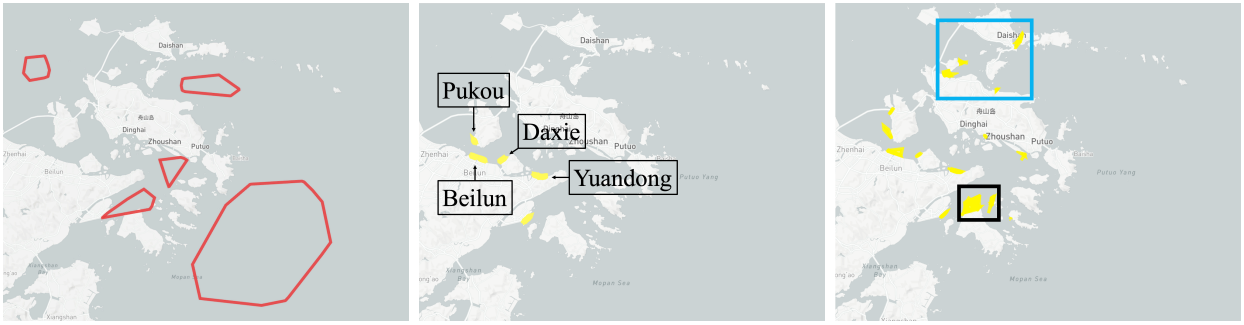

(d) Anchorages (IMA-DBSCAN) **(e)** Berths (IMA-DBSCAN) **(f)** Berths (ST-DBSCAN)

Figure A.3: Identification of Anchorage and Berth Areas in the Port of Ningbo-Zhoushan

Notes. In Figure (a), the sample data comprises the first 50,000 AIS observations taken in January 2020 within the Port of Ningbo-Zhoushan. These observations are represented by blue dots on the map, corresponding to coordinates ranging from 121.60°E to 123.00°E and from 29.50°N to 30.35°N. As a benchmark, using satellite maps and nautical charts, we identify the approximate areas of the anchorages with red polygons and the approximate locations of the berths with yellow rectangles. We apply two clustering algorithms, IMA-DBSCAN and ST-DBSCAN, to the sample data. The resulting clusters are depicted in Figures (b) and (c) respectively. Notably, blue dots in Figure (b) represent the identified anchorage areas, while those in Figure (c) represent noise, which outlines the general layout of anchorage areas but does not distinctly identify each one. In Figure (d), the anchorages from Figure (b) are shown separately in red. In Figure (e), the berths from Figure (b) are displayed separately in yellow. The four terminals are identified as Pukou, Daxie, Beilun, and Yuandong. Lastly, in Figure (f), the yellow areas depict the approximate positions of the berths as identified by ST-DBSCAN. The blue and black rectangles indicate misidentifications of noise as berths and confusion between anchorages and berths, respectively.

(a) Terminal Beilun **(b)** Terminal Daxie **(c)** Terminal Pukou **(d)** Terminal Yuandong

Figure A.4: Detailed Results of Berth Identification: IMA-DBSCAN (Top Row) vs. ST-DBSCAN (Bottom Row)

Notes. The figure displays the detailed results of berth identification for each of the four terminals: Beilun, Daxie, Pukou, and Yuandong, within the Port of Ningbo-Zhoushan. The berths identified by IMA-DBSCAN are presented in yellow on the top row, while those pinpointed by ST-DBSCAN are depicted in brown on the bottom row.

B. Discussion on the Shortcomings of Existing Indices of Supply Chain Disruptions

In this appendix, we elaborate on the shortcomings of using the shipping cost, the sub-components of the manufacturing PMI, and other indices of supply chain disruptions in the causality assessment.

Since our goal is to identify a supply chain disruption shock, the variables to include in the SVARs should in principle reflect how well the global supply chain is functioning. Shipping cost is a natural candidate, as supply chain issues could arise internationally due to a shortage of containers and port congestion (Klachkin 2021; Benigno et al. 2022). However, it should be noted that dynamics in the transportation sector are subject to both supply- and demand-side factors. An increase in the demand for tradable goods would fuel the derived demand for international shipping services, leading to a tighter transportation market and a higher shipping cost.

Another choice is the sub-components of the manufacturing PMI, such as "delivery times", which are used in Kamali and Wang (2021) and Benigno et al. (2022) to capture the extent of supply chain delays and hence act as a barometer of the effectiveness of the global supply chain.[9] Yet, since the PMI is computed based on responses to survey questions, it is inevitably subject to large, persistent, and time-varying measurement errors. Moreover, the PMI does not differentiate whether an increase in delivery times is caused by a disruption to the supply chain or the actual production itself.

In addition to the shipping cost and PMI sub-components, the Kiel trade indicator (Stamer 2021), which uses the same AIS data as ours, provides another angle to assess the widespread strain on the global supply chain; not only does it estimate imports and exports, but it also tracks containership traffic at major ports as well as freight on stationary ships. However, it has several drawbacks. First, the calculation of twenty-foot equivalent units (TEU) is problematic because the draught of a containership is not indicative of its

9. For instance, IHS Markit (Williamson 2021) calculates the suppliers' delivery times using responses to its PMI business surveys. Specifically, participating purchasing managers are asked if it takes their suppliers more or less time to provide inputs to their factories on average. The percentages of companies reporting an improvement, deterioration, or no change in delivery times are then weighted to derive the index.

loading status since loading and unloading operations could occur simultaneously. Second, variations in imports and exports are also subject to demand-side factors, leading to endogeneity issues. Third, the calculation of cargo capacity tied up at ports does not differentiate mooring positions of containerships (berth vs. anchorage), which, as argued in Talley and Ng (2016), could result in an overestimation of port congestion.

Other indices of supply chain disruptions employ either more advanced techniques (e.g., machine learning) or more granular data (e.g., import transactions). Burriel et al. (2023) develop a text-based index of supply disruptions, in which they apply the methodology by Baker, Bloom, and Davis (2016) using newspaper data. While such an index overcomes the endogeneity issue by selecting only supply-side events, it is not immune to measurement errors that naturally arise from word definitions; for instance, a disruption to "supply" is not the same as one to the "supply chain", as the former may stem from a shortage in labor supply. Another example is Smirnyagin and Tsyvinski (2022), who use the S&P Global Panjiva dataset, a comprehensive source of U.S. seaborne import records, to derive the U.S. supply disruptions index (SDI). They identify supply chain disruptions by monitoring regular and active consignee-shipper relationships over quarterly periods; a disruption occurs when a consistently active relationship goes inactive for a quarter and then resumes. While this identification isolates disruptions in the context of established trading relationships, potential endogeneity issues could still arise if, for instance, a consignee temporarily halts orders due to decreased demand, not because of a disruption in the supply chain. It might be challenging to disentangle these situations solely based on the activity status of consignee-shipper relationships. Moreover, while the SDI offers valuable insights into U.S. imports and is adept at delivering asset pricing predictions, the ACR, being a global index, aligns more closely with our specific goal of identifying *global* supply chain disruptions.

Figure B.1 plots the SDI alongside the ACR and GSCPI series. It is observed that the SDI and GSCPI align well and broadly capture the same patterns: fluctuations around the sample median before 2020, a massive but short-lived spike in 2020, and finally, a prolonged yet muted increase in 2021-2022. Figures B.2, B.3, and B.4 plot the estimation results with the SDI included in the SVAR as a measure of supply chain disruptions. Similar to those obtained using the GSCPI, the response of the GDP deflator to a supply chain shock is

around zero and statistically insignificant, and only a minimal fraction of the unexpected fluctuations in the GDP deflator is explained by supply chain disturbances. In terms of the historical decomposition of U.S. inflation, the SDI attributes the initial fall in inflation at the onset of the pandemic to both the collapse in demand and disruptions to the supply chain, and it attributes the subsequent rise in inflation from April 2020 to a combination of demand and supply shocks.

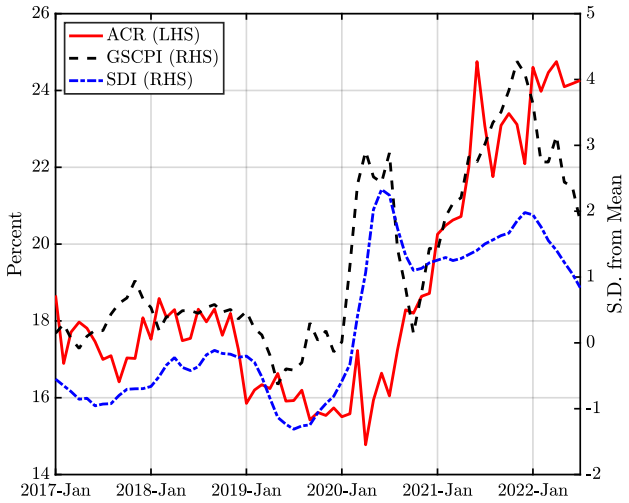

Figure B.1: Comparison Between the ACR, GSCPI, and SDI

Notes. The figure plots the ACR against the GSCPI (black dashed line) and SDI (blue dashed-dotted line) during the sample period from January 2017 to July 2022. The ACR is computed using the AIS data of containerships and the IMA-DBSCAN algorithm developed in Appendix A. The GSCPI is retrieved from the New York Fed's website (Source: https://www.newyorkfed.org/research/policy/gscpi#/overview (Accessed August 10, 2022)), while the SDI is retrieved from the author's website (Source: https://www.disruptions.supply (Accessed July 31, 2023)). The ACR is measured as a percentage, while the GSCPI and SDI are measured in standard deviations from the mean. All the series are seasonally adjusted.

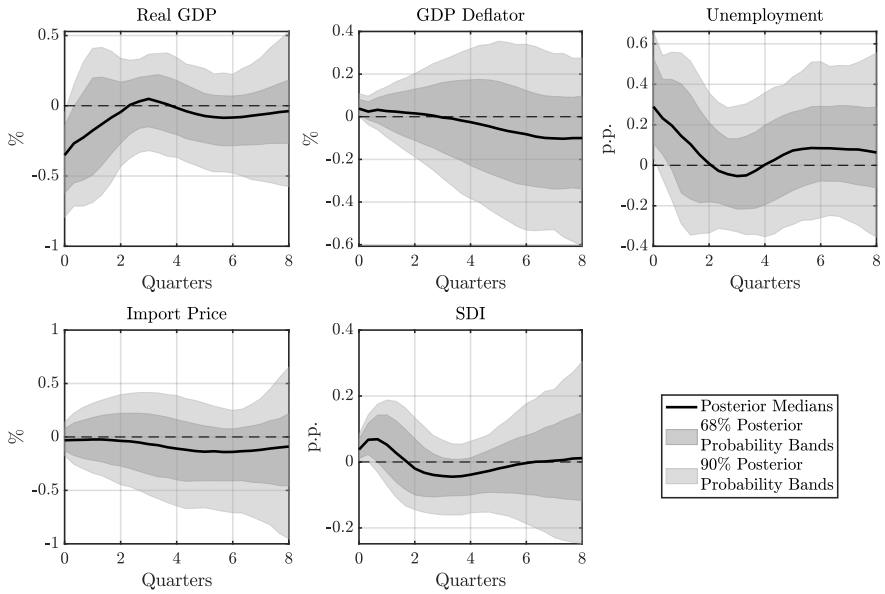

Figure B.2: IRFs to an Adverse Shock to Supply Chain: The SDI and Restrictions 1, 2, and 3

Notes. The IRFs to a one standard deviation adverse shock to supply chain are identified using the SDI index and Restrictions 1, 2, and 3. The solid line shows the point-wise posterior medians, and the shaded bands represent the 68% and 90% equal-tailed point-wise posterior probability bands. The figure is based on 100,000 independent draws.

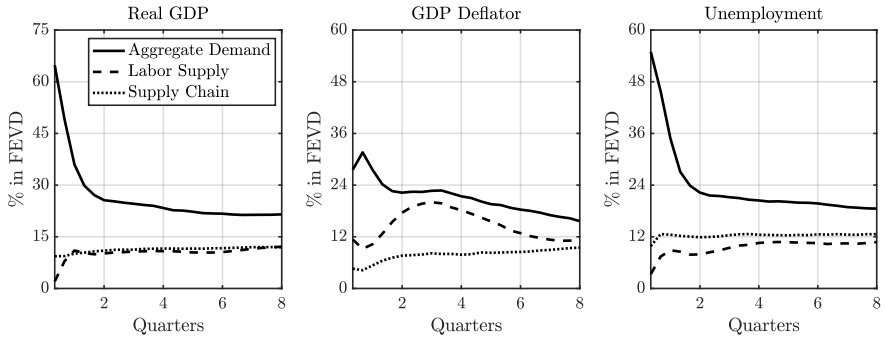

Figure B.3: FEVD from the SVAR: The SDI and Restrictions 1, 2, and 3

Notes. Each line presents the median fraction of the forecast error variance for each endogenous variable, explained by each of the three identified structural shocks at various time horizons. The FEVD is estimated using the SDI index and Restrictions 1, 2, and 3, and based on 100,000 independent draws.

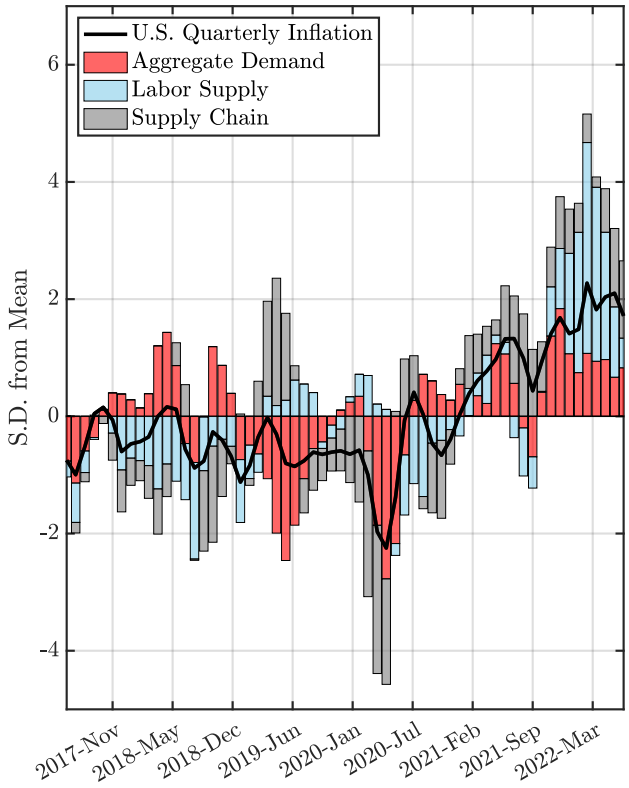

Figure B.4: HD of U.S. Inflation: The SDI and Restrictions 1, 2, and 3

Notes. The solid line represents the standardized quarterly inflation rate in the U.S., i.e., quarter-on-quarter growth of the GDP deflator. The shaded bar represents the standardized cumulative historical contribution of each of the three structural shocks identified using the SDI index and Restrictions 1, 2, and 3 to U.S. inflation. The estimation results are obtained with each variable measured in percent change from the previous period, and are calculated based on 100,000 independent draws.

C. Discussion on the Assumptions in the Model

In this appendix, we discuss two critical assumptions in the model: matching frictions on the international product market and endogenous separation of exporter-importer matches on transportation cost. First, to represent the matching frictions in a tractable manner, we assume that the number of trades between exporters and importers are governed by a matching function. Second, to succinctly capture the decision-making process between an exporter and an importer when their trade is subject to a transportation cost, we assume that upon meeting, both parties choose to endogenously separate from each other once the idiosyncratic transportation cost to pay lies above a reservation threshold. We discuss each of these two assumptions in turn.

The matching function. There is ample literature that studies the origins of matching frictions on the international product market, including but not limited to locating and building connections with overseas buyers (Benguria 2021; Krolikowski and McCallum 2021; Lenoir, Martin, and Mejean 2022), costly information acquisition about market conditions elsewhere (Allen 2014; Chaney 2014), and informal trade barriers such as common language (Melitz and Toubal 2014) and geography (Eaton and Kortum 2002). Different as these theories/evidence might be, they all show that there exist prevalent trade barriers between exporting and importing firms, implying that not all the unmatched exporters engage in trade, while not all the sourcing visits by importers are successful. Following in this vein, we assume a constant-returns-to-scale matching function that summarizes how unmatched exporters and visits of importers are transformed into trades through the matching process. As such, we abstract away from modeling the complex matching process while still preserving its main implication: the unmatched exporters only engage in trade with probability $f(\theta)G(\tau) < 1$ and the visits of importers to exporters are only successful with probability $q(\theta)G(\tau) < 1$.

Endogenous separation on transportation cost. Much in the same way the separation margin on the labor market could be modeled endogenously when workers face productivity shocks to their employment matches and bad draws possibly lead to separations (Bils, Chang, and Kim 2011; Menzio and Shi 2011; Fujita and Ramey 2012), the separation margin on the inter-

national product market could be modeled endogenously when exporters face idiosyncratic transportation costs to their trading relationships with importers and bad draws possibly lead to terminations of such relationships. Such a modeling assumption is reasonable only if we find convincing evidence that (1) transportation cost is taken into account when trading partners decide on a potential trade, and (2) there exists a threshold of transportation cost above which trading partners choose to sever their relationship.

The prediction that transportation cost affects the possibility of a trade has been examined empirically in the international trade literature. To name a few, evidence in Rodrigue (2020) underlines that across all modes, raising transportation costs by 10% reduces trade volumes by more than 20%. In the context of maritime transportation, Brancaccio, Kalouptsidi, and Papageorgiou (2020) exploit changes in tariffs across the trade network to estimate the elasticity of world trade value with respect to shipping costs. They estimate that a 1% change in shipping costs leads to approximately a 1% change in world trade value. Similarly, Wong (2022) estimates the containerized trade elasticity with respect to freight rates using the round-trip effect as an instrument (in particular, for route i, j, the author uses a Bartik-style instrument to proxy for the predicted trade value on route j, i). The author reports that a 1% increase in per unit container freight rates decreases containerized trade value by 2.8% when dyad-by-product controls are included in the regression. Together, these elasticities emphasize that transportation costs are indeed taken into account when trading partners choose to form a relationship, and that a rise in transportation cost deters international trade substantially.

Both theory and casual observation also suggest the presence of a reservation transportation cost, which trading partners often consider when assessing the profitability of a potential trade on the international product market. Notably, to reconcile the empirical evidence that export and import intensities vary across plants, Kasahara and Lapham (2013) extend the model in Melitz (2003) by allowing for heterogeneity in transportation costs. Incorporating heterogeneous transportation costs provides a plausible self-selection mechanism regarding trade decisions, as plants with low transportation costs self-select into exporting and importing. As such, there must exist a threshold value of transportation cost below

which plants choose to engage in trade.[10] Casual observations are also consistent with this theoretical prediction. For instance, according to the Global Transport Costs Dataset for International Trade (UNCTAD 2021), the cost of transporting medical care commodities by sea from China to the U.S. normally accounts for 5% of their Free On Board values. When the transportation cost rises above 5%, exporters in China will reconsider whether it is still profitable to export medical care commodities to the U.S. Hence, following the Covid-19 pandemic, as the transportation cost skyrocketed while the initial increase in the final price of medical care commodities was not on par, trades collapsed as exporters in China exited the market, leading to a great shortage of medical supplies in the U.S. Furthermore, it is noted that the reservation transportation cost is largely fixed in the short run, given that transportation technology and price outlook for shipping fuel are unlikely to vary in few years' time. As such, our modeling assumption regarding the flexible-price aggregate supply is consistent with the reality.

Lastly, the modeling assumption that transportation cost follows a log-normal distribution is borrowed from Kasahara and Lapham (2013). We make this crude but convenient assumption for two reasons. First, since transportation cost varies across countries, routes, directions, and commodities in reality (Brown, Englert, and Hoffmann 2021), an assumption that it is randomly distributed according to a distribution is more plausible than a fixed value (for instance, the "iceberg" formulation of trade costs as in Samuelson (1954)). Second, using a log-normally distributed transportation cost provides us with a purely exogenous measure of transportation cost. With the scale parameter of the log-normal distribution of transportation costs acting as the model counterpart to the ACR, our model mimics the positive relationship between the ACR and shipping costs, as shown in Figure 5a in the main text.[11]

10. A similar argument can be found in the discussion of transport infrastructure and its effects on firm's exporting decision. For instance, Naudé and Matthee (2011) argue that the availability of transport infrastructure will have a threshold effect – a certain minimum of transport infrastructure is required for a firm to start exporting, but once the threshold is reached, improved infrastructure will not necessarily have a large impact on the extent of an individual firm's exports. Since the availability of transport infrastructure (at least partially) determines the transportation cost, this argument is consistent with the presence of a reservation transportation cost that firms take into account when making an exporting decision.

11. Alternatively, we could augment the current model with a full-fledged transportation sector in which the interactions between exporters and shipowners determine the transportation cost. Such an endogenous setting can be found in Brancaccio, Kalouptsidi, and Papageorgiou (2020) and Bai and Li (2022). Nonetheless, we maintain the current setting for its tractability.

D. Long Proofs

D.1. Proof of Proposition 1

We first derive Equation (14). Rewriting Equations (12) and (13) and applying the property $\theta = f(\theta)/q(\theta)$, we obtain that:

$$\theta(p, \bar{z}) = \frac{1-\eta}{\eta\rho}\big(p - \bar{z} + \beta \mathbb{E}_{z'} S(z')\big). \tag{D.1}$$

Then we rewrite $\mathbb{E}_{z'} S(z')$. Using the definition of $S(z)$, we have:

$$S(z) = p - z + \big(1 - \eta f(\theta)\big)\beta \mathbb{E}_{z'} S(z').$$

Subtracting Equation (12) from the above equation yields $S(z) = \bar{z} - z$. Replacing $S(z')$ in $\mathbb{E}_{z'} S(z')$ with $\bar{z} - z'$, we derive that:

$$\begin{aligned}
\mathbb{E}_{z'} S(z') &= \int_0^{\bar{z}} (\bar{z} - z') dG(z') \\
&= (\bar{z} - z') G(z') \Big|_0^{\bar{z}} + \int_0^{\bar{z}} G(z') dz' \\
&= \int_0^{\bar{z}} G(z') dz'.
\end{aligned}$$

Subsequently, replacing $\mathbb{E}_{z'} S(z')$ in Equation (D.1) with $\int_0^{\bar{z}} G(z') dz'$ gives Equation (14).

The first property is obvious. Since θ cannot be negative, for a given $\bar{z}$, p is bounded on $[p^{min}, +\infty)$, where p^{min} is such that it solves $p^{min} - \bar{z} + \beta \int_0^{\bar{z}} G(z') dz' = 0$ for any $\bar{z} > 0$. As for the second and third properties, we derive that:

$$\frac{\partial \theta(p, \bar{z})}{\partial p} = \frac{1-\eta}{\eta\rho} > 0.$$

Hence, the product market tightness $\theta(p, \bar{z})$ is strictly increasing and linear on $[p^{min}, +\infty)$.

The fourth property is also obvious from the definition of $\bar{z}^{max}$, as θ cannot be negative. In terms of the fifth and last properties, we derive that:

$$\frac{\partial \theta(p, \bar{z})}{\partial \bar{z}} = \frac{1-\eta}{\eta\rho}\big(-1 + \beta G(\bar{z})\big) < 0,$$

$$\frac{\partial^2\theta(p,\bar{z})}{\partial\bar{z}^2} = \frac{(1-\eta)\beta}{\eta\rho}\frac{1}{\bar{z}\sigma}\phi(\frac{\log\bar{z}-\gamma}{\sigma}) > 0,$$

where $\phi(.)$ is the standard normal probability density function. Hence, the product market tightness $\theta(p,\bar{z})$ is strictly decreasing and convex on $(0,\bar{z}^{max}]$.

D.2. Proof of Proposition 2

The first property is obvious. When $p = p^{min}$, $\theta(p^{min}) = 0$, $f\big(\theta(p^{min})\big) = 0$, and $c_s^{flex}(p^{min}) = 0$. When $p \to +\infty$, $\lim_{p\to+\infty}\theta(p) = +\infty$, $\lim_{p\to+\infty} f\big(\theta(p)\big) = 1$, and hence $\lim_{p\to+\infty} c_s^{flex}(p) = G(\tau)l$. In terms of the second and third properties, we derive that:

$$\frac{dc_s^{flex}(p)}{dp} = \frac{1-\eta}{\eta\rho}\frac{\big(1-G(\tau)\big)q(\theta)^{1+\xi}G(\tau)l}{\big(1-G(\tau)+f(\theta)G(\tau)\big)^2} > 0,$$

$$\begin{aligned}\frac{d^2c_s^{flex}(p)}{dp^2} =& -\Big(\frac{1-\eta}{\eta\rho}\Big)^2\big(1-G(\tau)\big)G(\tau)l \\ &\cdot\frac{\big(1-G(\tau)+f(\theta)G(\tau)\big)\theta^{\xi-1}(1+\xi)(1+\theta^{\xi})^{-\frac{1+\xi}{\xi}-1}+2G(\tau)q(\theta)^{2(1+\xi)}}{\big(1-G(\tau)+f(\theta)G(\tau)\big)^3} < 0.\end{aligned}$$

Hence, the flexible-price aggregate supply c_s^{flex} is strictly increasing and concave on $[p^{min},+\infty)$.

D.3. Proof of Proposition 4

Since we look for a flexible-price equilibrium with positive consumption, we restrict our search of price p within the range $[p^{min},+\infty)$. The equilibrium condition (21) can be re-written as:

$$\frac{f\big(\theta(p)\big)p}{1-G(\tau)+f\big(\theta(p)\big)G(\tau)} = \frac{\chi^{\epsilon}}{1+\chi^{\epsilon}}\frac{\mu}{G(\tau)l}. \tag{D.2}$$

For any $\tau > 0$, the right hand side is a constant that is strictly positive. For the left hand side, when $p = p^{min}$, $\theta(p^{min}) = 0$, and $f\big(\theta(p^{min})\big) = 0$, it has a limit of zero; when $p \to +\infty$, $\lim_{p\to+\infty}\theta(p) = +\infty$, and $\lim_{p\to+\infty} f\big(\theta(p)\big) = 1$, it has a limit of positive infinity. For $p \in [p^{min},+\infty)$, the derivative of the left hand side with respect to p is given by:

$$\frac{d}{dp}\Big[\frac{f\big(\theta(p)\big)p}{1-G(\tau)+f\big(\theta(p)\big)G(\tau)}\Big] = \frac{\big(1-G(\tau)\big)\frac{1-\eta}{\eta\rho}q(\theta)^{1+\xi}p + f(\theta)\big(1-G(\tau)+f(\theta)G(\tau)\big)}{\big(1-G(\tau)+f(\theta)G(\tau)\big)^2} > 0.$$

Therefore, the left hand side is strictly increasing from zero to positive infinity on $[p^{min}, +\infty)$. As such, there is a unique $p \in [p^{min}, +\infty)$ that solves Equation (D.2).

D.4. Proof of Proposition 5

We first consider an adverse shock to aggregate demand. No matter whether the negative aggregate demand shock is represented by a decrease in money supply μ or in the taste for consumption of goods χ, the right hand side of Equation (D.2) will decrease. To balance both sides of Equation (D.2), price p will decrease, since the derivative of the left hand side with respect to p is positive (see the proof for Proposition 4). As p decreases, by the second property in Proposition 1 and the second property in Proposition 2, product market tightness θ and consumption (or equivalently, output) c will decrease. Since both p and θ decrease, according to Equation (10), import price r will decline as well. For the matching cost, $G(\tau)l - c$, and spare capacity (or equivalently, unemployment), $l - c$, since they both are strictly decreasing in c, they will increase following an adverse shock to aggregate demand.

Next, we consider an adverse shock to labor supply (or equivalently, productive capacity), which is parameterized by a decrease in l. On impact, the right hand side of Equation (D.2) increases. Similar to the above reasoning, price p will increase. As p increases, by the second property in Proposition 1 and Proposition 3, product market tightness θ will increase while consumption (or equivalently, output) c will fall. Again, since both p and θ increase, according to Equation (10), import price r will rise. As for the matching cost and spare capacity (or equivalently, unemployment), they can be alternatively expressed as:

$$matching\ cost = \frac{\big(1 - G(\tau)\big)\big(1 - f(\theta)\big)}{1 - \big(1 - f(\theta)\big)G(\tau)} G(\tau) l,$$

$$spare\ capacity = \frac{1 - G(\tau)}{1 - G(\tau) + f(\theta)G(\tau)} l,$$

respectively. With θ increasing and l decreasing following an adverse production shock, it is easy to verify that both the matching cost and spare capacity will decrease.

Lastly, we consider an adverse shock to supply chain, which is represented by an increase in γ, i.e., the scale parameter of the log-normal distribution of transportation costs $G(.)$. We first look at the effect on price. Using the re-arranged equilibrium condition (D.2), we define

a function $\mathbb{T} : [p^{min}, +\infty) \times \mathbb{R} \to \mathbb{R}$:

$$\mathbb{T}(p,\gamma) = \frac{\chi^{\epsilon}}{1+\chi^{\epsilon}} \frac{\mu}{G(\tau) l} - \frac{f(\theta) p}{1 - G(\tau) + f(\theta) G(\tau)}$$
$$= \frac{\chi^{\epsilon}}{1+\chi^{\epsilon}} \frac{\mu}{\Phi(\frac{\log \tau - \gamma}{\sigma}) l} - \frac{\left\{1 + \left[\frac{1-\eta}{\eta\rho}\left(p - \tau + \beta \int_0^{\tau} \Phi(\frac{\log z' - \gamma}{\sigma}) dz'\right)\right]^{-\xi}\right\}^{-\frac{1}{\xi}} p}{1 - \Phi(\frac{\log \tau - \gamma}{\sigma}) + \left\{1 + \left[\frac{1-\eta}{\eta\rho}\left(p - \tau + \beta \int_0^{\tau} \Phi(\frac{\log z' - \gamma}{\sigma}) dz'\right)\right]^{-\xi}\right\}^{-\frac{1}{\xi}} \Phi(\frac{\log \tau - \gamma}{\sigma})},$$

where $\Phi(.)$ is the standard normal cumulative density function. Assuming the existence of a tuple $(p_0, \gamma_0) \in [p^{min}, +\infty) \times \mathbb{R}$ such that $\mathbb{T}(p_0, \gamma_0) = 0$ and $\partial \mathbb{T}(p,\gamma)/\partial p|_{p=p_0, \gamma=\gamma_0} \neq 0$, by the Implicit Function Theorem, there is a neighborhood of (p_0, γ_0) such that whenever γ is sufficiently close to γ_0, there is a unique p so that $\mathbb{T}(p,\gamma) = 0$. This assignment makes p a continuous function of γ. Applying implicit differentiation to $\mathbb{T}(p,\gamma)$ around (p_0, γ_0) yields:

$$\frac{dp(\gamma)}{d\gamma} = -\frac{\partial \mathbb{T}(p,\gamma)/\partial \gamma}{\partial \mathbb{T}(p,\gamma)/\partial p}.$$

In terms of $\partial \mathbb{T}(p,\gamma)/\partial \gamma$, we derive that:

$$\frac{\partial \mathbb{T}(p,\gamma)}{\partial \gamma} = \frac{\chi^{\epsilon}}{1+\chi^{\epsilon}} \frac{\mu}{l} \frac{\frac{1}{\sigma} g(\tau)}{G(\tau)^2} + \frac{\big(1 - G(\tau)\big) \frac{(1-\eta)\beta}{\eta\rho} \big[\int_0^{\tau} \frac{1}{\sigma} g(z') dz'\big] q(\theta)^{1+\xi} p}{\big(1 - G(\tau) + f(\theta) G(\tau)\big)^2}$$
$$+ \frac{\big(1 - f(\theta)\big) f(\theta) p \frac{1}{\sigma} g(\tau)}{\big(1 - G(\tau) + f(\theta) G(\tau)\big)^2} > 0,$$

where $g(\tau) \equiv \phi[(\log \tau - \gamma)/\sigma]$, $g(z') \equiv \phi[(\log z' - \gamma)/\sigma]$, while $\phi(.)$ is the standard normal probability density function. In terms of $\partial \mathbb{T}(p,\gamma)/\partial p$, it can be written as:

$$\frac{\partial \mathbb{T}(p,\gamma)}{\partial p} = -\frac{\big(1 - G(\tau)\big) \frac{1-\eta}{\eta\rho} q(\theta)^{1+\xi} p + f(\theta)\big(1 - G(\tau) + f(\theta) G(\tau)\big)}{\big(1 - G(\tau) + f(\theta) G(\tau)\big)^2} < 0.$$

By combining $\partial \mathbb{T}(p,\gamma)/\partial \gamma$ with $\partial \mathbb{T}(p,\gamma)/\partial p$ and collecting terms, we have:

$$\begin{aligned} \frac{dp(\gamma)}{d\gamma} =& \big[\big(1 - G(\tau)\big) \frac{1-\eta}{\eta\rho} q(\theta)^{1+\xi} p + f(\theta)\big(1 - G(\tau) + f(\theta) G(\tau)\big)\big]^{-1} \\ & \cdot \Big\{\big(1 - G(\tau) + f(\theta) G(\tau)\big) f(\theta) \frac{1}{\sigma} g(\tau) \frac{p}{G(\tau)} \\ & + \big(1 - G(\tau)\big) \frac{(1-\eta)\beta}{\eta\rho} \big[\int_0^{\tau} \frac{1}{\sigma} g(z') dz'\big] q(\theta)^{1+\xi} p \\ & + \big(1 - f(\theta)\big) f(\theta) p \frac{1}{\sigma} g(\tau)\Big\} > 0. \end{aligned} \tag{D.3}$$

Hence, price p will increase on impact of an adverse shock to supply chain. In terms of

consumption (or equivalently, output), it is written as:

$$c(\gamma) = \frac{\chi^{\epsilon}}{1+\chi^{\epsilon}} \frac{\mu}{p(\gamma)},$$

where p is an implicit function of γ. Therefore, the derivative of c with respect to γ is:

$$\begin{aligned}
\frac{dc(\gamma)}{d\gamma} = &- \frac{\chi^{\epsilon}}{1+\chi^{\epsilon}} \frac{\mu}{p} \big[\big(1-G(\tau)\big) \frac{1-\eta}{\eta\rho} q(\theta)^{1+\xi} p + f(\theta)\big(1-G(\tau)+f(\theta)G(\tau)\big) \big]^{-1} \\
&\cdot \Big\{ \big(1-G(\tau)+f(\theta)G(\tau)\big) f(\theta) \frac{1}{\sigma} g(\tau) \frac{1}{G(\tau)} \\
&+ \big(1-G(\tau)\big) \frac{(1-\eta)\beta}{\eta\rho} \big[\int_0^{\tau} \frac{1}{\sigma} g(z')dz' \big] q(\theta)^{1+\xi} \\
&+ \big(1-f(\theta)\big) f(\theta) \frac{1}{\sigma} g(\tau) \Big\} < 0.
\end{aligned}$$

Hence, consumption (or equivalently, output) c will fall. Next, in terms of product market tightness, it is given by:

$$\theta(\gamma) = \frac{1-\eta}{\eta\rho} \big(p(\gamma) - \tau + \beta \int_0^{\tau} \Phi(\frac{\log z' - \gamma}{\sigma}) dz' \big). \tag{D.4}$$

Accordingly, the derivative of θ with respect to γ is:

$$\begin{aligned}
\frac{d\theta(\gamma)}{d\gamma} = &\frac{1-\eta}{\eta\rho} \big[\big(1-G(\tau)\big) \frac{1-\eta}{\eta\rho} q(\theta)^{1+\xi} p + f(\theta)\big(1-G(\tau)+f(\theta)G(\tau)\big) \big]^{-1} \\
&\cdot \Big\{ \big(1-G(\tau)+f(\theta)G(\tau)\big) f(\theta) \frac{1}{\sigma} g(\tau) \frac{p}{G(\tau)} + \big(1-f(\theta)\big) f(\theta) p \frac{1}{\sigma} g(\tau) \\
&- \big(1-G(\tau)+f(\theta)G(\tau)\big) f(\theta) \beta \big[\int_0^{\tau} \frac{1}{\sigma} g(z')dz' \big] \Big\},
\end{aligned} \tag{D.5}$$

whose value depends on the values of θ and p; as we will discuss later in Appendix D.5, this dependence is crucial for the state-dependence result of a contractionary monetary policy shock. Similarly, by substituting Equation (D.4) into Equation (10), the import price can be expressed as:

$$r(\gamma) = p(\gamma) + (1-\eta)\beta \int_0^{\tau} \Phi(\frac{\log z' - \gamma}{\sigma}) dz' + (1-\eta)(z-\tau).$$

Differentiating $r(\gamma)$ with respect to γ yields:

$$\begin{aligned}\frac{dr(\gamma)}{d\gamma} =&\big[\big(1-G(\tau)\big)\frac{1-\eta}{\eta\rho}q(\theta)^{1+\xi}p + f(\theta)\big(1-G(\tau)+f(\theta)G(\tau)\big)\big]^{-1}\\ &\cdot\Big\{\big(1-G(\tau)+f(\theta)G(\tau)\big)f(\theta)\frac{1}{\sigma}g(\tau)\frac{p}{G(\tau)}\\ &+\big(1-G(\tau)\big)\frac{(1-\eta)\beta}{\rho}\big[\int_0^\tau \frac{1}{\sigma}g(z')dz'\big]q(\theta)^{1+\xi}p\\ &+\big(1-f(\theta)\big)f(\theta)p\frac{1}{\sigma}g(\tau)\\ &-\big(1-G(\tau)+f(\theta)G(\tau)\big)f(\theta)(1-\eta)\beta\big[\int_0^\tau \frac{1}{\sigma}g(z')dz'\big]\Big\},\end{aligned}$$

whose value is also dependent on the values of θ and p. As for the matching cost, given that it is measured by the difference between $G(\tau)l$ and c, its derivative with respect to γ can be written as:

$$\begin{aligned}\frac{d}{d\gamma}\big[\textit{matching cost}(\gamma)\big] =&\big[\big(1-G(\tau)\big)\frac{1-\eta}{\eta\rho}q(\theta)^{1+\xi}p + f(\theta)\big(1-G(\tau)+f(\theta)G(\tau)\big)\big]^{-1}\\ &\cdot\Big(\frac{\chi^\epsilon}{1+\chi^\epsilon}\frac{\mu}{p}\Big\{\big(1-G(\tau)+f(\theta)G(\tau)\big)f(\theta)\frac{1}{\sigma}g(\tau)\frac{1}{G(\tau)}\\ &+\big(1-G(\tau)\big)\frac{(1-\eta)\beta}{\eta\rho}\big[\int_0^\tau \frac{1}{\sigma}g(z')dz'\big]q(\theta)^{1+\xi}\\ &+\big(1-f(\theta)\big)f(\theta)\frac{1}{\sigma}g(\tau)\Big\}\\ &-\big(1-G(\tau)\big)\frac{1-\eta}{\eta\rho}q(\theta)^{1+\xi}p\frac{1}{\sigma}g(\tau)l\\ &-f(\theta)\big(1-G(\tau)+f(\theta)G(\tau)\big)\frac{1}{\sigma}g(\tau)l\Big),\end{aligned}$$

whose value is again dependent on the values of θ and p. On the contrary, since the spare capacity (or equivalently, unemployment) is measured by the difference between l and c, its derivative with respect to γ is positive, i.e.,

$$\begin{aligned}\frac{d}{d\gamma}\big[\textit{spare capacity}(\gamma)\big] =&\frac{\chi^\epsilon}{1+\chi^\epsilon}\frac{\mu}{p}\big[\big(1-G(\tau)\big)\frac{1-\eta}{\eta\rho}q(\theta)^{1+\xi}p + f(\theta)\big(1-G(\tau)+f(\theta)G(\tau)\big)\big]^{-1}\\ &\cdot\Big\{\big(1-G(\tau)+f(\theta)G(\tau)\big)f(\theta)\frac{1}{\sigma}g(\tau)\frac{1}{G(\tau)}\\ &+\big(1-G(\tau)\big)\frac{(1-\eta)\beta}{\eta\rho}\big[\int_0^\tau \frac{1}{\sigma}g(z')dz'\big]q(\theta)^{1+\xi}\\ &+\big(1-f(\theta)\big)f(\theta)\frac{1}{\sigma}g(\tau)\Big\} > 0.\end{aligned}$$

D.5. Proof of Proposition 6

We start the proof by re-visiting the function $\mathbb{T} : [p^{min}, +\infty) \times \mathbb{R}^+ \times \mathbb{R} \to \mathbb{R}$:

$$\mathbb{T}(p,\mu,\gamma) = \frac{\chi^\epsilon}{1+\chi^\epsilon}\frac{\mu}{G(\tau)l} - \frac{f(\theta)p}{1-G(\tau)+f(\theta)G(\tau)}$$
$$= \frac{\chi^\epsilon}{1+\chi^\epsilon}\frac{\mu}{\Phi(\frac{\log\tau-\gamma}{\sigma})l} - \frac{\left\{1+\left[\frac{1-\eta}{\eta\rho}\left(p-\tau+\beta\int_0^\tau\Phi(\frac{\log z'-\gamma}{\sigma})dz'\right)\right]^{-\xi}\right\}^{-\frac{1}{\xi}}p}{1-\Phi(\frac{\log\tau-\gamma}{\sigma})+\left\{1+\left[\frac{1-\eta}{\eta\rho}\left(p-\tau+\beta\int_0^\tau\Phi(\frac{\log z'-\gamma}{\sigma})dz'\right)\right]^{-\xi}\right\}^{-\frac{1}{\xi}}\Phi(\frac{\log\tau-\gamma}{\sigma})},$$

where $\Phi(.)$ is the standard normal cumulative density function. Subsequently, assuming the existence of a tuple $(p_0,\mu_0,\gamma_0) \in [p^{min},+\infty)\times\mathbb{R}^+\times\mathbb{R}$ such that $\mathbb{T}(p_0,\mu_0,\gamma_0)=0$ and $\partial\mathbb{T}(p,\mu,\gamma)/\partial p|_{p=p_0,\mu=\mu_0,\gamma=\gamma_0} \neq 0$, by the Implicit Function Theorem, there is a neighborhood of (p_0,μ_0,γ_0) such that whenever (μ,γ) is sufficiently close to (μ_0,γ_0), there is a unique p so that $\mathbb{T}(p,\mu,\gamma)=0$. This assignment makes p a continuous function of μ and γ. Applying implicit differentiation to $\mathbb{T}(p,\mu,\gamma)$ around (p_0,μ_0,γ_0) yields:

$$\frac{\partial p(\mu,\gamma)}{\partial\mu} = -\frac{\partial\mathbb{T}(p,\mu,\gamma)/\partial\mu}{\partial\mathbb{T}(p,\mu,\gamma)/\partial p}.$$

The numerator can be written as:

$$\frac{\partial\mathbb{T}(p,\mu,\gamma)}{\partial\mu} = \frac{\chi^\epsilon}{1+\chi^\epsilon}\frac{1}{G(\tau)l} > 0,$$

whereas the denominator is given by:

$$\frac{\partial\mathbb{T}(p,\mu,\gamma)}{\partial p} = -\frac{\big(1-G(\tau)\big)\frac{1-\eta}{\eta\rho}q(\theta)^{1+\xi}p + f(\theta)\big(1-G(\tau)+f(\theta)G(\tau)\big)}{\big(1-G(\tau)+f(\theta)G(\tau)\big)^2} < 0.$$

By combining $\partial\mathbb{T}(p,\mu,\gamma)/\partial\mu$ with $\partial\mathbb{T}(p,\mu,\gamma)/\partial p$, we derive that:

$$\frac{\partial p(\mu,\gamma)}{\partial\mu} = \frac{\chi^\epsilon}{1+\chi^\epsilon}\frac{1}{G(\tau)l}\frac{\big(1-G(\tau)+f(\theta)G(\tau)\big)^2}{\big(1-G(\tau)\big)\frac{1-\eta}{\eta\rho}q(\theta)^{1+\xi}p + f(\theta)\big(1-G(\tau)+f(\theta)G(\tau)\big)}$$
$$= \frac{1}{\mu}\left[\frac{\big(1-G(\tau)\big)\frac{1-\eta}{\eta\rho}q(\theta)^{1+\xi}}{f(\theta)\big(1-G(\tau)+f(\theta)G(\tau)\big)} + \frac{1}{p}\right]^{-1} > 0.$$

In terms of the partial derivative $\partial c(\mu,\gamma)/\partial\mu$, using the expression of the aggregate demand in Equation (20), we can derive that:

$$\begin{aligned}\frac{\partial c(\mu,\gamma)}{\partial\mu} &= \frac{\chi^{\epsilon}}{1+\chi^{\epsilon}}\frac{\big(1-G(\tau)\big)^{\frac{1-\eta}{\eta\rho}}q(\theta)^{1+\xi}}{\big(1-G(\tau)\big)^{\frac{1-\eta}{\eta\rho}}q(\theta)^{1+\xi}p+f(\theta)\big(1-G(\tau)+f(\theta)G(\tau)\big)}\\ &= \frac{\chi^{\epsilon}}{1+\chi^{\epsilon}}\Big[p+\frac{f(\theta)\big(1-G(\tau)+f(\theta)G(\tau)\big)}{\big(1-G(\tau)\big)^{\frac{1-\eta}{\eta\rho}}q(\theta)^{1+\xi}}\Big]^{-1}.\end{aligned}$$

Hence, both $\partial p(\mu,\gamma)/\partial\mu$ and $\partial c(\mu,\gamma)/\partial\mu$ depend on the fraction:

$$\frac{\big(1-G(\tau)\big)^{\frac{1-\eta}{\eta\rho}}q(\theta)^{1+\xi}}{f(\theta)\big(1-G(\tau)+f(\theta)G(\tau)\big)}. \tag{D.6}$$

Next, we study the dependence of the fraction (D.6) on γ, as it directly determines the signs of $\partial^2 p(\mu,\gamma)/\partial\mu\partial\gamma$ and $\partial^2 c(\mu,\gamma)/\partial\mu\partial\gamma$. It is given by:

$$\begin{aligned}&\frac{\partial}{\partial\gamma}\Big[\frac{\big(1-G(\tau)\big)^{\frac{1-\eta}{\eta\rho}}q(\theta)^{1+\xi}}{f(\theta)\big(1-G(\tau)+f(\theta)G(\tau)\big)}\Big] = \frac{f(\theta)\big(1-G(\tau)+f(\theta)G(\tau)\big)\big[\frac{1}{\sigma}g(\tau)^{\frac{1-\eta}{\eta\rho}}q(\theta)^{1+\xi}\big]}{\big[f(\theta)\big(1-G(\tau)+f(\theta)G(\tau)\big)\big]^2}\\ &-\frac{f(\theta)\big(1-G(\tau)+f(\theta)G(\tau)\big)\big[\big(1-G(\tau)\big)^{\frac{1-\eta}{\eta\rho}}\frac{\partial\theta(\mu,\gamma)}{\partial\gamma}(1+\xi)\theta^{\xi-1}(1+\theta^{\xi})^{-\frac{1+\xi}{\xi}-1}\big]}{\big[f(\theta)\big(1-G(\tau)+f(\theta)G(\tau)\big)\big]^2}\\ &-\frac{\big(1-G(\tau)\big)^{\frac{1-\eta}{\eta\rho}}q(\theta)^{1+\xi}\big[\frac{\partial\theta(\mu,\gamma)}{\partial\gamma}q(\theta)^{1+\xi}\big(1-G(\tau)+f(\theta)G(\tau)\big)\big]}{\big[f(\theta)\big(1-G(\tau)+f(\theta)G(\tau)\big)\big]^2}\\ &-\frac{\big(1-G(\tau)\big)^{\frac{1-\eta}{\eta\rho}}q(\theta)^{1+\xi}\big[f(\theta)\big(\frac{1}{\sigma}g(\tau)+\frac{\partial\theta(\mu,\gamma)}{\partial\gamma}q(\theta)^{1+\xi}G(\tau)-f(\theta)\frac{1}{\sigma}g(\tau)\big)\big]}{\big[f(\theta)\big(1-G(\tau)+f(\theta)G(\tau)\big)\big]^2},\end{aligned}$$

and is proportional to:

$$\begin{aligned}&\frac{\partial}{\partial\gamma}\Big[\frac{\big(1-G(\tau)\big)^{\frac{1-\eta}{\eta\rho}}q(\theta)^{1+\xi}}{f(\theta)\big(1-G(\tau)+f(\theta)G(\tau)\big)}\Big] \propto f(\theta)^2\frac{1}{\sigma}g(\tau)\\ &-f(\theta)\big(1-G(\tau)+f(\theta)G(\tau)\big)\big(1-G(\tau)\big)\frac{\partial\theta(\mu,\gamma)}{\partial\gamma}(1+\xi)\frac{\theta^{\xi-1}}{1+\theta^{\xi}}\\ &-\big(1-G(\tau)\big)\frac{\partial\theta(\mu,\gamma)}{\partial\gamma}q(\theta)^{1+\xi}\big(1-G(\tau)+f(\theta)G(\tau)\big)\\ &-\big(1-G(\tau)\big)f(\theta)\frac{\partial\theta(\mu,\gamma)}{\partial\gamma}q(\theta)^{1+\xi}G(\tau),\end{aligned}$$

where $g(\tau)\equiv\phi[(\log\tau-\gamma)/\sigma]$ and $\phi(.)$ is the standard normal probability density function.

When the partial derivative of θ with respect to γ satisfies:

$$\frac{\partial\theta(\mu,\gamma)}{\partial\gamma} > \frac{f(\theta)^2\frac{1}{\sigma}g(\tau)}{\big(1-G(\tau)\big)f(\theta)q(\theta)^{1+\xi}G(\tau)} = \frac{\theta(1+\theta^{\xi})\frac{1}{\sigma}g(\tau)}{\big(1-G(\tau)\big)G(\tau)} > 0,$$

it is easy to verify that:

$$\frac{\partial}{\partial\gamma}\Big[\frac{\big(1-G(\tau)\big)\frac{1-\eta}{\eta\rho}q(\theta)^{1+\xi}}{f(\theta)\big(1-G(\tau)+f(\theta)G(\tau)\big)}\Big] < 0,$$

and the values of the cross derivatives can thus be determined:

$$\begin{aligned}\frac{\partial^2 p(\mu,\gamma)}{\partial\mu\partial\gamma} = &-\Big\{\frac{\partial}{\partial\gamma}\Big[\frac{\big(1-G(\tau)\big)\frac{1-\eta}{\eta\rho}q(\theta)^{1+\xi}}{f(\theta)\big(1-G(\tau)+f(\theta)G(\tau)\big)}\Big] - \frac{\partial p(\mu,\gamma)}{\partial\gamma}\frac{1}{p^2}\Big\}\\ &\cdot\Big[\frac{\big(1-G(\tau)\big)\frac{1-\eta}{\eta\rho}q(\theta)^{1+\xi}}{f(\theta)\big(1-G(\tau)+f(\theta)G(\tau)\big)}+\frac{1}{p}\Big]^{-2}\frac{1}{\mu} > 0,\end{aligned}$$

$$\begin{aligned}\frac{\partial^2 c(\mu,\gamma)}{\partial\mu\partial\gamma} = &-\Big\{\frac{\partial p(\mu,\gamma)}{\partial\gamma} - \frac{\partial}{\partial\gamma}\Big[\frac{\big(1-G(\tau)\big)\frac{1-\eta}{\eta\rho}q(\theta)^{1+\xi}}{f(\theta)\big(1-G(\tau)+f(\theta)G(\tau)\big)}\Big]\Big[\frac{\big(1-G(\tau)\big)\frac{1-\eta}{\eta\rho}q(\theta)^{1+\xi}}{f(\theta)\big(1-G(\tau)+f(\theta)G(\tau)\big)}\Big]^{-2}\Big\}\\ &\cdot\Big[p+\frac{f(\theta)\big(1-G(\tau)+f(\theta)G(\tau)\big)}{\big(1-G(\tau)\big)\frac{1-\eta}{\eta\rho}q(\theta)^{1+\xi}}\Big]^{-2}\frac{\chi^{\epsilon}}{1+\chi^{\epsilon}} < 0,\end{aligned}$$

where $\partial p(\mu,\gamma)/\partial\gamma > 0$ according to Equation (D.3). With them, it is straightforward to derive the rest of the cross derivatives: specifically, for the product market tightness,

$$\frac{\partial\theta(\mu,\gamma)}{\partial\mu} = \frac{1-\eta}{\eta\rho}\frac{\partial p(\mu,\gamma)}{\partial\mu} > 0,\ \ \frac{\partial^2\theta(\mu,\gamma)}{\partial\mu\partial\gamma} = \frac{1-\eta}{\eta\rho}\frac{\partial^2 p(\mu,\gamma)}{\partial\mu\partial\gamma} > 0;$$

for the import price,

$$\frac{\partial r(\mu,\gamma)}{\partial\mu} = \frac{\partial p(\mu,\gamma)}{\partial\mu} > 0,\ \ \frac{\partial^2 r(\mu,\gamma)}{\partial\mu\partial\gamma} = \frac{\partial^2 p(\mu,\gamma)}{\partial\mu\partial\gamma} > 0;$$

for the matching cost,

$$\frac{\partial}{\partial\mu}\big[\textit{matching cost}(\mu,\gamma)\big] = -\frac{\partial c(\mu,\gamma)}{\partial\mu} < 0,\ \ \frac{\partial^2}{\partial\mu\partial\gamma}\big[\textit{matching cost}(\mu,\gamma)\big] = -\frac{\partial^2 c(\mu,\gamma)}{\partial\mu\partial\gamma} > 0;$$

and lastly, for the spare capacity (or equivalently, unemployment),

$$\frac{\partial}{\partial\mu}\big[\textit{spare capacity}(\mu,\gamma)\big] = -\frac{\partial c(\mu,\gamma)}{\partial\mu} < 0,\ \ \frac{\partial^2}{\partial\mu\partial\gamma}\big[\textit{spare capacity}(\mu,\gamma)\big] = -\frac{\partial^2 c(\mu,\gamma)}{\partial\mu\partial\gamma} > 0.$$

E. Fixed-Price Aggregate Supply

In contrast to the flexible-price aggregate supply as discussed in the main text, we consider here the alternative pricing mechanism in which the price of goods is fixed while the reservation transportation cost can vary. A careful exposition of such a fixed-price mechanism is essential to understand how the matching frictions and endogenous separation mechanism could affect aggregate supply differently. The fixed-price aggregate supply is defined below, and its key analytical properties are summarized in Proposition 2′.

Definition 2″. *For an arbitrary price $\kappa \in (0, +\infty)$, the fixed-price aggregate supply c_s^{fix} is the function of reservation transportation cost $\bar{z}$ defined by:*

$$c_s^{fix}(\bar{z}) = \frac{\left\{1 + \left[\frac{1-\eta}{\eta\rho}\left(\kappa - \bar{z} + \beta \int_0^{\bar{z}} G(z')dz'\right)\right]^{-\xi}\right\}^{-\frac{1}{\xi}} G(\bar{z})l}{1 - G(\bar{z}) + \left\{1 + \left[\frac{1-\eta}{\eta\rho}\left(\kappa - \bar{z} + \beta \int_0^{\bar{z}} G(z')dz'\right)\right]^{-\xi}\right\}^{-\frac{1}{\xi}} G(\bar{z})}, \tag{E.1}$$

for all $\bar{z} \in (0, \bar{z}^{max}]$, where $\bar{z}^{max}$ satisfies:

$$\kappa - \bar{z}^{max} + \beta \int_0^{\bar{z}^{max}} G(z')dz' = 0. \tag{E.2}$$

Proposition 2′. *The fixed-price aggregate supply c_s^{fix} has the following properties:*

1. $\lim_{\bar{z}\to 0^+} c_s^{fix}(\bar{z}) = 0$;
2. $c_s^{fix}(\bar{z}^{max}) = 0$; *and*
3. *There exists at least one $\bar{z}^* \in (0, \bar{z}^{max}]$ such that $dc_s^{fix}(\bar{z})/d\bar{z}|_{\bar{z}=\bar{z}^*} = 0$.*

Proof. It is straightforward to prove the first property. When $\bar{z} \to 0^+$, $\lim_{\bar{z}\to 0^+} \theta(\bar{z}) = (1-\eta)\kappa/(\eta\rho)$, $\lim_{\bar{z}\to 0^+} f\big(\theta(\bar{z})\big) = \{1 + [(1-\eta)\kappa/(\eta\rho)]^{-\xi}\}^{-1/\xi} > 0$. At the same time, when $\bar{z} \to 0^+$, $\lim_{\bar{z}\to 0^+} G(\bar{z}) = 0$. Therefore, $\lim_{\bar{z}\to 0^+} c_s^{fix}(\bar{z}) = 0$. In terms of the second property, it is obvious from the definition of $\bar{z}^{max}$, together with that $f(0) = 0$. Regarding the last

property, the derivative of c_s^{fix} with respect to $\bar{z}$ can be written as:

$$\frac{dc_s^{fix}(\bar{z})}{d\bar{z}} = \big(1 - G(\bar{z}) + f(\theta)G(\bar{z})\big)^{-2} \cdot \Big[\underbrace{\big(1 - G(\bar{z})\big)\frac{1-\eta}{\eta\rho}\big(-1 + \beta G(\bar{z})\big)\theta^{-\xi-1}f(\theta)^{1+\xi}G(\bar{z})l}_{\substack{\text{Product Market Tightness} \\ \text{Channel} < 0}} + \underbrace{f(\theta)\frac{1}{\bar{z}\sigma}g(\bar{z})l}_{\substack{\text{Separation Margin} \\ \text{Channel} > 0}} \Big],$$

where $G(\bar{z}) \equiv \Phi[(\log \bar{z} - \gamma)/\sigma]$, $g(\bar{z}) \equiv \phi[(\log \bar{z} - \gamma)/\sigma]$, while $\Phi(.)$ and $\phi(.)$ are the standard normal cumulative density function and probability density function respectively. The product market tightness channel is negative, because a higher reservation transportation cost would reduce the total surplus to be shared between exporters and importers at the margin, hence dampening the incentives for importers to visit exporters, leading to a slack product market as well as a lower aggregate supply. The separation margin channel is positive, because a larger proportion of matches that would otherwise have been dismissed could now continue, hence contributing to a higher aggregate supply. These two channels jointly determine the fixed-price aggregate supply, and the extent to which one channel dominates the other depends on both the parameter values and reservation transportation cost itself.

When $\bar{z} \to 0^+$, it can be shown that:

$$\lim_{\bar{z}\to 0^+} \frac{dc_s^{fix}(\bar{z})}{d\bar{z}} = \Big\{1 + \Big[\frac{(1-\eta)\kappa}{\eta\rho}\Big]^{-\xi}\Big\}^{-\frac{1}{\xi}} \lim_{\bar{z}\to 0^+} \frac{1}{\bar{z}\sigma} g(\bar{z})l > 0,$$

since the probability density function of a log-normal distribution is always positive. When $\bar{z} \to \bar{z}^{max}$, it can be derived that:

$$\lim_{\bar{z}\to \bar{z}^{max}} \frac{dc_s^{fix}(\bar{z})}{d\bar{z}} = \frac{1}{1 - G(\bar{z}^{max})} \frac{1-\eta}{\eta\rho}\big(-1 + \beta G(\bar{z}^{max})\big)G(\bar{z}^{max})l < 0.$$

Consider an infinitesimal number $\epsilon > 0$ such that $dc_s^{fix}(\bar{z})/d\bar{z}|_{\bar{z}=\epsilon}$ and $\lim_{\bar{z}\to 0^+} dc_s^{fix}(\bar{z})/d\bar{z}$ have the same sign. By the Intermediate Value Theorem, since $dc_s^{fix}(\bar{z})/d\bar{z}$ is continuous on $[\epsilon, \bar{z}^{max}]$, there must exist at least one $\bar{z}^* \in [\epsilon, \bar{z}^{max}]$ such that $dc_s^{fix}(\bar{z})/d\bar{z}|_{\bar{z}=\bar{z}^*} = 0$. Since $[\epsilon, \bar{z}^{max}]$ is a sub-interval of $(0, \bar{z}^{max}]$, the last property thus holds. ■

To plot the fixed-price aggregate supply, we also need to pin down its curvature. Since the value of the second derivative of c_s^{fix} cannot be determined analytically, we resort to

numerical methods for an approximation.[12] Figure E.1 plots the fixed-price aggregate supply, its theoretical upper bound if the matching frictions were absent, and the productive capacity. As seen, the non-monotonic behavior of the fixed-price aggregate supply clearly illustrates the two aforementioned, counteracting channels at play; specifically, when the reservation transportation cost is relatively low, the separation margin channel dominates the product market tightness channel, and vice versa. Therefore, there exists a level of reservation transportation cost such that the aggregate supply is maximized. Such a behavior is similar to the one considered in Michaillat and Saez (2015), where both the matching frictions on the product market and matching cost per visit give rise to the non-standard behavior of the aggregate supply curve.[13]

In terms of the other variables of interest, as the reservation transportation cost increases, the matching cost, i.e., $G(\bar{z})l-c$, increases, the transportation cost, i.e., $(1-G(\bar{z}))l$, decreases, while the spare capacity (or equivalently, unemployment), i.e., $l-c$, first decreases then increases.

12. Nevertheless, the second derivative of c_s^{fix} with respect to $\bar{z}$ is given by:

$$\frac{d^2c_s^{fix}(\bar{z})}{d\bar{z}^2} = \big(1-G(\bar{z})+f(\theta)G(\bar{z})\big)^2\cdot\Big(\frac{(1-\eta)l}{\eta\rho}\frac{1}{\bar{z}\sigma}g(\bar{z})\big(-1+2\beta G(\bar{z})+2G(\bar{z})-3\beta G(\bar{z})^2\big)q(\theta)^{1+\xi}$$
$$-\frac{(1-\eta)l}{\eta\rho}\big(1-G(\bar{z})\big)G(\bar{z})\big(-1+\beta G(\bar{z})\big)^2\frac{1-\eta}{\eta\rho}\theta^{\xi-1}(1+\xi)\big(1+\theta^{\xi}\big)^{-\frac{1+\xi}{\xi}-1}$$
$$+\frac{1-\eta}{\eta\rho}\big(-1+\beta G(\bar{z})\big)\theta^{-\xi-1}\big(1+\theta^{-\xi}\big)^{-\frac{1}{\xi}-1}\frac{1}{\bar{z}\sigma}g(\bar{z})l-f(\theta)l\Big\{\frac{1}{\bar{z}^2\sigma}g(\bar{z})+\frac{\log\bar{z}-\gamma}{\bar{z}^2\sigma^3\sqrt{2\pi}}\exp\Big[-\frac{(\log\bar{z}-\gamma)^2}{2\sigma^2}\Big]\Big\}\Big)$$
$$-\Big[\frac{(1-\eta)l}{\eta\rho}\big(1-G(\bar{z})\big)G(\bar{z})\big(-1+\beta G(\bar{z})\big)q(\theta)^{1+\xi}+f(\theta)\frac{1}{\bar{z}\sigma}g(\bar{z})l\Big]$$
$$\cdot\Big[\frac{1-\eta}{\eta\rho}\big(-1+\beta G(\bar{z})\big)\theta^{-\xi-1}\big(1+\theta^{-\xi}\big)^{-\frac{1}{\xi}-1}G(\bar{z})-\big(1-f(\theta)\big)\frac{1}{\bar{z}\sigma}g(\bar{z})\Big]2\big(1-G(\bar{z})+f(\theta)G(\bar{z})\big),$$

13. In contrast to our fixed-price aggregate supply curve which is plotted in the $(c,\bar{z})$ plane, the aggregate supply curve in Michaillat and Saez (2015) is plotted in the (c,x) plane, where x refers to the product market tightness. See Figure I of their paper for details.

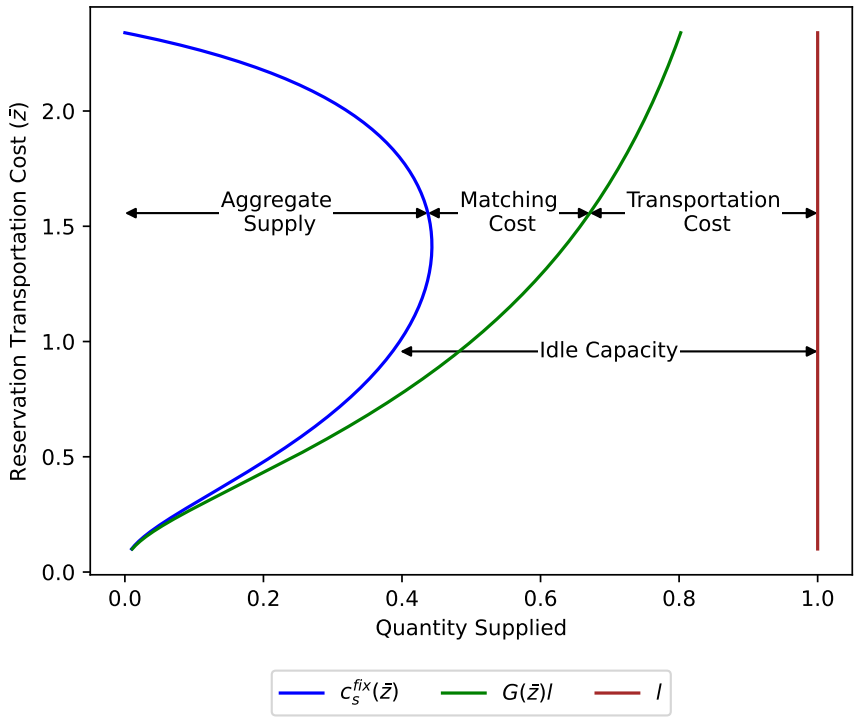

Figure E.1: Supply Side of the Economy When the Price of Goods Is Fixed

Notes. The figure plots the fixed-price aggregate supply $c_s^{fix}(\bar{z})$, its theoretical upper bound if the matching frictions were absent $G(\bar{z})l$, and the productive capacity l for certain values of reservation transportation cost $\bar{z}$. The gap between $c_s^{fix}(\bar{z})$ and $G(\bar{z})l$ represents the matching cost, the gap between $G(\bar{z})l$ and l represents the transportation cost (measured in units of goods), whereas the gap between $c_s^{fix}(\bar{z})$ and l represents the spare capacity of exporters, or equivalently, the unemployment. In the numerical approximation, parameter values are $\eta = 0.5, \rho = 0.5, \kappa = 1.2, \beta = 0.99, \xi = 2, l = 1, \gamma = 0$, and $\sigma = 1$. $\bar{z}$ takes its values from 1,000 evenly spaced numbers over $[0.1, \bar{z}^{max}]$, where $\bar{z}^{max}$ is solved numerically using its definition in (E.2).

F. Robustness of SVAR Results

F.1. The Fitted ACR

In this appendix, we conduct a robustness check of our baseline results by using a fitted ACR index in our estimation after regressing the port-specific ACR on the Oxford Stringency (OS) index (Mathieu et al. 2020) and port fixed effects.[14] Such a robustness check is intended to resolve the potential endogeneity concern regarding the ACR index when there are non-negligible changes in the container capacity between shipping routes that arise due to demand shifters which ultimately contribute to port congestion.

The OS index is essentially an indicator of mobility curtailment policies. Specifically, the authors of the OS index compile information on when and which measures governments take to contain the spread of the Covid-19 virus. The particular index we use is a simple average of nine individual component indicators, which measure the intensity of school closures, workplace closures, cancellation of public events, restrictions on public gatherings, closures of public transport, stay-at-home requirements, public information campaigns, restrictions on internal movements, and international travel controls, respectively. Since the OS index is dedicated to measuring the strictness of government policies, its variations are not subject to any demand-side factor. More importantly, strict containment policies enacted by local governments, as measured by a high value of the OS index, are expected to have contributed significantly to the escalation of port congestion worldwide, hence serving as the main cause of the global supply chain disruptions.[15] As such, the OS index could be applied as an instrument to the ACR index, and the resulting fitted ACR index could help us isolate the causal effects of global supply chain disruptions.

In the actual implementation, we first calculate the monthly average OS index for the country where each of the major container ports worldwide is located. In the process, we

14. We thank Kun Wang for suggesting this robustness check.

15. The pandemic-related containment measures have put enormous strain on the global supply chain, disrupting the international shipping of tradable goods to the U.S. from around the world (Attinasi et al. 2021; Grimes and Edgecliffe-Johnson 2021; Dempsey 2022). For instance, lock-downs introduced to combat Covid-19 have limited the availability of workers to process cargo in ports as well as their work arrangements, leading to a slow-down of container processing, an escalation of port congestion, and hence a supply chain disruption cascading both upstream and downstream.

truncate our sample at 2020M1 as the OS index is only available after then. Subsequently, we regress the port-specific ACR on the corresponding OS index and port fixed effects, and extract the fitted values, i.e., $\widehat{\text{ACR}}$. Lastly, we replace the ACR index with $\widehat{\text{ACR}}$ in our estimation. Once again, Restrictions 1, 2, and 3 are imposed on IRFs, and the estimation is undertaken using the Bayesian approach as in Arias, Rubio-Ramirez, and Waggoner (2018), Arias, Caldara, and Rubio-Ramírez (2019), and Arias et al. (2023). While all the other specifications are kept the same as those in the baseline, due to the reduced sample length, we include only one lag in the estimation and compute the IRFs and FEVD for only one year after impact to reduce parameter uncertainty.

As shown in Figures F.1 to F.3, the IRFs to each structural shock are quantitatively similar to those in Figures 9 to 11.

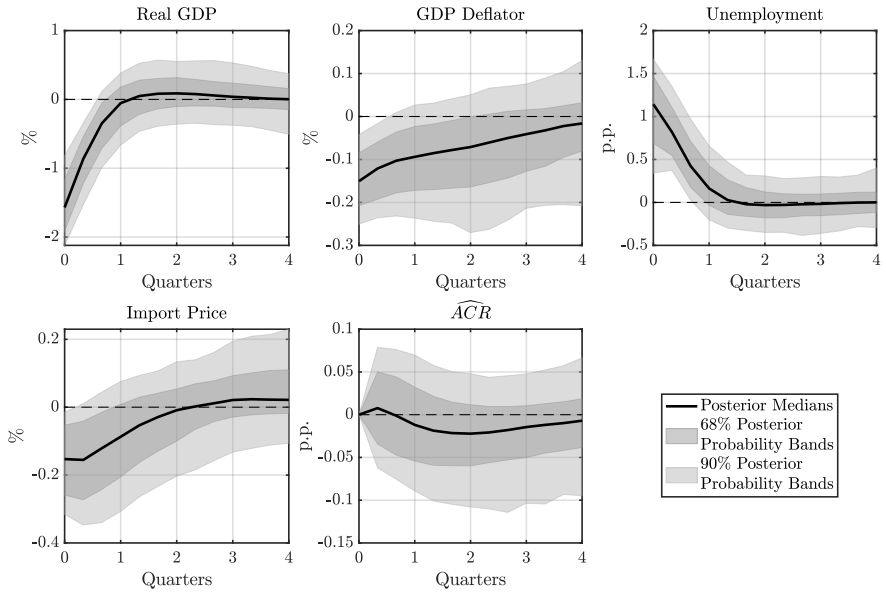

Figure F.1: IRFs to an Adverse Shock to Aggregate Demand: $\widehat{\text{ACR}}$ and Restrictions 1, 2, and 3

Notes. The IRFs to a one standard deviation adverse shock to aggregate demand are identified using $\widehat{\text{ACR}}$ and Restrictions 1, 2, and 3. The solid line shows the point-wise posterior medians, and the shaded bands represent the 68% and 90% equal-tailed point-wise posterior probability bands. The figure is based on 100,000 independent draws.

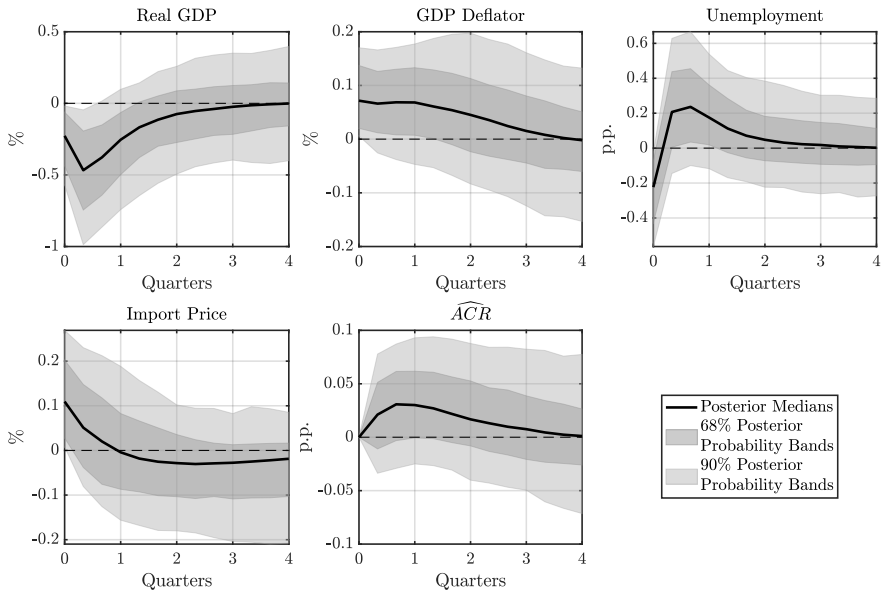

Figure F.2: IRFs to an Adverse Shock to Labor Supply: $\widehat{\text{ACR}}$ and Restrictions 1, 2, and 3

Notes. The IRFs to a one standard deviation adverse shock to labor supply are identified using $\widehat{\text{ACR}}$ and Restrictions 1, 2, and 3. The solid line shows the point-wise posterior medians, and the shaded bands represent the 68% and 90% equal-tailed point-wise posterior probability bands. The figure is based on 100,000 independent draws.

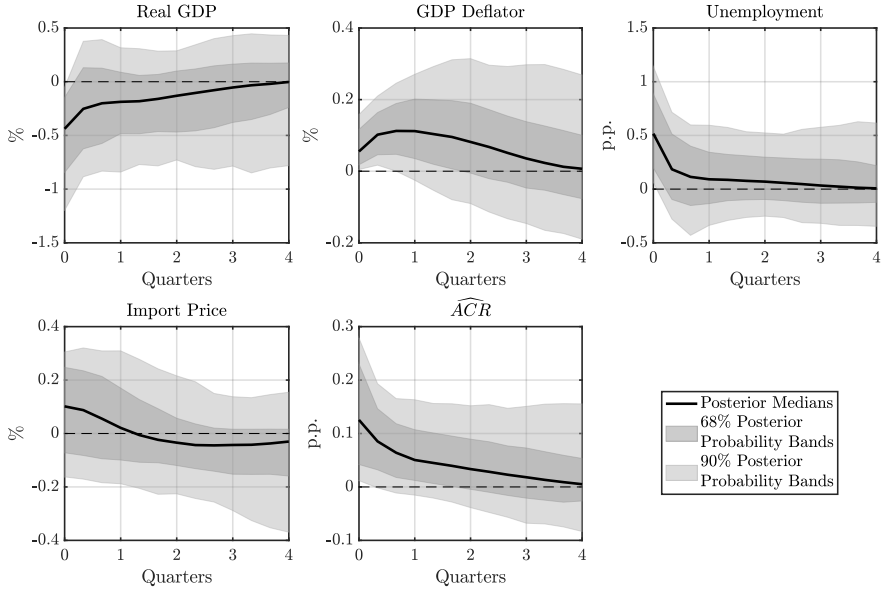

Figure F.3: IRFs to an Adverse Shock to Supply Chain: $\widehat{\text{ACR}}$ and Restrictions 1, 2, and 3

Notes. The IRFs to a one standard deviation adverse shock to supply chain are identified using $\widehat{\text{ACR}}$ and Restrictions 1, 2, and 3. The solid line shows the point-wise posterior medians, and the shaded bands represent the 68% and 90% equal-tailed point-wise posterior probability bands. The figure is based on 100,000 independent draws.

F.2. PCE Goods Price Index

In light of the fact that disruptions to the global supply chain predominantly impacted the trade of goods over services, we check the robustness of our baseline results by replacing the monthly U.S. series of the GDP deflator with the PCE goods price index in the SVAR model. As shown in Figures F.4 to F.8, the estimation results are quantitatively similar to those outlined in Section 4.1. Furthermore, it is noted in Figure F.6 that the stagflationary effects of a supply chain disturbance are more pronounced than those in Figure 11, confirming that the propagation of a supply chain shock is mostly through a severing of trading relationships in goods.

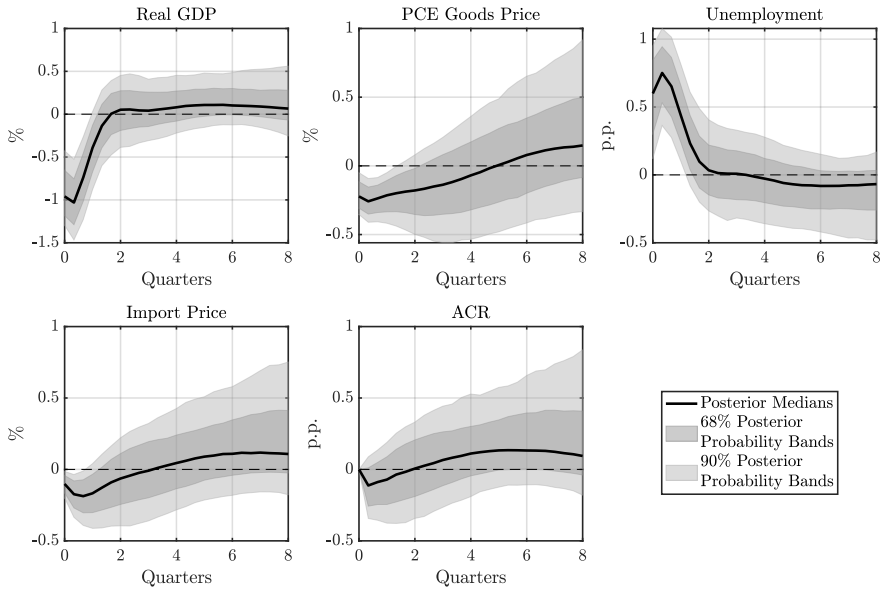

Figure F.4: IRFs to an Adverse Shock to Aggregate Demand: PCE Goods Price Index

Notes. The IRFs to a one standard deviation adverse shock to aggregate demand are identified using an SVAR specification with the PCE goods price index included. The solid line shows the point-wise posterior medians, and the shaded bands represent the 68% and 90% equal-tailed point-wise posterior probability bands. The figure is based on 100,000 independent draws.

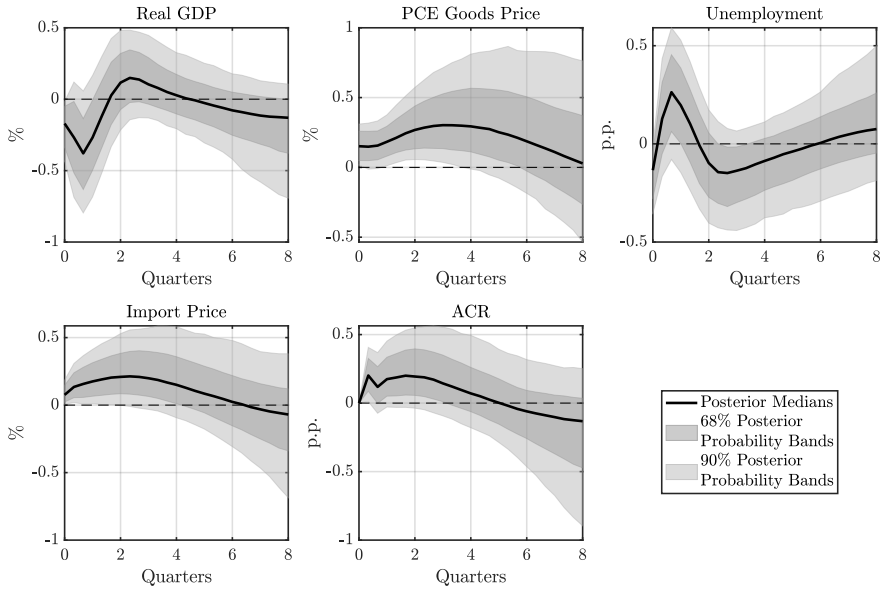

Figure F.5: IRFs to an Adverse Shock to Labor Supply: PCE Goods Price Index

Notes. The IRFs to a one standard deviation adverse shock to labor supply are identified using an SVAR specification with the PCE goods price index included. The solid line shows the point-wise posterior medians, and the shaded bands represent the 68% and 90% equal-tailed point-wise posterior probability bands. The figure is based on 100,000 independent draws.

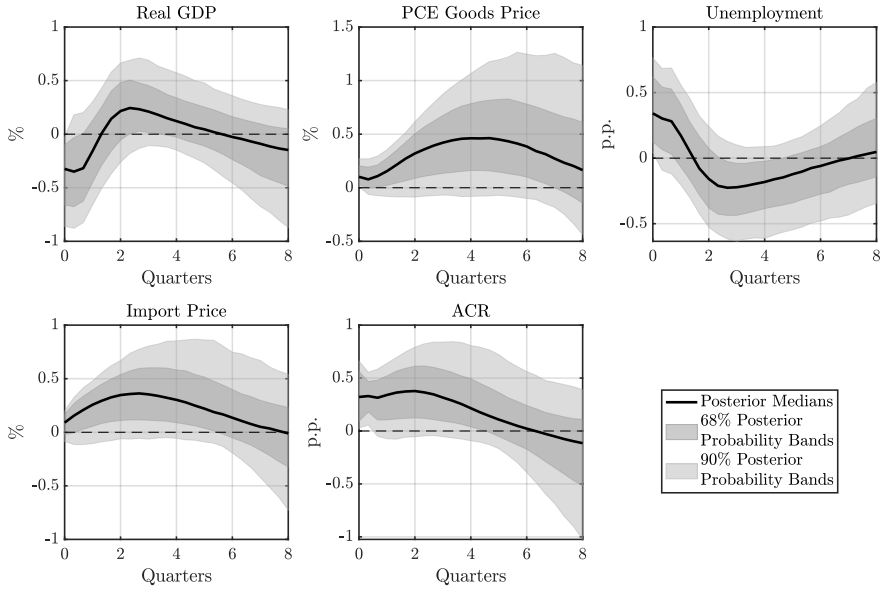

Figure F.6: IRFs to an Adverse Shock to Supply Chain: PCE Goods Price Index

Notes. The IRFs to a one standard deviation adverse shock to supply chain are identified using an SVAR specification with the PCE goods price index included. The solid line shows the point-wise posterior medians, and the shaded bands represent the 68% and 90% equal-tailed point-wise posterior probability bands. The figure is based on 100,000 independent draws.

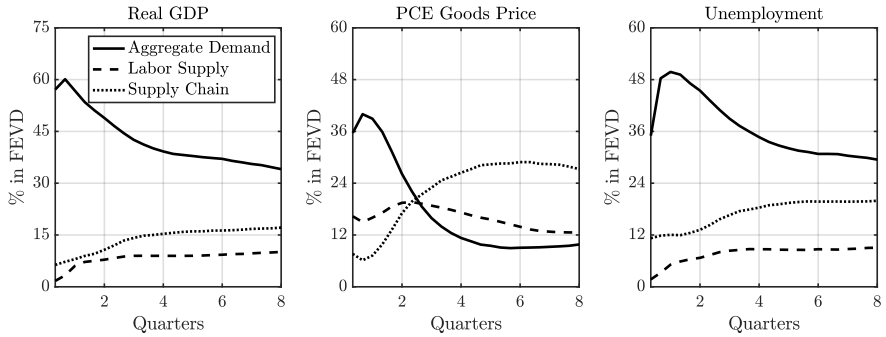

Figure F.7: FEVD from the SVAR: PCE Goods Price Index

Notes. Each line presents the median fraction of the forecast error variance for each endogenous variable, explained by each of the three identified structural shocks at various time horizons. The FEVD is estimated using an SVAR specification with the PCE goods price index included, and based on 100,000 independent draws.

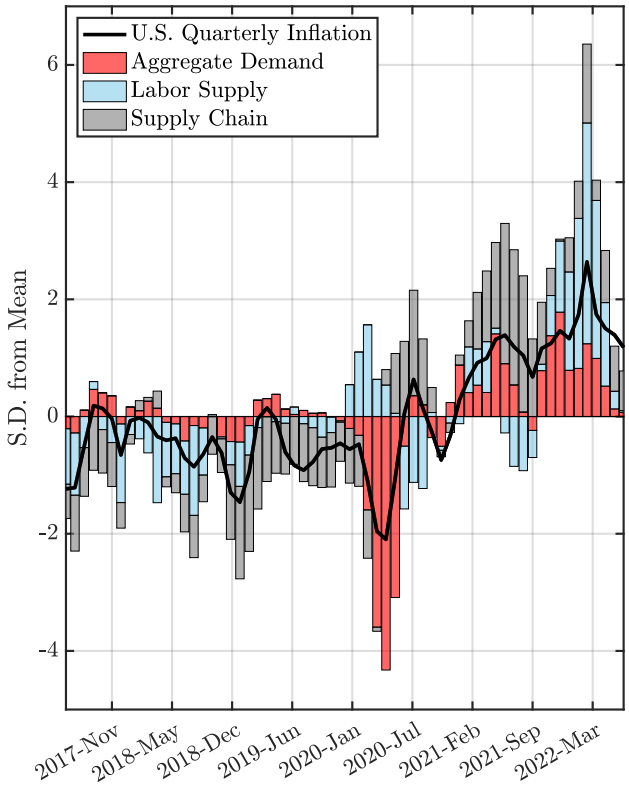

Figure F.8: HD of U.S. Goods Inflation

Notes. The solid line represents the standardized quarterly goods inflation rate in the U.S., i.e., quarter-on-quarter growth of the PCE goods price index. The shaded bar represents the standardized cumulative historical contribution of each of the three structural shocks identified using an SVAR specification with the PCE goods price index included to U.S. goods inflation. The estimation results are obtained with each variable measured in percent change from the previous period, and are calculated based on 100,000 independent draws.

F.3. Different Lag Structures and Longer Restrictions

In Figures F.9 to F.14, we show that our baseline results are robust to considering different lag structures, i.e., one or three lags. We do not consider four lags or beyond due to parameter uncertainty resulting from our limited sample length. We also extend the horizons at which we impose the sign restrictions – i.e., from $k = 1$ to $k = 1, 2$ – to put more disciplines on the behaviors of the IRFs. As shown in Figures F.15 to F.17, our baseline results still hold.

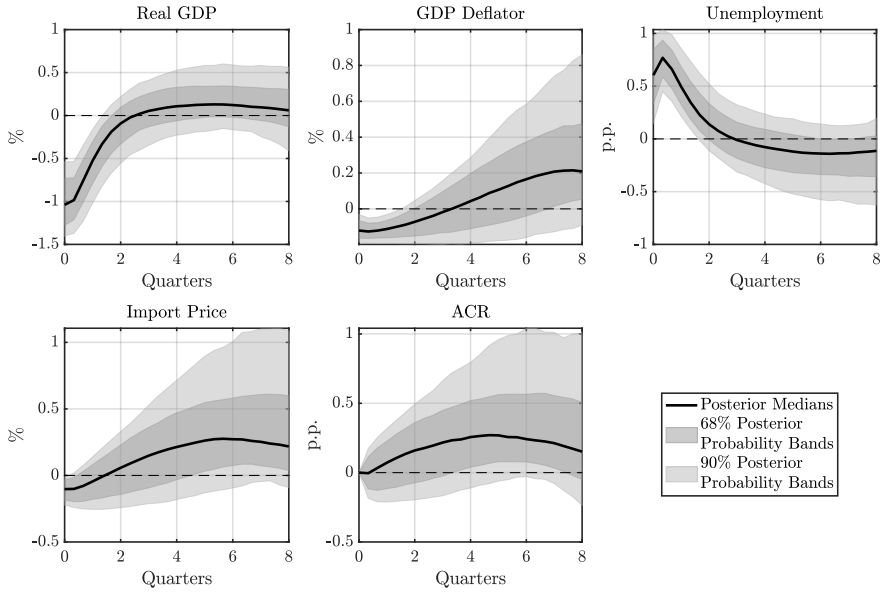

Figure F.9: IRFs to an Adverse Shock to Aggregate Demand: $L = 1$

Notes. The IRFs to a one standard deviation adverse shock to aggregate demand are identified using an SVAR specification as in Equation (24) with one lag, as well as Restrictions 1, 2, and 3. The solid line shows the point-wise posterior medians, and the shaded bands represent the 68% and 90% equal-tailed point-wise posterior probability bands. The figure is based on 100,000 independent draws.

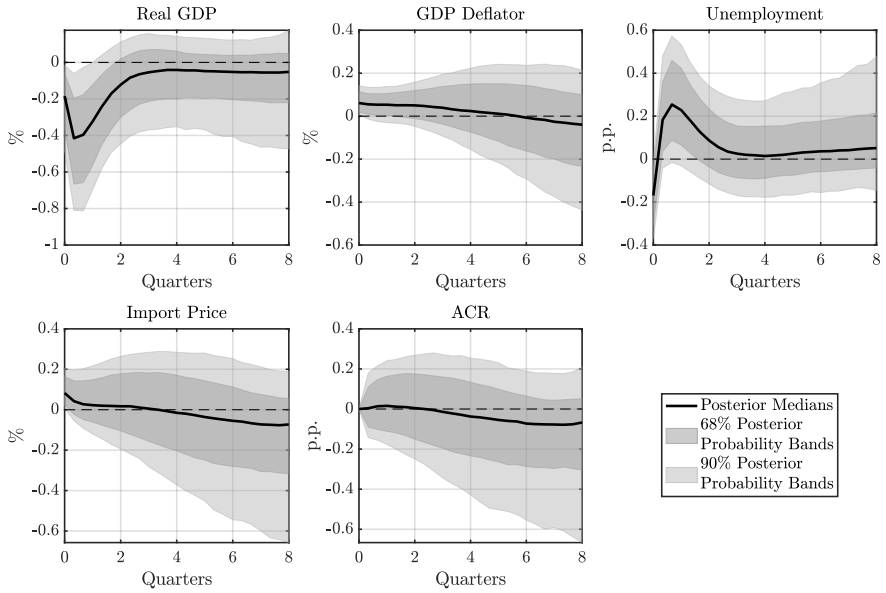

Figure F.10: IRFs to an Adverse Shock to Labor Supply: $L = 1$

Notes. The IRFs to a one standard deviation adverse shock to labor supply are identified using an SVAR specification as in Equation (24) with one lag, as well as Restrictions 1, 2, and 3. The solid line shows the point-wise posterior medians, and the shaded bands represent the 68% and 90% equal-tailed point-wise posterior probability bands. The figure is based on 100,000 independent draws.

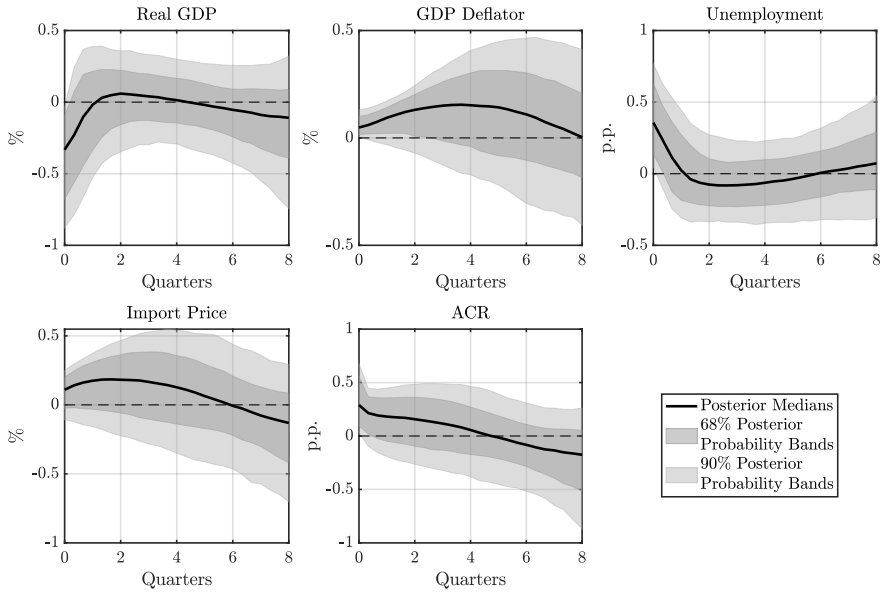

Figure F.11: IRFs to an Adverse Shock to Supply Chain: $L = 1$

Notes. The IRFs to a one standard deviation adverse shock to supply chain are identified using an SVAR specification as in Equation (24) with one lag, as well as Restrictions 1, 2, and 3. The solid line shows the point-wise posterior medians, and the shaded bands represent the 68% and 90% equal-tailed point-wise posterior probability bands. The figure is based on 100,000 independent draws.

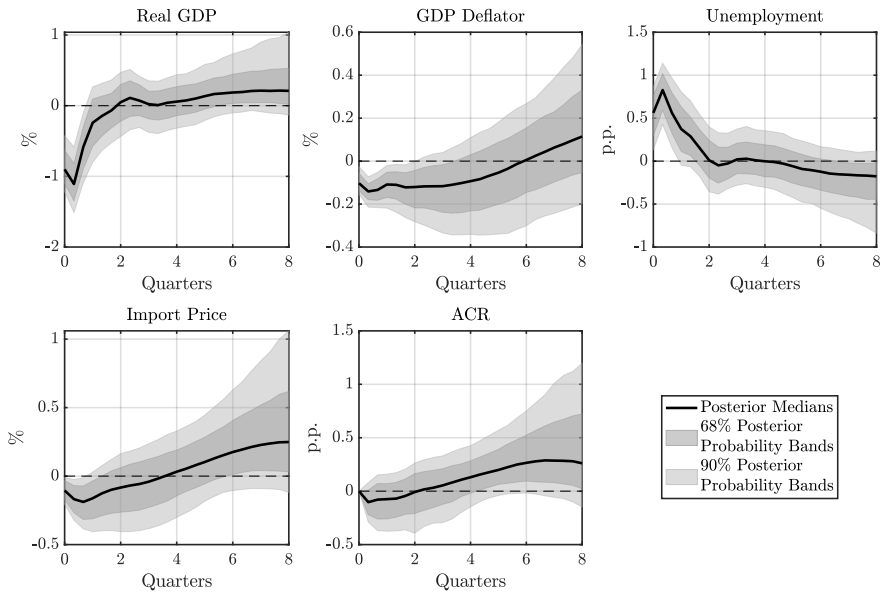

Figure F.12: IRFs to an Adverse Shock to Aggregate Demand: $L = 3$

Notes. The IRFs to a one standard deviation adverse shock to aggregate demand are identified using an SVAR specification as in Equation (24) with three lags, as well as Restrictions 1, 2, and 3. The solid line shows the point-wise posterior medians, and the shaded bands represent the 68% and 90% equal-tailed point-wise posterior probability bands. The figure is based on 100,000 independent draws.

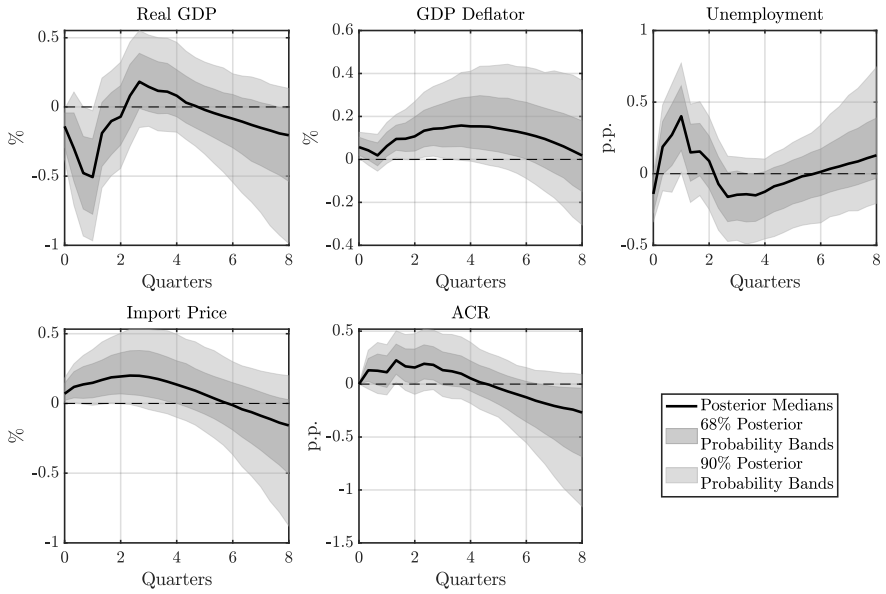

Figure F.13: IRFs to an Adverse Shock to Labor Supply: $L = 3$

Notes. The IRFs to a one standard deviation adverse shock to labor supply are identified using an SVAR specification as in Equation (24) with three lags, as well as Restrictions 1, 2, and 3. The solid line shows the point-wise posterior medians, and the shaded bands represent the 68% and 90% equal-tailed point-wise posterior probability bands. The figure is based on 100,000 independent draws.

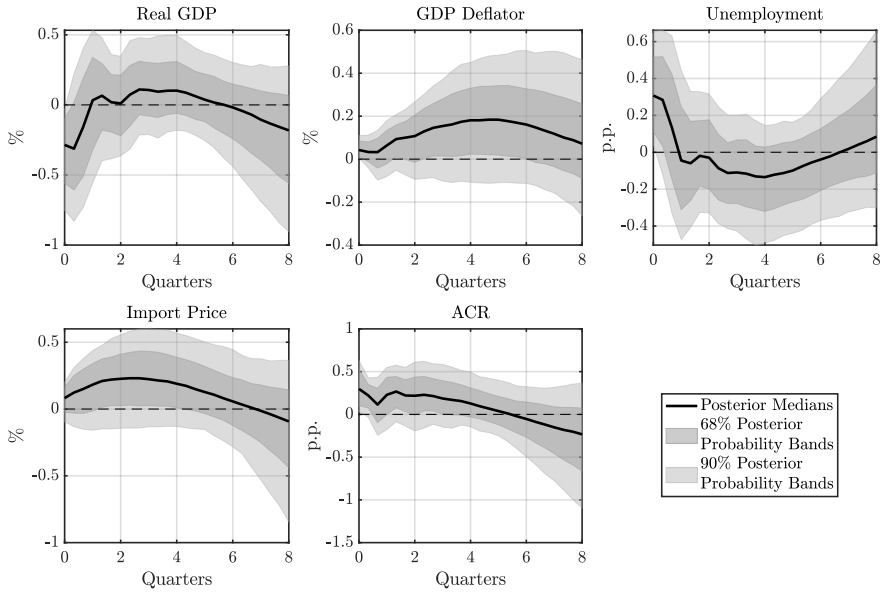

Figure F.14: IRFs to an Adverse Shock to Supply Chain: $L = 3$

Notes. The IRFs to a one standard deviation adverse shock to supply chain are identified using an SVAR specification as in Equation (24) with three lags, as well as Restrictions 1, 2, and 3. The solid line shows the point-wise posterior medians, and the shaded bands represent the 68% and 90% equal-tailed point-wise posterior probability bands. The figure is based on 100,000 independent draws.

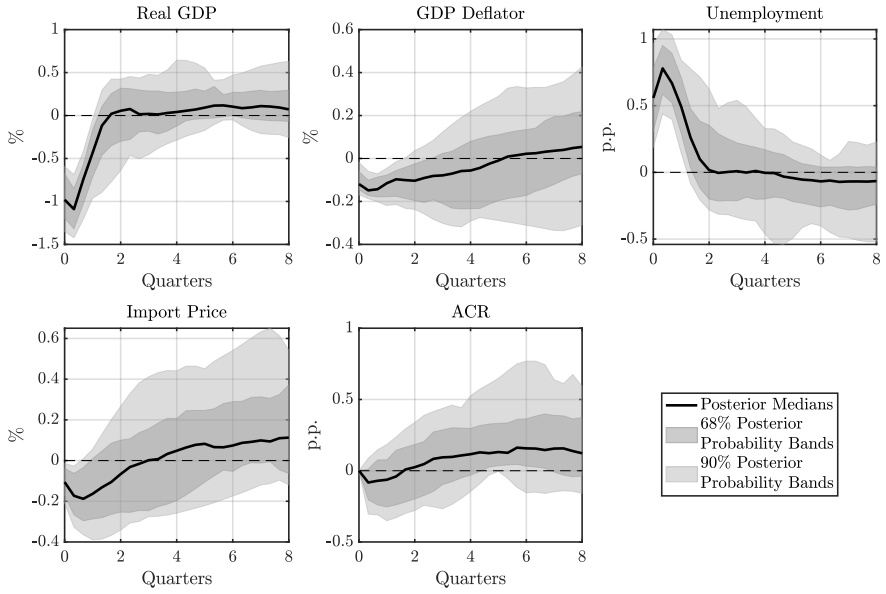

Figure F.15: IRFs to an Adverse Shock to Aggregate Demand: $k = 1, 2$

Notes. The IRFs to a one standard deviation adverse shock to aggregate demand are identified using a set of restrictions that are the same as Restrictions 1, 2, and 3, except that the sign restrictions on IRFs are imposed for longer horizons, i.e., $k = 1$ to $k = 1, 2$. The solid line shows the point-wise posterior medians, and the shaded bands represent the 68% and 90% equal-tailed point-wise posterior probability bands. The figure is based on 100,000 independent draws.

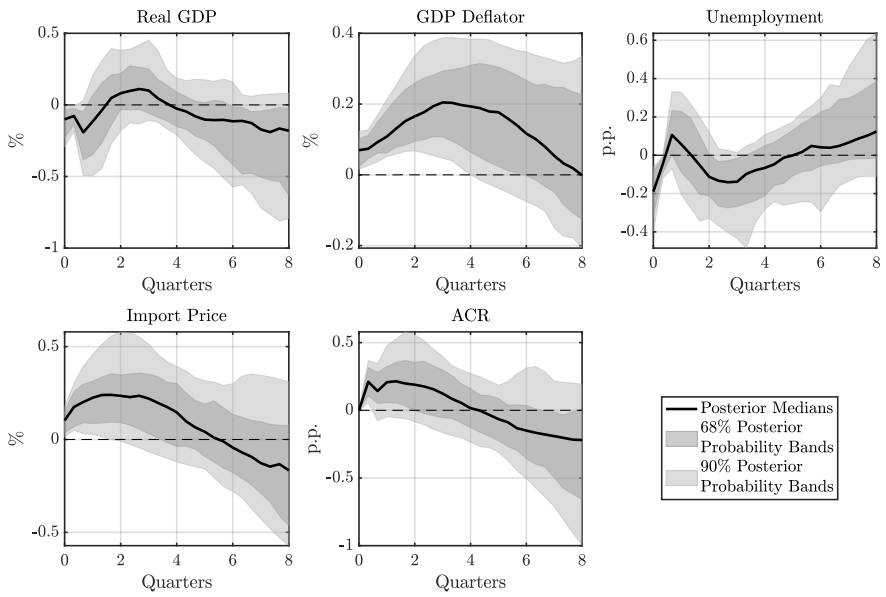

Figure F.16: IRFs to an Adverse Shock to Labor Supply: $k = 1, 2$

Notes. The IRFs to a one standard deviation adverse shock to labor supply are identified using a set of restrictions that are the same as Restrictions 1, 2, and 3, except that the sign restrictions on IRFs are imposed for longer horizons, i.e., $k = 1$ to $k = 1, 2$. The solid line shows the point-wise posterior medians, and the shaded bands represent the 68% and 90% equal-tailed point-wise posterior probability bands. The figure is based on 100,000 independent draws.

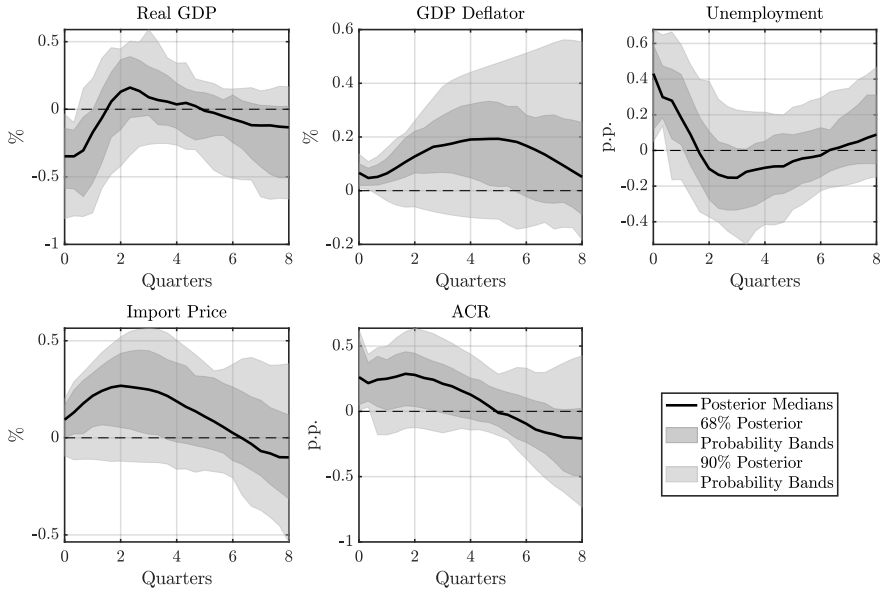

Figure F.17: IRFs to an Adverse Shock to Supply Chain: $k = 1, 2$

Notes. The IRFs to a one standard deviation adverse shock to supply chain are identified using a set of restrictions that are the same as Restrictions 1, 2, and 3, except that the sign restrictions on IRFs are imposed for longer horizons, i.e., $k = 1$ to $k = 1, 2$. The solid line shows the point-wise posterior medians, and the shaded bands represent the 68% and 90% equal-tailed point-wise posterior probability bands. The figure is based on 100,000 independent draws.

F.4. Prior Robustness

Figures F.18, F.19, and F.20 show that the main conclusions from our baseline SVAR analysis are robust to using the prior robust approach for the SVARs proposed by Giacomini and Kitagawa (2021). Such an approach removes the need to specify the prior for the structural parameter given the reduced-form parameter, which is the component of the prior that is responsible for the asymptotic disagreement between Bayesian and frequentist inference. This is mainly achieved by constructing a class of priors that shares a single prior for the reduced-form parameter but allows for arbitrary conditional priors for the structural parameters given the reduced-form parameter.

In practice, we apply their Algorithm 1 to numerically approximate the set of posterior means and the associated robust credible regions for the IRFs of the selected endogenous variables to each structural shock. We make two modifications in the implementation of Algorithm 1. First, in Step 2 of Algorithm 1, to draw the orthonormal Q's subject to Restrictions 1, 2, and 3, we apply the QR decomposition method as in Arias, Rubio-Ramirez, and Waggoner (2018) instead of the original linear projection approach. These two ways of drawing Q are comparable in terms of both the resulting distribution of Q and computational cost. Second, we replace Step 3 of Algorithm 1 with Step 3′ of Algorithm 2 to approximate the lower and upper bounds of the prior robust posterior means, as well as those associated with the robust credible regions.

In Figures F.18, F.19, and F.20, the solid line shows the point-wise posterior medians, and the shaded area represents the 68% equal-tailed point-wise posterior probability bands. Their underlying data are from our baseline estimation outlined in Section 4.1. Alongside the posterior medians and probability bands, we plot the set of prior robust posterior means using dotted curves, and the corresponding 68% robust credible regions using dashed-dotted curves. Their underlying data are based on 1,000 independent draws of the reduced-form parameters and 100,000 orthogonal matrices draws for each reduced-form parameter.

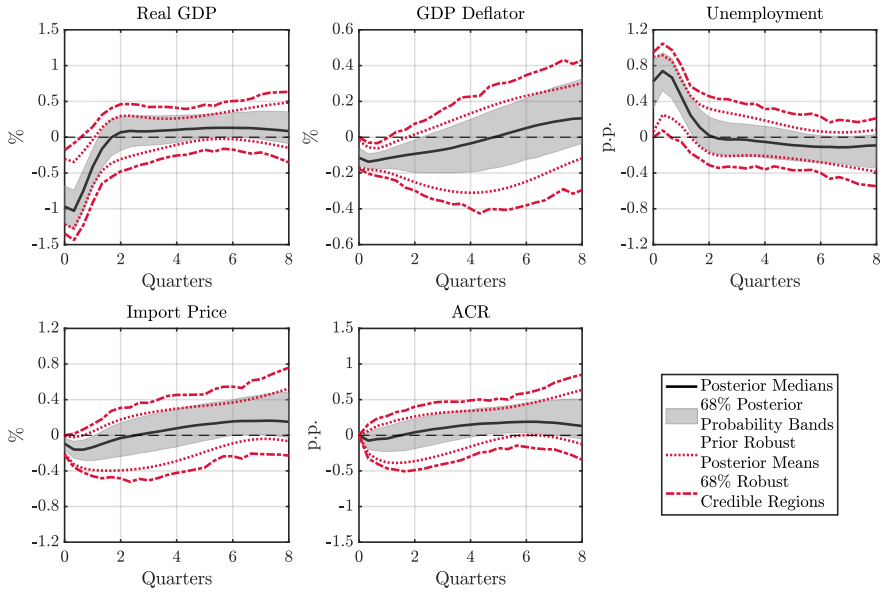

Figure F.18: IRFs to an Adverse Shock to Aggregate Demand Using the Prior Robust Approach in Giacomini and Kitagawa (2021)

Notes. The IRFs to a one standard deviation adverse shock to aggregate demand are estimated using the prior robust approach for the SVARs proposed by Giacomini and Kitagawa (2021). The solid line shows the point-wise posterior medians, and the shaded area represents the 68% equal-tailed point-wise posterior probability bands, which are based on the data from our baseline estimation outlined in Section 4.1. The dotted curves illustrate the set of prior robust posterior means, and the dashed-dotted curves depict the 68% robust credible regions. These curves are obtained from 1,000 independent draws of the reduced-form parameters and 100,000 orthogonal matrix draws for each reduced-form parameter.

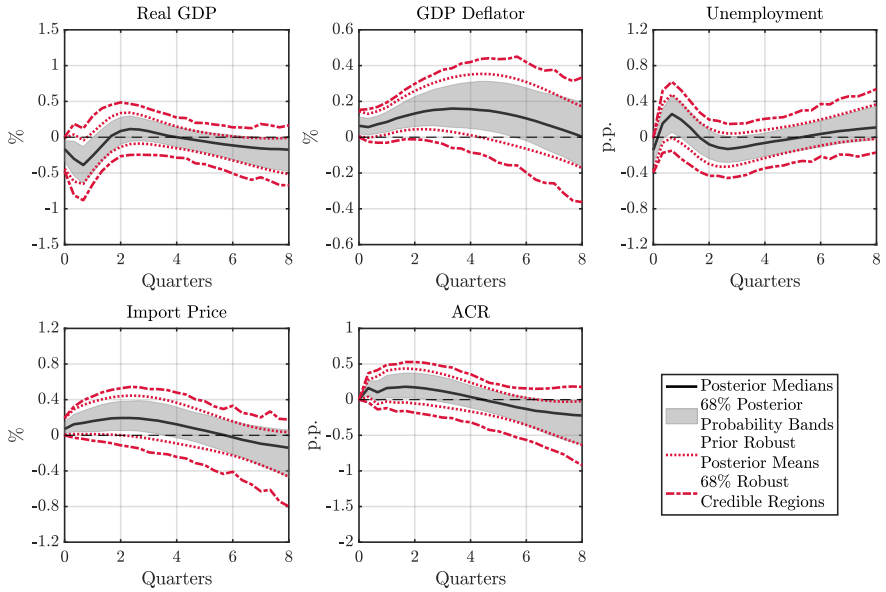

Figure F.19: IRFs to an Adverse Shock to Labor Supply Using the Prior Robust Approach in Giacomini and Kitagawa (2021)

Notes. The IRFs to a one standard deviation adverse shock to labor supply are estimated using the prior robust approach for the SVARs proposed by Giacomini and Kitagawa (2021). The solid line shows the point-wise posterior medians, and the shaded area represents the 68% equal-tailed point-wise posterior probability bands, which are based on the data from our baseline estimation outlined in Section 4.1. The dotted curves illustrate the set of prior robust posterior means, and the dashed-dotted curves depict the 68% robust credible regions. These curves are obtained from 1,000 independent draws of the reduced-form parameters and 100,000 orthogonal matrix draws for each reduced-form parameter.

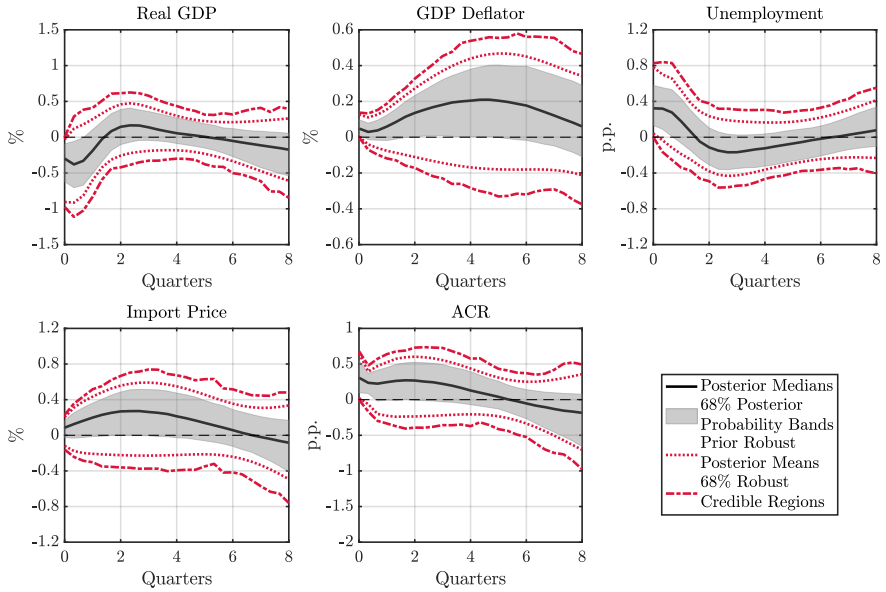

Figure F.20: IRFs to an Adverse Shock to Supply Chain Using the Prior Robust Approach in Giacomini and Kitagawa (2021)

Notes. The IRFs to a one standard deviation adverse shock to supply chain are estimated using the prior robust approach for the SVARs proposed by Giacomini and Kitagawa (2021). The solid line shows the point-wise posterior medians, and the shaded area represents the 68% equal-tailed point-wise posterior probability bands, which are based on the data from our baseline estimation outlined in Section 4.1. The dotted curves illustrate the set of prior robust posterior means, and the dashed-dotted curves depict the 68% robust credible regions. These curves are obtained from 1,000 independent draws of the reduced-form parameters and 100,000 orthogonal matrix draws for each reduced-form parameter.

F.5. No Zero Restrictions When Estimating with the GSCPI

As argued in the introduction and Section 4.2, the GSCPI index is not a pure supply chain disruption measure, as not only could the movements in its underlying data be driven by the demand-side factors (e.g., a high demand for tradable goods translates to a high shipping price), but also there is no differentiation between the supply-side factors (e.g., a rise in "delivery times" could originate from either a supply chain disruption or a labor shortage). As a result, the zero restrictions in Restrictions 1, 2, and 3 are no longer valid in the identification of the adverse shocks to aggregate demand and labor supply.[16]

Therefore, we conduct a robustness check by relaxing the zero restrictions when estimating the SVAR model with the GSCPI index included as an endogenous variable. Specifically, the identification restrictions are now the following:

Restriction 1′. ***An adverse shock to aggregate demand*** *leads to a negative response of real GDP, GDP deflator, and import price, as well as to a positive response of unemployment at* $k = 1$.

Restriction 2′. ***An adverse shock to labor supply*** *leads to a negative response of real GDP and unemployment, as well as to a positive response of GDP deflator and import price at* $k = 1$.

Restriction 3′. ***An adverse shock to supply chain*** *leads to a negative response of real GDP, as well as to a positive response of GDP deflator, unemployment, and GSCPI at* $k = 1$.

The estimation is still conducted using the Bayesian approach as in Arias, Rubio-Ramirez, and Waggoner (2018), Arias, Caldara, and Rubio-Ramírez (2019), and Arias et al. (2023). All the estimation specifications are kept the same as those applied in the baseline. As can be clearly seen in Figures F.21, F.22, and F.23, the biases of using the GSCPI index as a measure of global supply chain disruptions still persist.

16. Nevertheless, we still apply Restrictions 1, 2, and 3 in the identification of the structural shocks in Section 4.2 so as to control for any potential discrepancy that may arise due to differences in the identification restrictions.

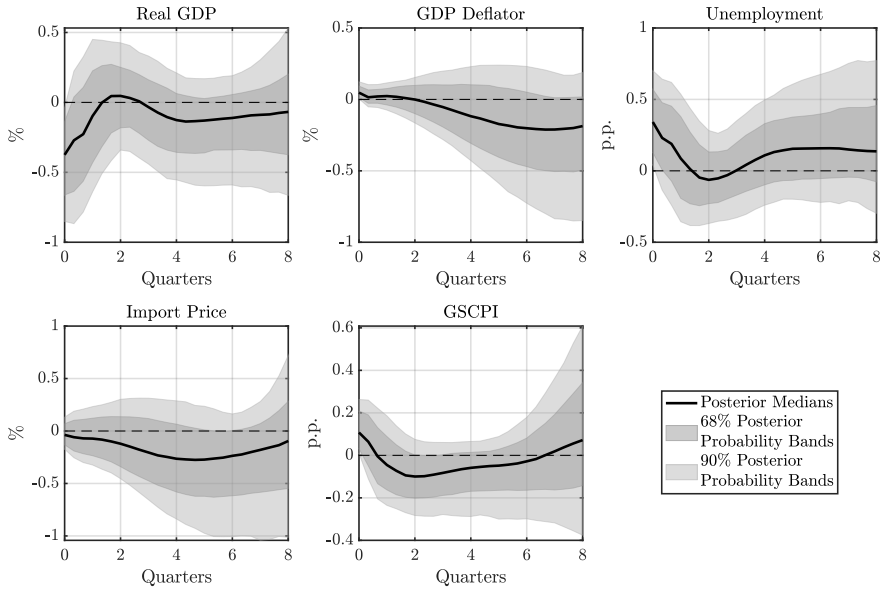

Figure F.21: IRFs to an Adverse Shock to Supply Chain: The GSCPI and Restrictions 1′, 2′, and 3′

Notes. The IRFs to a one standard deviation adverse shock to supply chain are identified using the GSCPI index and Restrictions 1′, 2′, and 3′. The solid line shows the point-wise posterior medians, and the shaded bands represent the 68% and 90% equal-tailed point-wise posterior probability bands. The figure is based on 100,000 independent draws.

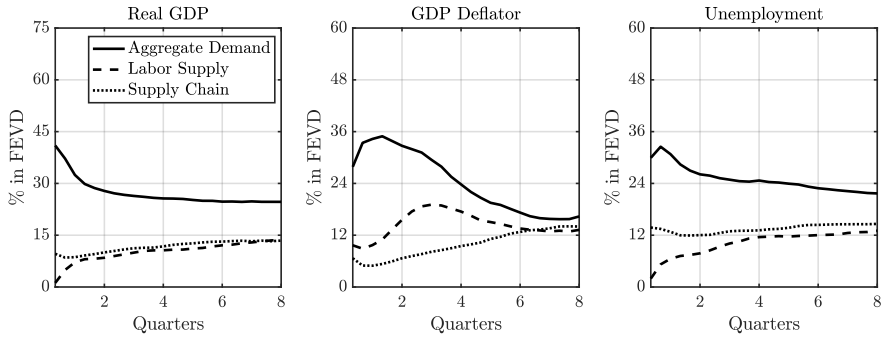

Figure F.22: FEVD from the SVAR: The GSCPI and Restrictions 1′, 2′, and 3′

Notes. Each line presents the median fraction of the forecast error variance for each endogenous variable, explained by each of the three identified structural shocks at various time horizons. The FEVD is estimated using the GSCPI index and Restrictions 1′, 2′, and 3′, and based on 100,000 independent draws.

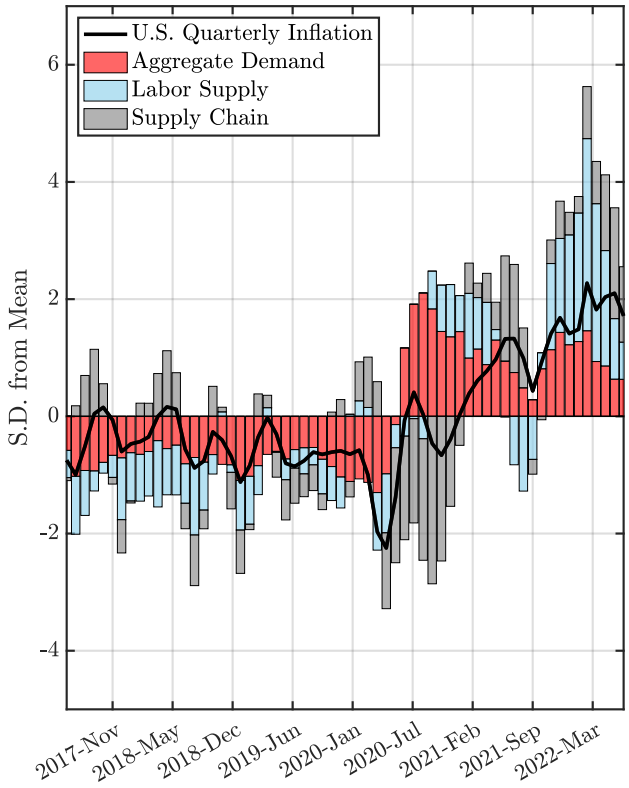

Figure F.23: HD of U.S. Inflation: The GSCPI and Restrictions 1′, 2′, and 3′

Notes. The solid line represents the standardized quarterly inflation rate in the U.S., i.e., quarter-on-quarter growth of the GDP deflator. The shaded bar represents the standardized cumulative historical contribution of each of the three structural shocks identified using the GSCPI index and Restrictions 1′, 2′, and 3′ to U.S. inflation. The estimation results are obtained with each variable measured in percent change from the previous period, and are calculated based on 100,000 independent draws.

G. Priors and Identification in TVAR

G.1. Priors

Our formulation of the prior in the TVAR model follows Bańbura, Giannone, and Reichlin (2010), Mumtaz and Zanetti (2012), and Pizzinelli, Theodoridis, and Zanetti (2020), and the same prior has been applied to the parameters in both the supply chain disrupted ($\mathbb{D}$) and undisrupted ($\mathbb{U}$) regimes. Specifically, we write the TVAR model in Equation (26) compactly as a system of multivariate regressions:

$$\boldsymbol{y} = (\boldsymbol{M}_{\mathbb{D}}\boldsymbol{x}_{\mathbb{D}} + \boldsymbol{u}_{\mathbb{D}})\boldsymbol{I} + (\boldsymbol{M}_{\mathbb{U}}\boldsymbol{x}_{\mathbb{U}} + \boldsymbol{u}_{\mathbb{U}})(\boldsymbol{1}_{T\times T} - \boldsymbol{I}), \tag{G.1}$$

where $\boldsymbol{y} = [\boldsymbol{y}_1 \ \dots \ \boldsymbol{y}_T]$ is an $n \times T$ matrix, $\boldsymbol{x}_{\mathbb{D}} = [\boldsymbol{x}_{\mathbb{D},1} \ \dots \ \boldsymbol{x}_{\mathbb{D},T}]$ is an $m \times T$ matrix with $\boldsymbol{x}_{\mathbb{D},t} = [\boldsymbol{y}'_{t-1} \ \dots \ \boldsymbol{y}'_{t-L} \ \boldsymbol{\omega}'_t]'$, $\boldsymbol{x}_{\mathbb{U}} = [\boldsymbol{x}_{\mathbb{U},1} \ \dots \ \boldsymbol{x}_{\mathbb{U},T}]$ is an $m \times T$ matrix with $\boldsymbol{x}_{\mathbb{U},t} = [\boldsymbol{y}'_{t-1} \ \dots \ \boldsymbol{y}'_{t-L} \ \boldsymbol{\omega}'_t]'$, $\boldsymbol{\omega}_t = [1, t]'$ is a 2×1 vector of a constant and a linear trend, $\boldsymbol{u}_{\mathbb{D}} = [\boldsymbol{\Sigma}_{\mathbb{D}}^{1/2}\boldsymbol{\epsilon}_1 \ \dots \ \boldsymbol{\Sigma}_{\mathbb{D}}^{1/2}\boldsymbol{\epsilon}_T]$ is an $n \times T$ matrix, $\boldsymbol{u}_{\mathbb{U}} = [\boldsymbol{\Sigma}_{\mathbb{U}}^{1/2}\boldsymbol{\epsilon}_1 \ \dots \ \boldsymbol{\Sigma}_{\mathbb{U}}^{1/2}\boldsymbol{\epsilon}_T]$ is an $n \times T$ matrix, $\boldsymbol{\Sigma}_{\mathbb{D}}$ and $\boldsymbol{\Sigma}_{\mathbb{U}}$ are the covariance matrices, $\boldsymbol{I} = diag[I_1 \ \dots \ I_T]$ is a $T \times T$ diagonal matrix, $\boldsymbol{M}_{\mathbb{D}} = [\boldsymbol{B}'_{\mathbb{D},1} \ \dots \ \boldsymbol{B}'_{\mathbb{D},L} \ \boldsymbol{C}'_{\mathbb{D}}]$ and $\boldsymbol{M}_{\mathbb{U}} = [\boldsymbol{B}'_{\mathbb{U},1} \ \dots \ \boldsymbol{B}'_{\mathbb{U},L} \ \boldsymbol{C}'_{\mathbb{U}}]$ are two $n \times m$ matrices containing the TVAR coefficients associated with each regime, and $m = nL + 2$. Given Equation (G.1), for each regime $r \in \{\mathbb{D}, \mathbb{U}\}$, we assume that the prior distribution of the parameter vector, $vec(\boldsymbol{M}_r)$, has a Normal-Inverse-Wishart conjugate form.[17] Such a form can be written as:

$$\begin{aligned} vec(\boldsymbol{M}_r)|\boldsymbol{\Sigma}_r &\sim N\Big(vec(\boldsymbol{M}_r^0), \boldsymbol{\Sigma}_r \otimes \boldsymbol{\Omega}_r^0\Big), \\ \boldsymbol{\Sigma}_r &\sim IW\Big(\boldsymbol{S}_r^0, \alpha_r^0\Big), \end{aligned} \tag{G.2}$$

where $vec(\boldsymbol{M}_r^0)$ is the prior mean of the parameter vector, $\boldsymbol{\Omega}_r^0$ controls the tightness around this prior, $\boldsymbol{S}_r^0$ is the prior scale matrix of the Inverse-Wishart (IW) distribution, and α_r^0 denotes the prior degrees of freedom. Essentially, the prior in Equation (G.2) is a generalization of the Minnesota prior discussed in Litterman (1986) and assumes that the endogenous variables follow a random walk or an AR(1) process. This is based on the idea that recent lags provide more reliable information on the dynamics of the system and therefore the estima-

17. $vec(\cdot)$ denotes the operator that stacks the columns of a matrix into a vector.

tion should assign them a higher weighting. Unlike the original formulation in Litterman (1986) however, the prior in Equation (G.2) does not assume a diagonal, fixed, and known covariance matrix, making it more suitable for our structural analysis.

The Normal-Inverse-Wishart prior implies that, while the prior expectations and variances of the coefficient matrices for the constant and linear trend, $\boldsymbol{C}_r$, are diffuse, those associated with the autoregressive matrices, $\boldsymbol{B}_{r,l}$, can be written as:

$$\begin{aligned}\mathbb{E}[(\boldsymbol{B}_{r,l})_{i,j}] &= \begin{cases}\beta^0_{r,i}, & \text{if } i=j,\ l=1;\\ 0, & \text{otherwise;}\end{cases}\\ \mathbb{V}[(\boldsymbol{B}_{r,l})_{i,j}] &= \lambda\sigma_i^2/\sigma_j^2,\end{aligned} \tag{G.3}$$

where $\beta^0_{r,1},\ldots,\beta^0_{r,n}$ are the prior means of the autoregressive coefficients, $\sigma_1,\ldots,\sigma_n$ are the prior error standard deviations, and the hyper-parameter λ controls the overall tightness of the prior distribution such that a larger λ corresponds to a looser prior. As described in Bańbura, Giannone, and Reichlin (2010) and commonly used in the literature of Bayesian SVARs, the prior moments in Equation (G.3) can be implemented by adding $T_{r,d}$ dummy observations $\boldsymbol{y}_{r,d}$ and $\boldsymbol{x}_{r,d}$ to the system of regressions in Equation (G.1) that correspond to each regime, with $\boldsymbol{y}_{r,d}$ and $\boldsymbol{x}_{r,d}$ satisfying:

$$\boldsymbol{y}_{r,d} = \begin{bmatrix} diag[\beta^0_{r,1}\sigma_1 & \ldots & \beta^0_{r,n}\sigma_n]/\lambda \\ \mathbf{0}_{n(L-1)\times n} \\ diag[\sigma_1 & \ldots & \sigma_n] \\ \mathbf{0}_{2\times n}\end{bmatrix},\ \boldsymbol{x}_{r,d} = \begin{bmatrix} J_L \otimes diag[\sigma_1 & \ldots & \sigma_n]/\lambda & \mathbf{0}_{nL\times 1} & \mathbf{0}_{nL\times 1} \\ \mathbf{0}_{n\times nL} & & \mathbf{0}_{n\times 1} & \mathbf{0}_{n\times 1} \\ \mathbf{0}_{1\times nL} & & \xi & 0 \\ \mathbf{0}_{1\times nL} & & 0 & \xi\end{bmatrix},$$

where $J_L = diag[1 \quad \ldots \quad L]$ and the hyper-parameter ξ controls the prior on the constant and the linear trend such that a small number makes the prior uninformative. Subsequently, the prior moments in Equation (G.2) are simply functions of $\boldsymbol{y}_{r,d}$ and $\boldsymbol{x}_{r,d}$, which are given by:

$$\begin{aligned}\boldsymbol{M}^0_r &= \boldsymbol{y}_{r,d}\boldsymbol{x}'_{r,d}(\boldsymbol{x}_{r,d}\boldsymbol{x}'_{r,d})^{-1},\\ \boldsymbol{\Omega}^0_r &= (\boldsymbol{x}_{r,d}\boldsymbol{x}'_{r,d})^{-1},\\ \boldsymbol{S}^0_r &= (\boldsymbol{y}_{r,d}-\boldsymbol{M}^0_r\boldsymbol{x}_{r,d})(\boldsymbol{y}_{r,d}-\boldsymbol{M}^0_r\boldsymbol{x}_{r,d})',\\ \alpha^0_r &= T_{r,d}-m.\end{aligned}$$

With the Normal-Inverse-Wishart prior being conjugate, the conditional posterior distribution of the parameter vector is also Normal-Inverse-Wishart (Bańbura, Giannone, and Reichlin 2010; Mumtaz and Zanetti 2012):

$$vec(\boldsymbol{M}_r)|\boldsymbol{\Sigma}_r, \boldsymbol{y} \sim N\Big(vec(\tilde{\boldsymbol{M}}_r), \boldsymbol{\Sigma}_r \otimes (\tilde{\boldsymbol{x}}_r \tilde{\boldsymbol{x}}_r')^{-1}\Big),$$
$$\boldsymbol{\Sigma}_r|\boldsymbol{y} \sim IW\Big(\tilde{\boldsymbol{S}}_r, T_{r,d} + 2 + T - m\Big),$$

where the parameters associated with the posterior are given by:

$$\tilde{\boldsymbol{M}}_r = \tilde{\boldsymbol{y}}_r \tilde{\boldsymbol{x}}_r' (\tilde{\boldsymbol{x}}_r \tilde{\boldsymbol{x}}_r')^{-1},$$
$$\tilde{\boldsymbol{S}}_r^0 = (\tilde{\boldsymbol{y}}_r - \tilde{\boldsymbol{M}}_r \tilde{\boldsymbol{x}}_r)(\tilde{\boldsymbol{y}}_r - \tilde{\boldsymbol{M}}_r \tilde{\boldsymbol{x}}_r)',$$

in which the terms $\tilde{\boldsymbol{y}}_r$ and $\tilde{\boldsymbol{x}}_r$ are the matrices of $\boldsymbol{y}_r$ and $\boldsymbol{x}_r$ augmented with the dummy observations $\boldsymbol{y}_{r,d}$ and $\boldsymbol{x}_{r,d}$ respectively.[18]

Following Mumtaz and Zanetti (2012) and Pizzinelli, Theodoridis, and Zanetti (2020), we obtain the values of the prior mean of each autoregressive coefficient, $\beta_{r,i}^0$, as well as the prior error standard deviation, σ_i, from the OLS estimation of a univariate AR(1) model for each endogenous variable. In addition, we set $\lambda = 0.25$ to ensure fast lag decay towards zero. Finally, in terms of the prior distribution of $\overline{ACR}$, we assume that it is normally distributed, with the mean set at the median of the ACR series and the standard deviation calibrated to deliver a Markov Chain Monte Carlo (MCMC) acceptance rate of approximately 70%.

G.2. Identification Using the PFA

Following Uhlig (2005) and Mountford and Uhlig (2009), the identification scheme we employ in the study of the state-dependent effects of a contractionary monetary policy shock amounts to finding an impulse vector a that minimizes a given criterion function $f(\cdot)$ on the space of all impulse vectors. This function penalizes positive impulse responses of real GDP, GDP deflator, and import price as well as negative impulse responses of the Federal Funds Rate and unemployment at horizons $k = 1, \ldots, K$, while satisfying the zero restriction imposed on the impulse response of ACR at horizon $k = 1$. The scheme is applied separately for the observations in each regime. Hence, for simplicity, we drop the regime-specific notation

18. $\boldsymbol{y}_r$ is the part of $\boldsymbol{y}$ that is associated with regime $r \in \{\mathbb{D}, \mathbb{U}\}$.

$r \in \{\mathbb{D}, \mathbb{U}\}$ in the following description.

The PFA is implemented numerically as follows. Define the penalty function as:

$$f(x) = \begin{cases} x, & \text{if } x \leq 0; \\ 100x, & \text{if } x > 0, \end{cases} \tag{G.4}$$

which penalizes positive responses in linear proportion and rewards negative responses in linear proportion, albeit at a slope 100 times smaller than the slope for penalties on the positive side. For the true VAR coefficients, let $r_{j,a}(k),\ k = 1, \ldots, K$ be the impulse response of variable j and σ_j be the standard deviation of the series for variable j. Let $\iota_j = -1$ if j is the index of Federal Funds Rate or unemployment in the data vector, and $\iota_j = 1$ if j is the index of real GDP, GDP deflator, or import price in the data vector. Define the contractionary monetary policy impulse vector as that impulse vector a, which minimizes the total penalty $\varphi(a)$ subject to the zero restriction imposed on the impulse response of the ACR index at horizon $k = 1$:

$$\varphi(a) = \sum_{j \in \left\{ \begin{array}{c} \text{“Federal Funds Rate”}, \\ \text{“real GDP”}, \\ \text{“GDP deflator”}, \\ \text{“unemployment”}, \\ \text{“import price”} \end{array} \right\}} \Big[\sum_{k=1}^{K} f\Big(\iota_j \frac{r_{j,a}(k)}{\sigma_j} \Big) \Big].$$

The re-scaling by σ_j is necessary to make the deviations across different impulse responses comparable to each other. Note that the sign of the penalty direction is flipped for the Federal Funds Rate and unemployment. Since the true VAR is unknown, we find the contractionary monetary policy vector for each draw from the posterior. Such a step involves numerical minimization, and we keep all the draws and accordingly calculate all the corresponding impulse vectors. As a result, the IRFs in the main text are calculated based on these.

G.3. Posterior and Identified Regimes

The posterior distribution of the threshold $\overline{ACR}$ is plotted in Figure G.1, while the time series of the identified regimes using the median of such a posterior is plotted in Figure G.2.

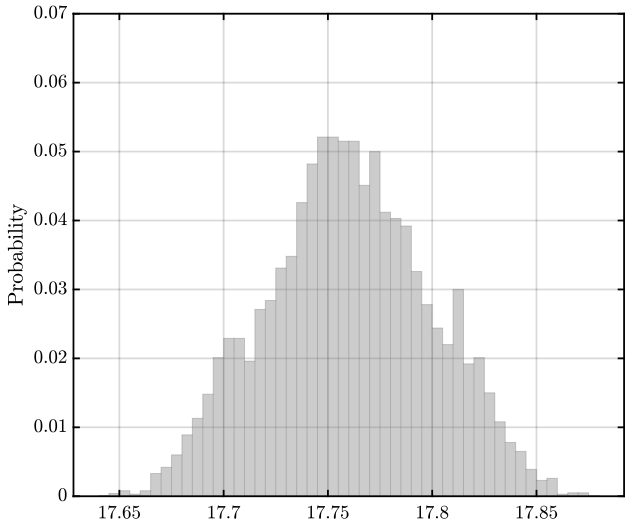

Figure G.1: Posterior Distribution of the Threshold $\overline{ACR}$

Notes. The figure plots the posterior distribution of the ACR threshold value, i.e., $\overline{ACR}$, based on 10,000 independent draws.

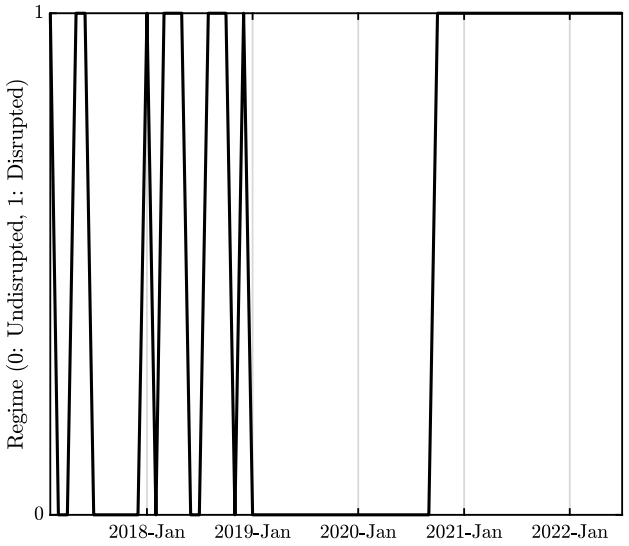

Figure G.2: Regimes Based on the Median of the Posterior $\overline{ACR}$

Notes. The solid line, switching from zero to one, represents the current regime as identified by the median of the posterior distribution of the ACR threshold, i.e., $median(\overline{ACR}) = 17.7595$. The value of one corresponds to the supply chain disrupted ($\mathbb{D}$) regime, while the value of zero corresponds to the supply chain undisrupted ($\mathbb{U}$) regime.

H. Robustness of TVAR Results

In Figures H.1 and H.2, we show that our state-dependence results are robust to considering different lag structures in the TVAR model, i.e., two or three lags. We do not consider four lags or beyond due to parameter uncertainty resulting from our limited sample length. We also show in Figure H.3 that the results are robust when a looser prior is undertaken in the estimation, i.e., $\lambda = 0.5$. Furthermore, we extend the horizons at which we impose the sign restrictions – i.e., from $k = 1$ to $k = 1, 2, 3$ – so as to put more disciplines on the behaviors of IRFs. As shown in Figure H.4, once again, our benchmark results still hold.

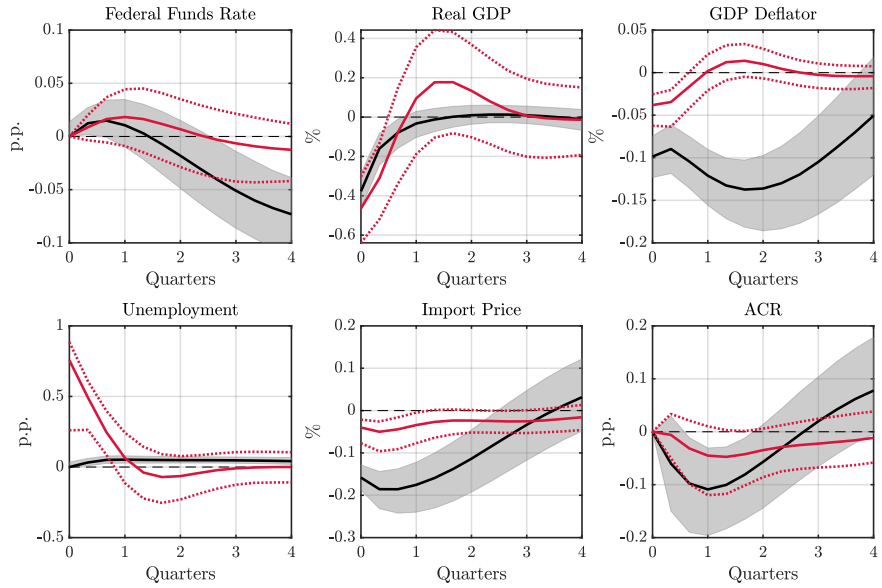

Figure H.1: State-Dependent Effects of a Contractionary Monetary Policy Shock: $L = 2$

Notes. The figure shows the IRFs to a one standard deviation contractionary monetary policy shock identified using a TVAR specification as in Equation (26) with two lags, as well as Restriction 4, for both the supply chain disrupted and undisrupted regimes. The black solid (red solid) line shows the point-wise posterior medians, and the black shaded area (red dotted lines) depicts the 68% equal-tailed point-wise posterior probability bands for the supply chain disrupted (undisrupted) regime. The figure is based on 10,000 independent draws from the posterior.

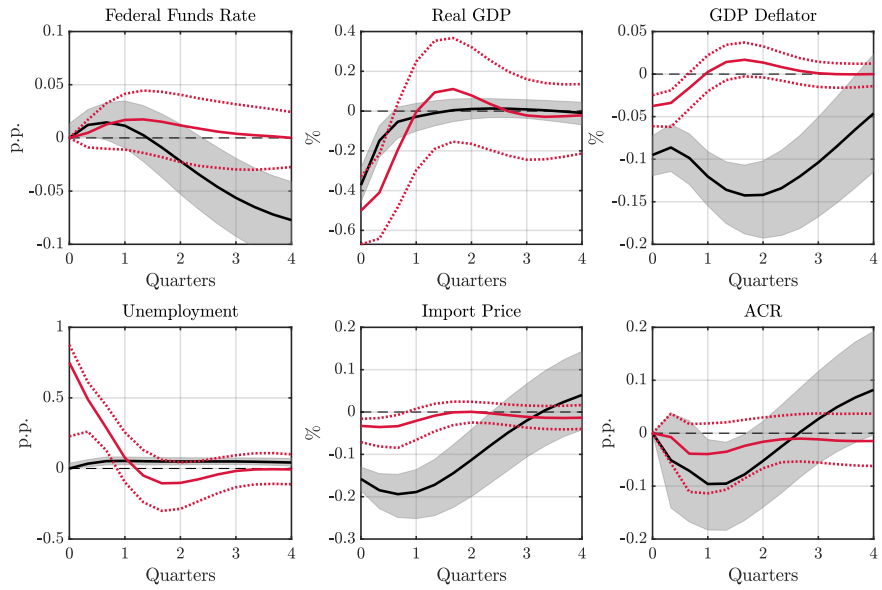

Figure H.2: State-Dependent Effects of a Contractionary Monetary Policy Shock: $L = 3$

Notes. The figure shows the IRFs to a one standard deviation contractionary monetary policy shock identified using a TVAR specification as in Equation (26) with three lags, as well as Restriction 4, for both the supply chain disrupted and undisrupted regimes. The black solid (red solid) line shows the point-wise posterior medians, and the black shaded area (red dotted lines) depicts the 68% equal-tailed point-wise posterior probability bands for the supply chain disrupted (undisrupted) regime. The figure is based on 10,000 independent draws from the posterior.

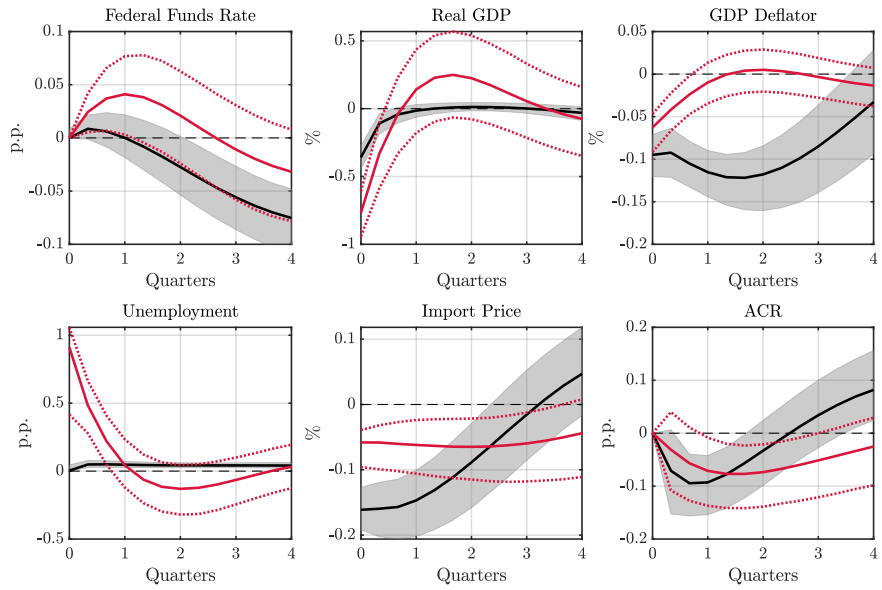

Figure H.3: State-Dependent Effects of a Contractionary Monetary Policy Shock: $\lambda = 0.5$

Notes. The figure shows the IRFs to a one standard deviation contractionary monetary policy shock identified using a TVAR specification as in Equation (26) with $\lambda = 0.5$, as well as Restriction 4, for both the supply chain disrupted and undisrupted regimes. The black solid (red solid) line shows the point-wise posterior medians, and the black shaded area (red dotted lines) depicts the 68% equal-tailed point-wise posterior probability bands for the supply chain disrupted (undisrupted) regime. The figure is based on 10,000 independent draws from the posterior.

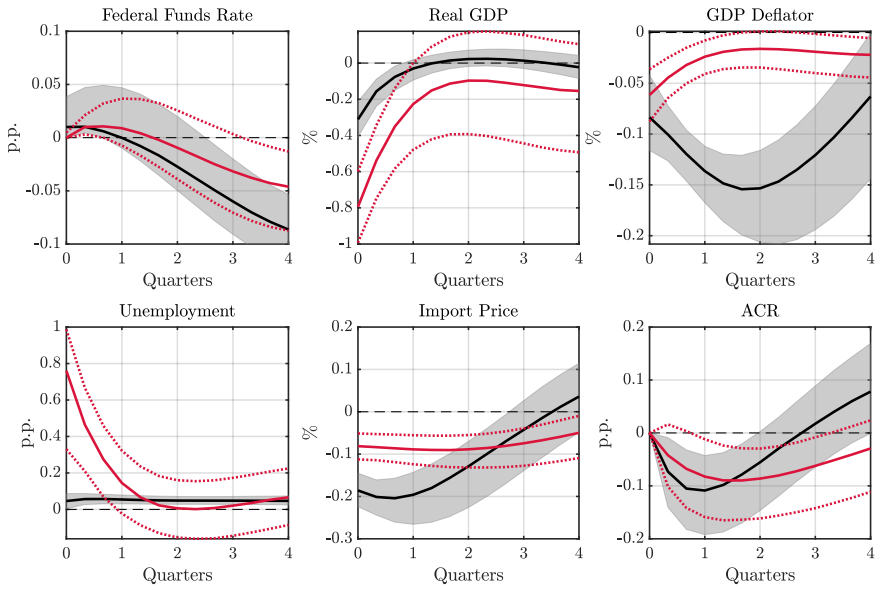

Figure H.4: State-Dependent Effects of a Contractionary Monetary Policy Shock: $k = 1, 2, 3$

Notes. The figure shows the IRFs to a one standard deviation contractionary monetary policy shock identified using Restriction 4 for both the supply chain disrupted and undisrupted regimes. Restriction 4 is imposed for longer horizons, i.e., $k = 1, 2, 3$. The black solid (red solid) line shows the point-wise posterior medians, and the black shaded area (red dotted lines) depicts the 68% equal-tailed point-wise posterior probability bands for the supply chain disrupted (undisrupted) regime. The figure is based on 10,000 independent draws from the posterior.

I. State-Dependence Results Using the LPs

In this appendix, as a robustness check to our state-dependence results obtained using the TVAR model, we work with LPs to identify a contractionary monetary policy shock and analyze how it affects the macro aggregates for the U.S. economy depending on the level of global supply chain disruptions. LPs are a flexible approach that allows us to address the state-dependence of monetary policy without making strong parametric assumptions. Specifically, we use the LPs with interaction terms as in Ghassibe and Zanetti (2022), and our identification scheme consists of sign restrictions implemented as described in Plagborg-Møller and Wolf (2021). Consider the following $n \times (K+1)$ projections:

$$\begin{aligned} y_{i,t+k} =& I_t \left[\boldsymbol{\beta}'_{\mathbb{D},i,k,0} \boldsymbol{y}_t + \sum_{l=1}^{L} \boldsymbol{\beta}'_{\mathbb{D},i,k,l} \boldsymbol{y}_{t-l} + \boldsymbol{C}'_{\mathbb{D},i,k} \boldsymbol{\omega}_t \right] \\ &+ (1 - I_t) \left[\boldsymbol{\beta}'_{\mathbb{U},i,k,0} \boldsymbol{y}_t + \sum_{l=1}^{L} \boldsymbol{\beta}'_{\mathbb{U},i,k,l} \boldsymbol{y}_{t-l} + \boldsymbol{C}'_{\mathbb{U},i,k} \boldsymbol{\omega}_t \right] + u_{i,k,t}, \end{aligned} \tag{I.1}$$

where $1 \leq i \leq n$, $0 \leq k \leq K$, $\boldsymbol{y}_t$ is an $n \times 1$ vector of the same endogenous variables as in Section 5.2 save for the ACR index (since it is the variable we use to split the sample), $y_{i,t+k}$ is the value of the i-th variable in $\boldsymbol{y}_{t+k}$, $\boldsymbol{\omega}_t = [1, t]'$ is a 2×1 vector of a constant and a linear trend, and $u_{i,k,t}$ is the reduced-form error corresponding to the i-th variable. The vector of the reduced-form errors for $k = 1$, $\boldsymbol{u}_{1,t} = [u_{1,1,t} \ \ \dots \ \ u_{n,1,t}]'$, is assumed to have mean zero and covariance matrix equal to $\mathbb{E}(\boldsymbol{u}_{1,t}\boldsymbol{u}'_{1,t}) = \boldsymbol{\Sigma}$.

Similar to the setup in the TVAR model, I_t is a dummy variable that indicates whether the supply chain is disrupted. The supply chain disrupted regime is determined based on whether the one-month lag of the ACR index is above its median level over the sample. Figure I.1 shows the times series of the ACR index along with its 50th and 60th percentiles. As seen, there were frequent switches between the supply chain disrupted and undisrupted regimes before 2019. Subsequently, from early-2019 to mid-2020, the ACR index was constantly below its sample median. Such a pattern was reversed from mid-2020 onwards, as the ACR index started to climb up and the U.S. economy stepped into the disrupted regime. Note that the switches between the two regimes shown in Figure I.1 are almost identical to those

illustrated in Figure G.2 when the threshold $\overline{ACR}$ is determined endogenously in the TVAR estimation.

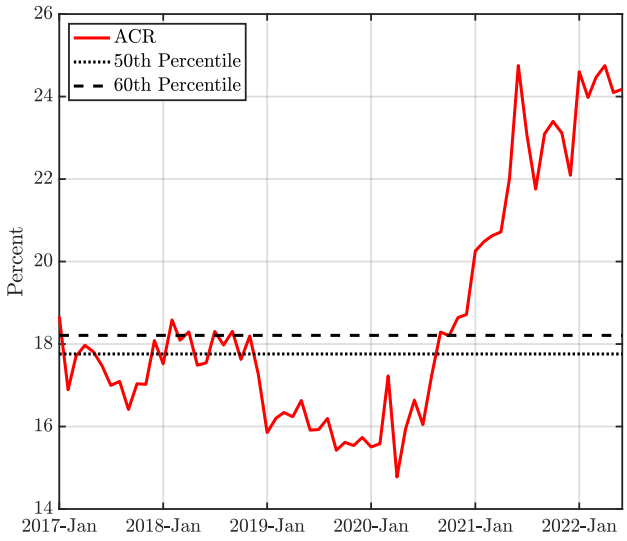

Figure I.1: ACR and Its 50th and 60th Percentiles

Notes. The figure plots the ACR index as well as its 50th and 60th percentiles during the sampling period from January 2017 to July 2022. The ACR index is computed using the AIS data of containerships and the IMA-DBSCAN algorithm developed in Appendix A. The index is presented in percentage terms and has been seasonally adjusted.

With the two regimes defined, the parameters $\boldsymbol{\beta}_{\mathbb{D},i,k,0}, \boldsymbol{\beta}_{\mathbb{D},i,k,l}$, and $\boldsymbol{C}_{\mathbb{D},i,k}$ correspond to the supply chain disrupted regime ($\mathbb{D}$), while the parameters $\boldsymbol{\beta}_{\mathbb{U},i,k,0}, \boldsymbol{\beta}_{\mathbb{U},i,k,l}$, and $\boldsymbol{C}_{\mathbb{U},i,k}$ correspond to the supply chain undisrupted regime ($\mathbb{U}$). Same as our choice of the lag structure in the TVAR model, we include only one lag in the estimation of the LPs so as to reduce parameter uncertainty.

In order to identify a contractionary monetary policy shock, we follow our theoretical prediction in Proposition 6 and come up with an identification scheme similar to that in Section 5.2. Yet, since the ACR is not included in the estimation, we drop the zero restriction in Restriction 4 and re-write it as the following:

Restriction 4′. ***A contractionary monetary policy shock*** *leads to a negative response of real GDP, GDP deflator, and import price, as well as to a positive response of unemployment and Federal Funds Rate at* $k = 1, 2, 3$. *In addition, the on-impact response of GDP deflator in p.p. is bounded to be smaller than that of Federal Funds Rate in p.p.*

Note that Restriction 4′ is similar to Restriction 4, except that we impose restrictions on the subsequent horizons to sharpen our identification, and an elasticity bound is imposed to discipline the identified set of IRFs corresponding to the GDP deflator. The latter variation is critical to ensure that our estimation is plausible, as in the absence of such a bound, the identified set would include a decline in the GDP deflator of 100 p.p. as being equally likely as a decline in the GDP deflator of 1 p.p. following an unexpected increase in the Federal Funds Rate of 0.05 p.p. Hence, we use a bound to rule out dubious IRFs following Kilian and Murphy (2012), Arias, Caldara, and Rubio-Ramírez (2019), and Arias et al. (2023).

With Restriction 4′, we compute the identified set of IRFs in each regime by numerically solving the quadratic program described in the supplement to Plagborg-Møller and Wolf (2021) using Algorithm 2 of Giacomini and Kitagawa (2021). Without loss of generality, we normalize the first shock to be the shock of interest. Let $\boldsymbol{S}$ denote a $15 \times n$ matrix that selects the IRFs which we restrict to be either positive or negative (there are in total 15 sign restrictions in Restriction 4′). Then, for each regime, we draw $D = 100,000$ orthogonal matrices $\boldsymbol{Q}_{r,d}$ (i.e., $\boldsymbol{Q}'_{r,d}\boldsymbol{Q}_{r,d} = \boldsymbol{Q}_{r,d}\boldsymbol{Q}'_{r,d} = \mathbf{1}_{n\times n}$) that satisfy the following:

$$\begin{aligned} \boldsymbol{S}\hat{\boldsymbol{B}}_{r,0:2}\hat{\boldsymbol{\Omega}}\boldsymbol{Q}_{r,d}\boldsymbol{e}_1 &\geq 0, \\ \frac{\boldsymbol{e}_3'\hat{\boldsymbol{B}}_{r,0}\hat{\boldsymbol{\Omega}}\boldsymbol{Q}_{r,d}\boldsymbol{e}_1}{\boldsymbol{e}_1'\hat{\boldsymbol{B}}_{r,0}\hat{\boldsymbol{\Omega}}\boldsymbol{Q}_{r,d}\boldsymbol{e}_1} + 1 &\geq 0, \end{aligned} \tag{I.2}$$

where $r \in \{\mathbb{D}, \mathbb{U}\}$, $1 \leq d \leq D$, $\hat{\boldsymbol{B}}_{r,0:2} = [\hat{\boldsymbol{B}}'_{r,0} \;\; \hat{\boldsymbol{B}}'_{r,1} \;\; \hat{\boldsymbol{B}}'_{r,2}]'$, $\hat{\boldsymbol{B}}_{r,k} = [\hat{\boldsymbol{\beta}}_{r,1,k,0} \;\; \dots \;\; \hat{\boldsymbol{\beta}}_{r,n,k,0}]'$, $\hat{\boldsymbol{\beta}}_{r,i,k,0}$ is the OLS estimate of $\boldsymbol{\beta}_{r,i,k,0}$, $\hat{\boldsymbol{\Omega}} = chol(\hat{\boldsymbol{\Sigma}})'$, $chol$ is the upper triangular Cholesky decomposition of $\hat{\boldsymbol{\Sigma}}$, and $\hat{\boldsymbol{\Sigma}}$ is the OLS estimate of $\boldsymbol{\Sigma}$.[19] Given that the entry (i, j) in $\hat{\boldsymbol{B}}_{r,k}\hat{\boldsymbol{\Omega}}\boldsymbol{Q}_{r,d}$ gives the response of the i-th variable to the j-th shock at horizon k, the first inequality condition in Equation (I.2) summarizes all the sign restrictions imposed on IRFs, while the second inequality condition contains the elasticity bound, as $(\boldsymbol{e}_3'\hat{\boldsymbol{B}}_{r,0}\hat{\boldsymbol{\Omega}}\boldsymbol{Q}_{r,d}\boldsymbol{e}_1)/(\boldsymbol{e}_1'\hat{\boldsymbol{B}}_{r,0}\hat{\boldsymbol{\Omega}}\boldsymbol{Q}_{r,d}\boldsymbol{e}_1)$ denotes the ratio between the on-impact responses of the GDP deflator and the Federal Funds Rate, where e_i is the i-th column of the n-dimensional identity matrix.

Given $\hat{\boldsymbol{B}}_{r,k}$ and $\hat{\boldsymbol{\Omega}}$, let $\{\boldsymbol{Q}_{r,d}\}_{d=1,\dots,D}$ be the draws that satisfy the restrictions in Equation

19. Vector inequalities are to be understood element-wise.

(I.2). The identified set of IRFs of the i-th variable at horizon k is thus given by:

$$\left[\min_{d}\left\{0.05\frac{\boldsymbol{e}_i'\hat{\boldsymbol{B}}_{r,k}\hat{\boldsymbol{\Omega}}\boldsymbol{Q}_{r,d}\boldsymbol{e}_1}{\boldsymbol{e}_1'\hat{\boldsymbol{B}}_{r,0}\hat{\boldsymbol{\Omega}}\boldsymbol{Q}_{r,d}\boldsymbol{e}_1}\right\}_{d=1,\ldots,D},\ \max_{d}\left\{0.05\frac{\boldsymbol{e}_i'\hat{\boldsymbol{B}}_{r,k}\hat{\boldsymbol{\Omega}}\boldsymbol{Q}_{r,d}\boldsymbol{e}_1}{\boldsymbol{e}_1'\hat{\boldsymbol{B}}_{r,0}\hat{\boldsymbol{\Omega}}\boldsymbol{Q}_{r,d}\boldsymbol{e}_1}\right\}_{d=1,\ldots,D}\right], \tag{I.3}$$

where the factor $0.05/(\boldsymbol{e}_1'\hat{\boldsymbol{B}}_{r,0}\hat{\boldsymbol{\Omega}}\boldsymbol{Q}_{r,d}\boldsymbol{e}_1)$ is a normalization so that in both regimes, the contractionary monetary policy shock raises the Federal Funds Rate by 0.05 p.p. on impact.

Figure I.2 plots the point-wise medians and 68% equal-tailed point-wise probability bands associated with the identified set of IRFs in each regime following a contractionary monetary policy shock. We show the IRFs from horizon $k = 0$ up to horizon $k = 6$. The shorter horizon relative to the horizon of the IRFs shown in the TVAR model (Figure 16) is due to parameter uncertainty associated with the LPs. Nevertheless, as clearly seen in Figure I.2, the state-dependent effects of a contractionary monetary policy shock are still observable, as the responses of real GDP and unemployment are weaker while those of the GDP deflator and import price are stronger when the global supply chain is disrupted (i.e., $ACR_{t-1} > 17.8\%$, which is the sample median of the ACR index).

As a robustness check, we also consider a threshold at the 60th percentile of the ACR index (i.e., 18.2%) to distinguish between the supply chain disrupted and undisrupted regimes. As shown in Figure I.3, the main results are robust. We do not consider thresholds higher than the 60th percentile because, as shown in Figure I.1, they would imply a sharp division of our sample at around mid-2020, which may lead to a biased result.

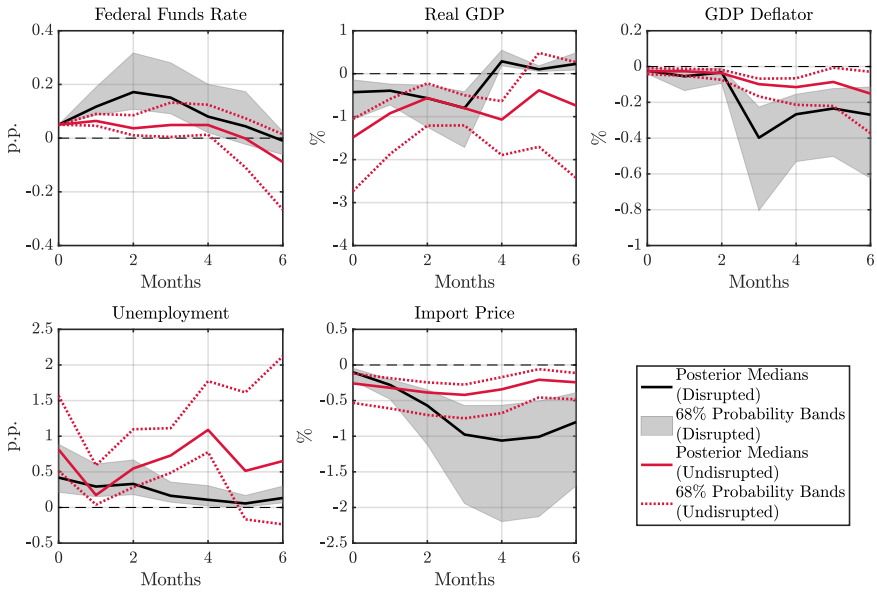

Figure I.2: State-Dependent Effects of a Contractionary Monetary Policy Shock: Using LPs With Interaction Terms and a Threshold at the Median of the ACR Index

Notes. The figure shows the IRFs to a contractionary monetary policy shock identified using LPs with interaction terms, as in Ghassibe and Zanetti (2022), along with Restriction 4′, for both the supply chain disrupted and undisrupted regimes. A threshold at the sample median of the ACR index (i.e., 17.8%) is applied to distinguish between the two regimes. The black solid (red solid) line shows the point-wise medians, and the black shaded area (red dotted lines) depicts the 68% equal-tailed point-wise probability bands for the supply chain disrupted (undisrupted) regime. The figure is based on 100,000 draws of orthogonal matrices.

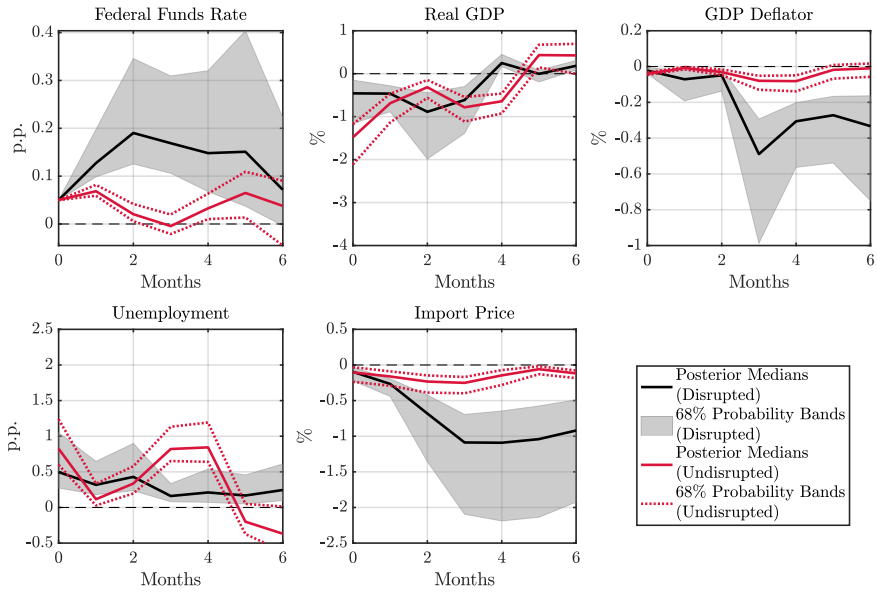

Figure I.3: State-Dependent Effects of a Contractionary Monetary Policy Shock: Using LPs With Interaction Terms and a Threshold at the 60th Percentile of the ACR Index

Notes. The figure shows the IRFs to a contractionary monetary policy shock identified using LPs with interaction terms, as in Ghassibe and Zanetti (2022), along with Restriction 4′, for both the supply chain disrupted and undisrupted regimes. A threshold at the 60th percentile of the ACR index (i.e., 18.2%) is applied to distinguish between the two regimes. The black solid (red solid) line shows the point-wise medians, and the black shaded area (red dotted lines) depicts the 68% equal-tailed point-wise probability bands for the supply chain disrupted (undisrupted) regime. The figure is based on 100,000 draws of orthogonal matrices.